IDŐJÁRÁS

QUARTERLY JOURNAL
OF THE HUNGARIAN METEOROLOGICAL SERVICE

Special Issue: Workshop on Environmental Fluid Mechanics as Elements in Agrometeorological Modeling

Guest Editors: **Tor Håkon Sivertsen** and **Peder A. Tyvand**

CONTENTS

Editorial I

Tor Håkon Sivertsen and *Janis Gailis:* Discussing a web-based system for administration, evaluation, and correction of meteorological and biological data in a perspective of actor-network theory 79

Arne Oddvar Skjelvåg, Ole Einar Tveito and *Inge Bjørdal:* Use of crop development models in agroclimatic mapping 91

Peder A. Tyvand: A diffusive Boussinesq plume 101

Oliver J. Brambles and *D. Andrew S. Rees:* Curved free convection plume paths in porous media 109

Tor Håkon Sivertsen: Discussing certain features of the transfer of wave energy in stationary gravity waves and stationary gravity-inertia waves in the atmosphere 123

Yuli D. Chashechkin: Internal waves and internal boundary currents. In memoriam Fridtjof Nansen 133

Kirill Karelsky, Arakel Petrosyan and *Igor Smirnov:* A new model for boundary layer flows interacting with particulates in land surface on complex terrain 149

Thomas K. Thiis, Willy K. Jeksrud† and *Andreas S. Fløe:* Numerical simulation of cross-flow ventilation of farm buildings in a cold, windy coast climate 161

Michael Bestehorn: Surface patterns on thin liquid films, reduced 2D-descriptions. Part I. Perfect fluids ... 171

Michael Bestehorn: Surface patterns on thin liquid films, reduced 2D-descriptions. Part II. Viscous fluids. 185

Lalić Branislava, Dragutin T. Mihailović, Slavica Radovanović, Jelica Balaž and *Ana Ćirišan:* Input data representativeness problem in plant disease forecasting models 199

Dragutin T. Mihailović and *Igor Balaž:* An essay on modeling problems of complex systems in environmental fluid mechanics 209

****

http://www.met.hu/Journal-Idojaras.php

VOL. 111 * NO. 2–3 * APRIL – SEPTEMBER 2007

IDŐJÁRÁS

Quarterly Journal of the Hungarian Meteorological Service

Editorial Office: P.O. Box 39, H-1675 Budapest, Hungary or
Gilice tér 39, H-1181 Budapest, Hungary
E-mail: bozo.l@met.hu or *antal.e@met.hu*
Fax: (36-1) 346-4809

Subscription by

mail: IDŐJÁRÁS, P.O. Box 39, H-1675 Budapest, Hungary;
E-mail: bozo.l@met.hu or *antal.e@met.hu*; *Fax: (36-1) 346-4809*

This special issue contains the proceedings from a workshop arranged at Ås in Norway in June 2006, called 'Workshop on environmental fluid mechanics as elements in agrometeorological modeling'.

Agrometeorology is a field of applied science aiming to develop operational systems for decision support in crop production and horticultural production. Both support of strategic decisions on what crops to grow at a certain farm or in a certain region, and support of tactical decisions on protecting the field crops against pests and disease, on timing the harvest, on irrigation scheduling etc. are covered by agro meteorological models. Furthermore, analyzing the environmental results of agricultural crop production is dependent on agrometeorological knowledge.

The models of agrometeorology contain results from the fields of physical meteorology, fluid dynamics, crop science, and biological sciences connected to operational crop protection. One major aim of this workshop has been to look into the sub-models of agrometeorology related to fluid dynamics and dynamical meteorology.

Norway once was a pioneering country for meteorology. Vilhelm Bjerknes (1862–1951) had important influence on the development of operational meteorology into a deterministic science based on the principles of hydrodynamics and synoptic systems for making observation. Before Bjerknes started his pioneering work in the beginning of the 20th century, there was no deterministic meteorology used operationally. The weather prognoses were mainly based on the combination of climate data, weather signs, and statistical inference. It was a great progress to be able to use deterministic weather forecasts instead of vague statistical prognoses. Life and death may depend on knowledge in advance, if a disastrous winter storm is heading for the western coast of Norway.

Today large-scale meteorology is established as a deterministic science, and numerical weather forecasts based on fluid dynamics as an important tool.

Agrometeorology is a special branch of physical meteorology. It works on the smallest length scale, where there is no direct influence of the Earth's rotation. The large-scale weather forecasts are sometimes used as input data in agrometeorological forecasts. In large-scale meteorology the horizontal transport of mass and energy is of primary importance. In small-scale meteorology the vertical fluxes play a dominant role. In order to understand and control the conditions for healthy growth of a plant crop, one needs to measure and model the vertical flow of energy and mass in the system of soil, water, air, and plants.

Agrometeorology is being developed at a crossroad between deterministic and statistical science. Plant growth and plant health inevitably bring statistical elements into the models of agrometeorology. Other elements of statistical uncertainty are leaf area, transpiration, humidity, albedo, and turbulent transport coefficients. It is a scientific goal to make agrometeorology models as deterministic as possible. However, the smaller the time and length scales involved, the statistical deviations will be relatively greater. Therefore, a model that works on the shortest length scales can never be fully deterministic in all aspects.

In this special issue of IDŐJÁRÁS *we are presenting some of the results from the workshop for an international audience. The issue contains one paper on the subject of administrating meteorological and biological data to be used operationally as input to models. Another paper on agroclimatic modeling, meant for decision support on strategic issues is included. Three papers are dealing with local meteorological features connected to the fluid dynamical concepts of plumes and internal gravity waves in the atmosphere. At the small special session on gravity waves an interesting contribution on the history of Fridtjof Nansen and gravity waves in the ocean, as well as theory on internal waves and*

boundary layers was presented, and this is one of the contributions in the proceedings. Numerical modeling of fluxes of particles and heat in the boundary layer near the ground are dealt with in this issue. Furthermore, two papers connected to fluid dynamical instabilities in films of fluid are included.

The important theme of 'representativeness' of input data to operational biometeorological models is the theme of one paper. Finally, we will mention an essay dealing with the non-linearity and chaotic behavior of the seemingly simple energy balance equation in the vicinity of the soil surface.

Looking into the future we think it is worthwhile to continue this discussion between biologists and researchers in the field of fluid dynamics to clarify the content and the scope of black boxes used operationally, and try to interpret complicated formulas using ordinary language. Two important related problems connected to operational models will be more and more relevant to deal with in the future: (a) determining the scope of qualitative modeling techniques, (b) developing methods for integrating data from different sources (automated networks of meteorological stations, weather radars, satellites, and manual observations) to be used in an optimal and intelligible way.

Acknowledgements

We would like to thank IDŐJÁRÁS *for giving us the opportunity to publish the proceedings from this workshop in a special issue. We also would like to thank Norwegian Institute for Agricultural and Environmental Research (both the Director of Research and the project 'Agrometorological Service of Norway'), the Norwegian Institute for Life Sciences (both the Director of Research and the Department of Mathematical Sciences and Technology), and Nordic Association of Agricultural Sciences for making it economically possible to arrange this workshop and publish the proceedings.*

Especially we will to thank the secretaries Karin K. Lyngmo and Signe Kroken for helping us with the arrangement and typewriting.

Tor Håkon Sivertsen[1] and Peder A. Tyvand[2]
Guest editors

[1]Norwegian Institute for Agricultural and Environmental Research
[2]Norwegian University of Life Sciences

IDŐJÁRÁS

Quarterly Journal of the Hungarian Meteorological Service
Vol. 111, No. 2–3, April–September 2007, pp. 79–89

Discussing a web-based system for administration, evaluation, and correction of meteorological and biological data in a perspective of actor-network theory

Tor Håkon Sivertsen[1] and Janis Gailis[2]

[1]*Norwegian Institute for Agricultural and Environmental Research, Høgskoleveien 7, N-1432 Ås, Norway; E-mail: thsivert@online.no*

[2]*Agder University College, Service Box 422, N-4604 Kristansand, Norway; E-mail: janis.gailis@hia.no*

(Manuscript received in final form January 29, 2007)

Abstract—The history of a web-based system for administrating data from a network of agrometeorological stations is shortly presented, and the module of this system containing the documentation of the instruments in this network is discussed in detail. The quality concept of meteorological data is the starting point for this discussion. The way of coupling the instruments and parameters on each meteorological station is shown, as well as the use of this information by controlling and correcting meteorological data.

Ideas of actor-network theory are discussed connected to the future challenges of data integration and use of data from different sources in applications.

Key-words: meteorological data, instruments, controlling data, documentation system, correcting meteorological data, actor-network theory

1. Introduction

The agrometeorological service of Norway is the owner of a network of agrometeorological stations, and during the growing season of 2006 the number of stations was 80. In 1998 and 1999 a web-based system for administration of this network of stations was developed, and this system was used operationally from May 2000 until March 2006. Documentation of the system, both the technical as well as theoretical parts, was published in an internal report at the Plant Protection Centre of The Norwegian Crop Research Institute in November 2002 (*Sivertsen* and *Gailis,* 2002), in Norwegian. The development of the software was based on ideas on object oriented analysis of the operational use of the results, put up by (*Brown,* 1997).

In January 2005 a description of the main theoretical elements of the system was published together with several ideas for refinement of the system to include methods for making measurements of meteorological parameters (networks of meteorological stations, weather radars, etc., as well as output from different models, meteorological prognoses on different spatial and temporal scales) (*Sivertsen,* 2005a).

Ideas for extending this system to include biological data, both long time series of measurements and model calculations were published in 2005 (*Sivertsen*, 2005b), together with technical information on constructing the most important tables of the database.

This system for administrating the stations contain a documentation system for meteorological parameters (*Sivertsen,* 2004, 2005a, c and d), and a documentation of instruments giving unique identification of each instrument at every station. In Section 2 the documentation of instruments, as well as the way the instruments and parameters are coupled, are described. The coupling of instrumentation and parameters is used for controlling the values of the meteorological parameters. Furthermore, routines for automated corrections of meteorological data, connected to the specific types of instruments is a part of this system.

The responsibility of the agrometeorological service of the Norwegian Institute for Agricultural and Environmental Research is to run the network of agrometeorological stations as well as to gather, store, control, and use meteorological and biological data originated from the stations and other sources to be used in applications for plant protection (for tactical and strategical decisions) and in research purposes on agricultural and environmental issues. Important future challenges are connected to the integration and use of data from different sources in an intelligent and optimal manner (*Sivertsen,* 2006).

A few elements of actor-network theory (*Latour*, 2005) are discussed in this paper. The ideas of this theory may be applied in inquiry of the exchange of data and applications on the internet by a heterogenous system of actors. Norwegian Institute for Agricultural and Environmental Research ought to act in this heterorgeneous world wide network according to the responsibility of the organization. When the institute is gathering data and information, this ought to be done according to an evaluation of what is needed for each specific task. The organization may demand specific quality on the data gathered and only use the data according to the known quality level of the data. When submitting data to other organizations and to the public, the Norwegian Institute for Agricultural and Environmental Research may explicitely document the quality and scope of these data. The institute may suggest in which context the information should be used and in which context the information should not be used.

Specifically, the Norwegian Institute for Agricultural and Environmental Research has been be engaged in standarazing formats for exchange of meteorological and biological data (*Sivertsen,* 2005c; *Mestre,* 2006). Such work is a task logically connected to the responsibility of the organization.

2. Connecting measurable quantities to the scientific principle

2.1. The concept of a parameter and the quality of data

When any physical, meteorological, or biological phenomenon is described by attaching quantitative attributes to it, this is called 'parameterization' in this paper (*Sivertsen*, 2004, 2005c and e). The main attributes of documenting measured parameters and parameters of models are given in the following manner (*Sivertsen*, 2005a and b) and (*Mestre*, 2006):

Measured parameters:

Name of the parameter
Unit
Definition
Method(s) for measuring the parameter
Representativeness for certain phenomena (models).

Parameters in models:

Name of the parameter
Unit
Definition of the parameter
Representativeness for certain phenomena in other models.

The term quality is derived from the Latin word 'qualitas' meaning the nature (good or bad), properties, or condition of something. If we know the nature and sources of meteorological and biological data, the value of the data is known.

The quality of the meteorological data may in a very short manner be described in this way (*Sivertsen,* 2005b):

(a) Connection of the data to the objects of nature (*Sivertsen,* 2005d);
(b) Properties, conditions, and quantitative values of the data, including completeness and representativeness;
(c) Identity of the data that is linked to the social system producing the data (giving the data authority);
(d) Availability of the data; and
(e) Presentation and use of the data including the context of the presentation.

The meteorological data of interest for the use in models, etc., of course are the numerical values of the parameters. Nevertheless, for discussions connected to the scope of the model systems, contained in the interpretation of the scientific principle given in *Fig. 1* (*Sivertsen*, 2005e), the knowledge of the definition of the parameters, technical details of the measurements, and other attributes of the metadata are of interest. Thus, the points (a), (b), and (c) above connected to the quality of the data are of relevance for the discussion in this paper.

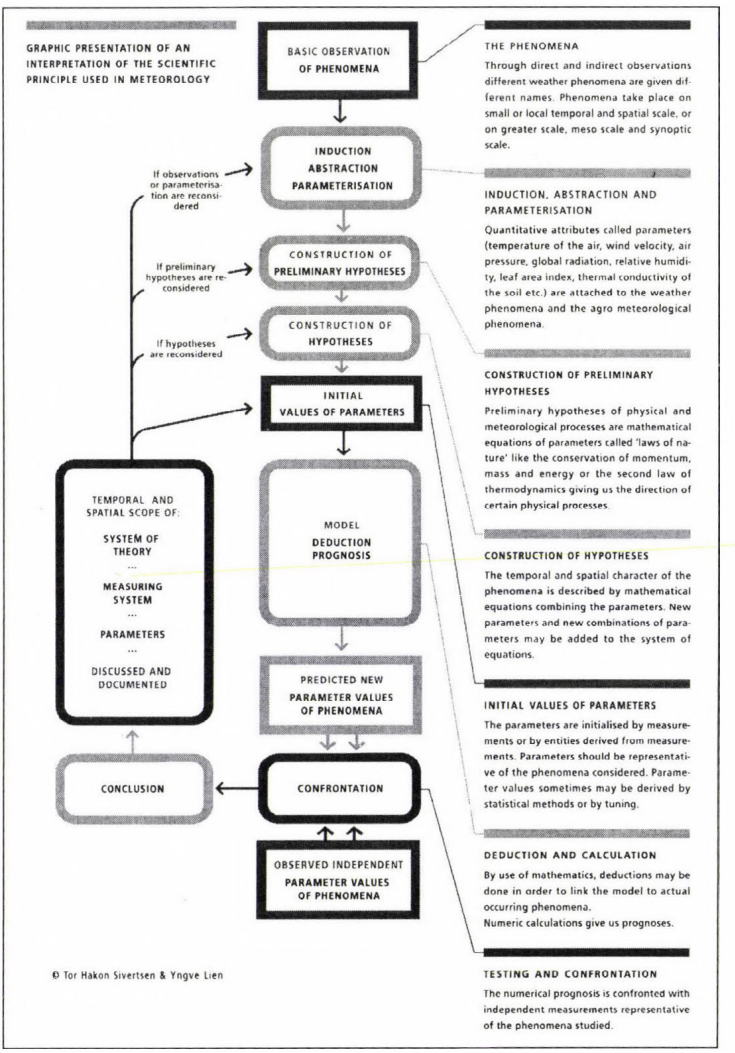

Fig. 1. Graphical representation of an interpretation of the scientific principle.

2.2. Documentation of the instruments

The instruments are documented in a hierarchy, and the four levels in this hierarchy have got the following names: (a) InstrumentType: the type name used by the producer of the instrumen, (b) SensorType: type of sensors connected to each type of instrument, (c) SensorGroupType: defined group of sensors connected to a certain type of instrument, and it may consist of only one type of sensor, (d) SensorGroup: the actual group of sensors connected to a type of instrument and a certain logger. This group of sensors (one sensor or several sensors) is used to measure one or several parameter values.

The highest level is the InstrumentType. This is a rather short description of the types of instruments used in the web-system. The instrument type is defined as the production name used by the company producing the instrument. Also the name of the producer, the country of the producing company, and a short description of the instrument are given as attributes in this table.

The second highest level is the SensorType. This level contains description of the different types of sensors connected to a certain type of instrument. An important part of the description, and the key of the table, is a short name, a symbolic name, constructed to give a very short description of the physical principle of the sensor. Here is a list of some short names used (the type of instrument and the producer's name are also given to clarify the system):

PHEV (photo electric vane) WAV15, Vaisala Oy, Finland

P2 (Pt 100) MP-100, Rotronic AG, Germany

CP (sensor measuring electric capacity of air) MP-100, Rotronic AG, Germany

TIPB (tipping bucket) ARG 100, Campbell Scientific, USA

P3 (Pt1000) HMP45A, Vaisala Oy, Finland

CPaa2 (sensor measuring electric capacity of air, second type) HMP45A, Vaisala Oy, Finland

TIPBH (tipping bucket, heated) ARG 100Heated, Campbell Scientific Ltd, USA

TIPBaa2 (tipping bucket, second instrumenttype) Rainmatic, Pronamic, Denmark

3CUP (3 cup anemometer) A100R, Vector Instruments, United Kingdom

3CUPH (3 cup anemometer, heated) WAA15, Vaisala Oy, Finland

3CUPHaa2 (3 cup anemometer, heated, second type) 432 Anemometer, Theodor Fiedrichs & Co, Germany

3CUPaa2 (3 cup anemometer, second type) Wind Speed Sensor 2740, Aanderaa Instrumnents, Norway.

In addition the calibration procedure of the sensor, the temperature range of usefulness, the measuring range, the precision of the measurement, if it can be used in darkness and if it is useful below 0 degrees Celsius, are given as attributes of the SensorType.

The third highest level is called SensorGroupType. This is a table of shortnames. Usually a few letters are added to the SensorType shortname or to a combination of SensorType short names to give an indication of which meteorological parameter are most usually recorded by an actual instrument with this SensorGroupType.

Below a few examples are presented:

ALBSN (measuring 'albedo') consists of the sensor types TCUPaa4 and TCDO

GRPHDD (measuring 'global radiation') consists of the sensor type PHDD

GRTCUP (measuring 'global radiation') consists of the sensor type TCUP

LWARTL (measuring 'leaf wetness') consists of the sensor type ARTL

PBUSTRI (measuring 'precipitation') consists of the sensor type BUSTRI

TP2 (measuring 'the temperature of the air') consists of the sensor type P2.

The lowest level in the description and classification of the instruments is the SensorGroup, which is a unique registration of one particular group of sensor on one particular logger. Most of the loggers are permanently placed on a certain site. We, therefore, always add three unique letters to the 'SensorGroupType' short name to tell at which site the 'SensorGroup' is placed.

An example is given below:

GRTCUPUDN is the SensorGroup measuring global radiation on the logger number 14 placed at Udnes.

In the case of certain SensorGroups, for example sensor groups measuring the temperature of the soil in different depths, the name of the sensor group also indicates in which depth the instrument is placed.

Two examples are given below:

JT10TTHERMUDN is the SensorGroup belonging to the SensorGroupType TTHERM measuring soil temperature in 10 cm depth on the logger number 14 at Udnes.

JT20TTHERMUDN is the SensorGroup belonging to the SensorGroupType TTHERM measuring soil temperature in 20 cm depth on the logger number 14 at Udnes.

2.3. Coupling of instruments and parameters

Through a user interface the different meteorological parameters may be coupled to the SensorGroups defined on each logger, and each parameter is also defined by a shortname:

One example:

The SensorGroup TP2UDN is connected to four parameters:

TM: The hourly mean air temperature 2m above the soil surface.

TN: The hourly minimum air temperature 2m above the soil surface.

TX: The hourly maximum air temperature 2m above the soil surface.

TT: The instantaneous air temperature 2m above the soil surface in the end of the hourly interval considered.

2.4. Data controlling and correction

One special feature of the system is the development and implementation of the unique characteristics and naming of each instrument at every station, and the unique coupling of the instrument, denoted to a SensorGroup, to every parameter measured at the station. Six different types of tests and corrections exist:

R-test: This range test of parameter values is often connected to the climate at the different sites.

J-test: Jump test (this is a temporal test comparing the values of a parameter at one recorded measurement and the previous recorded measurement (usually connected to climate and season of the year).

L-test: Consistency test connected to the parameters of one single SensorGroup. An example is testing the logical consistency of four hourly values of air temperature, TM (average temperature), TN (minimum temperature), TX (maximum temperature), and TT (temperature measured in the last minute of the hour).

LT-test: Consistency test connected to the parameters of two different SensorGroups. An example is comparing leaf wetness duration, BT, and precipitation, RR. Two different sensors are used. When it is raining, the sensor for measuring leaf wetness shall indicate leaf wetness.

CI-correction: This is an automated test of the parameters of one SensorGroup, followed by an automated correction, specific for the unique SensorGroupType in question. An example is correcting different types of gauge for measuring precipitation, using different physical principles. The sensors, using the tipping bucket system, are existing functions only in the warm season with no snow or

other types of hydrometeors precipitating from the clouds. These instruments normally need no corrections. At several sites the GEONOR instrument, using the principle of weigthing the snow or rain that is falling, is used. This instrument is functioning at all seasons, but the outcome will also have spurious small positive and negative values that ought to be corrected.

CTI-correction: This is an automated test of the parameters of two different SensorGroups, where the result from one group indicates the relevance of the results from the other. An example is: If the temperature of the air is below 0 degrees Celsius, this indicates that the parameter value of precipitation from the tipping bucket-systems are not correct.

The actual R, J, L, and LT tests are not very different from the tests used at other Nordic institutions in charge of running networks of meteorological stations (*Vejen et al.,* 2002). The main difference is that in the system described above, a test is defined as a test of the functioning of a SensorGroup, using values of the parameters connected to the SensorGroup as input. The knowledge of type of instrument also makes it easy to validate the results of the tests. The construction also makes it possible to implement the corrections named CI and CTI relatively easy.

3. Reflections on actor-network theory

The information system for administration of meteorological data, discussed in this paper was developed according to traditional (mainly object-oriented) methodologies (*Brown,* 1997). The whole concept is confined to the responsibility of the institute and the possible use of meteorological and biological models and data on the field of plant protection in the commercial agriculture of Norway.

Information technology provides an arena for network building in the global sense. The cooperation in such networks is essential for innovation. According to actor-network theory, the society consists of networks of heteorogeneous actors, both human and non-human. "Agents, texts, devices, architectures are all generated in forming part of, and are essential to, the network of the social" (*Law,* 1992).

In the Wikipedia one can read: "Actor-network theory is useful in exploration of why technologies, scientific theories, and/or social endeavours succeed or fail as the direct result of changes in their network integrity, in such an analysis the technologies or theory is positioned as token."

The network of agrometeorological stations considered and the data produced by using the measurements are fully financed by the Norwegian Ministry of Agriculture and Food. The Norwegian Institute for Agricultural and Environmental Research may be considered one of the most important

stakeholders of this system for managing and producing information beneficial for the Norwegian society. To a certain measure, stakeholders want to keep a network punctualized, where punctualization means that when a problem or issue is presented, the answer should be given inside the actual frame of the question. If the system is de-punctualized, the result may end in conflicts because stakeholders are loosing control. But a stakeholder do not have to define himself as a controlling agency. He mereiy may try to keep order in his relations in the processes of bringing up the problems and solving the problems, also through mobilisation of allies. But never the less it is in fact very difficult in the long run to act with integrity for any stakeholder. Integrity can not be retained without compassionate understanding of all the different relations.

4. Future challenges on integration of meteorological and biological data

When designing a system for administration of meteorological and biological data in the future, the requirements ought to be evaluated and presented by the Norwegian Institute for Agricultural and Environmental Research. The challenges seems to be the ability of creating a flexible and extendable system for administrating the data, containing the possibility of integrating, and utilizing data from different sources. In order to assure effective retrieval of data, cooperation with other organizations nationally and on the international level have to be organized. The processes/tasks of exchange of data from different sources as well as exchange of applications have to be organized through cooperation. The scientific and practical scope of the system may be discussed, also by allowing conceptual discussions.

Also the Norwegian Institute for Agricultural and Environmental Research may organize its own controlling system of data and document, the quality of the data produced by this organization, and the institute may make demands on the quality of the data produced by other organizations to define the usefulness of data from any source.

The exchange of meteorological data is formalized and may be further formalized through defining and using standardized schemes for exchange (*Sivertsen,* 2005e).

5. Conclusions

A documenting system of instruments may be used as a very effective feed back to the part of the organization in charge of the technical maintenance of the instrumentation.

Furthermore, meteorological data from agrometeorological networks of stations is used in many different meteorological and biological models. The

models are often used for practical decisions, and they normally need correct and complete time series of data. Documenting the data is then a tool for deciding the scope of the use of the data. So, the first step is to construct a system telling the status of the data in the database. The next step is to construct relevant sets of data for each model when specific data from the systems for making measurement is lacking. The system described in this paper is mainly a presentation of how incorrect or questionable data may be indicated. A few additional corrections specific for certain types of instruments may be relatively easily implemented by using the system.

The further steps of constructing complete time series when data is lacking may be organized in two somewhat different ways. One way of doing this is that the people in charge of running a model is asking the people in charge of producing the data to deliver them complete time series of data. Another way of constructing complete time series is that the model-people themselves make the corrections of the input data. The second way is often the most practical one, and probably the input part of each model ought to contain a module containing corrections of the input data (or alternative data is used when data is lacking).

The responsibility of the agrometeorological service of the Norwegian Institute for Agricultural and Environmental Research is to manage a network of agrometeorological stations as well as gathering, storing, controlling, and using data from the stations and from other sources to be used in applications for plant protection and research purposes. Important future challenges are connected to the integration and use of data from different sources in an intelligent and optimal manner.

References

Brown, D., 1997: *An Introduction to Object/Oriented Analysis.* John Wiley & Sons Inc., 700 pp.

Latour, B., 2005: *Resembling the Social. An introduction to Actor-Network Theory.* Oxford University Press Inc., New York.

Law, J., 1992: Notes on the theory of the actor-network: Ordering, strategy and heterogeneity. In *Systemic Practice and Action Research.* Springer, Netherlands, 379-393.

Mestre, A., 2006: Meteorological Information as input in agrometeorological models; analysis of the potential use of data from numerical weather models in agrometeorology. In COST ACTION 718 *Meteorological Applications for Agriculture* (eds.: *G. Maracchi, A. Mestre, L. Toulios, L. Kajfez-Bogataj*, and *A.A. Hocevar*). COST OFFICE, 2006.

Sivertsen, T.H., 2004: Invitation to Conceptual Discussions Concerning the Scope of the Scientific Method and Classification Systems of Meteorological Phenomena and Meteorological Parameters, Selected Papers of the International Conference "Fluxes and Structures in Fluids". St. Petersburg, Russia, June 23-26, 2003. Moscow. IPM RAS. 2004, 6 p.

Sivertsen, T.H., 2005a: Discussing the scientific method and a documentation systems of meteorological and biological parameters, Physics and Chemistry of the Earth Special Issue: *Agrometeorology*, 2003, *30* (1-3), 35-43.

Sivertsen, T.H., 2005b: Implementation of a General Documentation System for web-based administration and use of historical series of meteorological and biological data, Physics and Chemistry of the Earth Special Issue: *Agrometeorology*, 2003, *30* (1-3), 217-222.

Sivertsen, T.H., 2005c: Discussing scientific methods and the quality of meteorological data. In *Use and Availability of Meteorological Information from Different Sources as Input in Agrometeorological Models.* COST ACTIONS 718, *Meteorological Applications for Agriculture* (eds.: *G. Maracchi, A. Mestre, L. Toulios,* and *B. Gozzin).*

Sivertsen, T.H., 2005d: The Concept of Leaf Wetness used in Agro Meteorology. In *Leaf Wetness Duration: Analysis of the Agrometeorological requirements and Evaluation of New Estimation Methods*. COST ACTIONS 718 *Meteorological Applications for Agriculture* (eds.: *G. Maracchi, L. Kajfez Bogataj, S. Orlandini, A. Dalla Marta,* and *F. Rossi*).

Sivertsen, T.H., 2005e: *Reflections on the Theme of Classifying.* Documenting and Exchanging Meteorological Data. *Atmospheric Science Letters.* John Wiley & Sons.

Sivertsen, T.H., 2006: Quality considerations on meteorological parameters to be used for modelling UV-radiation. Proceedings from the session *Remote Sensing of Clouds and the Atmosphere.* Arranged by The International Society for Optical Engineering (SPIE), Stockholm, September 2006.

Sivertsen, T.H. and *Gailis, J.*, 2002: Weather data project containing: Complete list of documents, attachments and references in the documentation. The vision and requirements of the project. System architecture document. Glossary and Diary for the documentation. Internal Report of The Plant Protection Centre of The Norwegian Crop Research Institute (in Norwegian).

Vejen, F., Jacobsson, C., Fredrikson, U., Moe, M., Andersen, L., Hellsten, E., Rissanen, P., Pálsdottir, T., and *Arason, T.*, 2002: Quality Control of Meteorological Observations. Automatic Methods used in the Nordic Countries. *Report 8,* 2002, The Norwegian Meteorological Institute.

IDŐJÁRÁS

Quarterly Journal of the Hungarian Meteorological Service
Vol. 111, No. 2–3, April–September 2007, pp. 91–99

Use of crop development models in agroclimatic mapping

Arne Oddvar Skjelvåg[1*], Ole Einar Tveito[2] and Inge Bjørdal[3]

[1]*Department of Plant and Environmental Sciences, Norwegian University of Life Sciences, P.O. Box 5003, N-1432 Ås, Norway; E-mail: arne.skjelvag@umb.no*

[2]*Norwegian Meteorological Institute, P.O. Box 43 Blindern, N-0313 Oslo, Norway; E-mail: ole.einar.tveito@met.no*

[3]*The Norwegian Forest and Landscape Institute, P.O. Box 115, N-1430 Ås, Norway; E-mail: inge.bjordal@skogoglandskap.no*

(Manuscript received in final form January 31, 2007)

Abstract—An example is given from a pilot project on a coherent application of soil and weather data to produce crop security estimates of barley. GIS was used to interpolate daily weather elements from a network of weather stations to individually mapped soil type units, on average less than 1 ha, of arable land. Other model tools are: a soil moisture model to estimate soil drying from the day of snow thaw until sowing date, temperature sum functions to estimate daily advance in phenological development to emergence, heading, and yellow ripeness, and thereafter, a grain moisture model for logging of combine harvesting days, taking also daily precipitation into account. The outcome is probability estimates of getting at least a given number of combining options within a given calendar day.

Key-words: weather, interpolation, soil types, phenology, barley, crop security

1. Introduction

Agroclimatic mapping has mostly defined and classified agroclimatic zones that differ in climatic conditions for crop production (*Mischenko,* 1984). Simple temperature indices have often been used as the sole parameter to characterize climatic conditions for agriculture in general, or for specific crops or cropping systems (*Samnordisk planteforedling,* 1992). However, a modern approach should be such designed that it is agronomically meaningful, which implies the use of more weather elements and terms such as yield level and crop security.

* Corresponding author

Hutchinson et al. (1992) have briefly reviewed the development of zonation for large area mapping purposes as related to plant growth for all the time since Köppen's attempt by use of monthly temperature and precipitation records until the recent use of simple crop growth models (*Köppen*, 1900). An early Nordic example on use of a crop growth model is the geographical distribution of first cut hay yield estimates in Sweden (*Angus et al.*, 1980).

Soil and climatic data have been combined with crop growth models for estimation of production potential on a large scale (e.g., *Netherlands Scientific Council*, 1992). During recent decades there has been a great development in geographical information systems (GIS), and new options have appeared in coherent application of both soil and weather data. Soil inventory data are now easily available on electronic media, at least for parts of the arable land. Weather records have got a much more adaptable application through new interpolation techniques that allow for making weather estimates to any location surrounded by more or less distant weather stations (*Tveito* and *Førland*, 1999; *Tveito* and *Schöner*, 2002). Soil and weather make up the natural resource base for crop production. Thus, by using such data in crop growth and development models, a detailed map of crop performance may be produced. The objective of this work has been to demonstrate the feasibility of such an approach reported in detail by *Aune et al.* (2004).

2. *Materials and methods*

The procedure followed in the present project, located in two Norwegian municipalities, Inderøy and Steinkjer, at about 64°N 11.5°E, is as follows: The cultivated land, altogether ca. 21 kha, was mapped into homogeneous soil type area units according to *FAO* (1998). There was a wide range of soil types from coarse sand to clays and organic soils, as indicated in *Fig. 1* by soil moisture capacity of the top soil. Each of these approximately 31,000 units in the entire study area (*Fig. 2*) was defined by midpoint geographical coordinates and altitude, using a digital terrain model.

Daily weather records for the years 1991 to 2000 were interpolated to each individual soil type area unit according to *Tveito et al.* (2005). Thus, temperature was spatially interpolated by residual kriging after application of covariables as terrain, longitude, and latitude. Wind speed, air humidity, and snow depth were dealt with by inverse distance weighting. Precipitation was interpolated by triangulation with terrain adjustment. After interpolation daily potential evapotranspiration was calculated for each unit by the Penman II method (*Shaw*, 1983). A network of 98 Norwegian weather stations located from 62.5 to 66°N, were applied as basis for the interpolation of global radiation and the mentioned parameters. Most of the stations (77) only observe precipitation and snow cover.

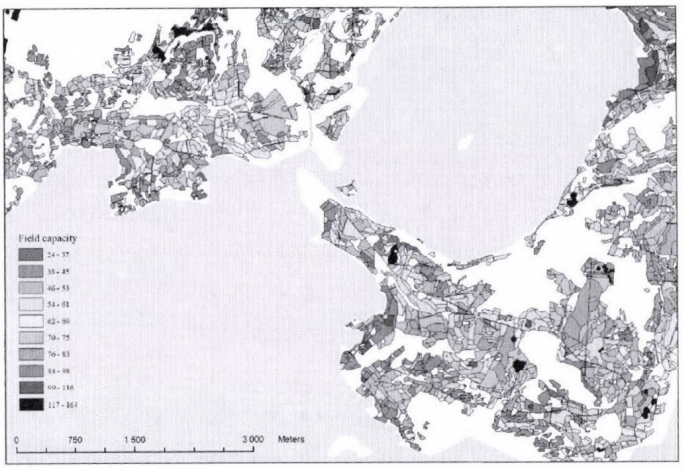

Fig. 1. Field capacity in mm of water of the 20 cm topsoil at soil type area units, on arable land northwest and southeast to the Straumen area of the Inderøy community.

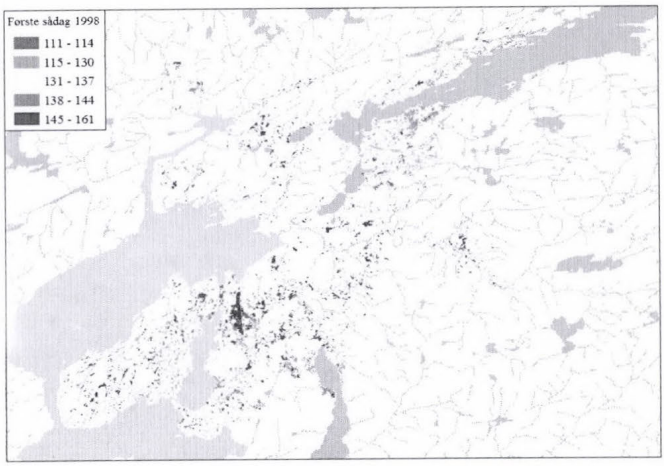

Fig. 2. First possible sowing date in 1998 on soil type area units covering all arable land in the Inderøy and Steinkjer communities. Day numbers of the year: 121 = May 1, 152 = June 1.

For each soil type area unit of the cultivated land, the first possible sowing date was determined on the basis of interpolated snow thaw time. Soil moisture at the first observed day of snowless ground was set to field capacity. Subsequently, estimates of top soil drying were made by the model of *Ritchie* (1972) until the required soil dryness for sowing day was met (*Skjelvåg,* 1986).

The daily advance in phenological development, (dP_i), was calculated by the formula

$$dP_i = (t_i - t_b)/ts_j, \qquad j = 1,2,3, \tag{1}$$

where t_i is the diurnal mean temperature, t_b is the base temperature, ts_j is the temperature sum, i is the number of days, and j is the number of phases. The formula is used with parameter values from the paper of *Bleken* (2001) when $t_i \geq t_b$, from sowing to emergence, further to heading, and in the third phase to yellow ripeness (40% grain moisture content) of 'Bamse' barley. Base temperatures were –1.57, –3.17, and 4.89 °C, and temperature sums were: 139, 685, and 383 °C of the three phases, respectively.

From yellow ripeness on, the daily calculations of grain moisture content was conducted by the model of *Stewart* and *Lievers* (1978), with coefficients and constants adjusted to 'Bamse' barley under Norwegian conditions (*Govasmark,* 2000). The driving variables are the potential evapotranspiration and precipitation.

Conditions for combine harvesting were evaluated daily from yellow ripeness until the end of the month of October for every individual soil type area unit. The requirement for being logged as a possible day for combining was an estimated grain moisture content less than or equal to a specified level starting at 20% on August 1, gradually increasing to 43% on October 1. Later it was increased to 45% on October 15 and kept at that level to the end of the month (*Aune et al.,* 2004). Furthermore, the recorded daily precipitation should be less than or equal to 2 mm.

The final result can be presented in various frequency statistics of number of possible days for combine harvesting of barley within certain dates. By defining requirements for number of combine harvesting days within given calendar time, one may calculate the probabilities to meet the specified performance for successful cropping at individual soil type area units.

3. Results

In addition to the snow cover observation and drying of the soil, sowing date is much determined by the soil moisture capacity of each soil type area unit. Within a small geographical area, the amount of soil moisture to be evaporated before sowing may vary considerably (*Fig. 1*). In this detailed segment there is a variation in field capacity of the 20 cm topsoil from about 25 mm of water to the sixfold of that.

As an example from the year 1998, three large and time spaced rainfalls interrupted soil drying and spring work. The combination of this with time of snow thaw and soil moisture capacity created a variation in the first possible

sowing day of about seven weeks from the April 24 to June 10 (*Fig. 2*). In this marginal area of grain production, the latter is considered close to the last possible sowing day of an early barley cultivar to reach maturity in an average growing season.

In the other end of the growing season, number of days suitable for combine harvesting of the barley crop varied considerably. Within the end of September and on average of ten years, the range of threshing options varied from a couple of days to more than two weeks (*Fig. 3*).

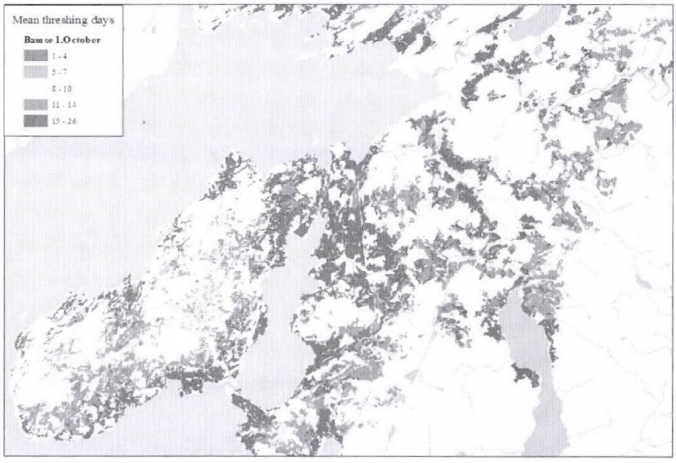

Fig. 3. Mean number of days with combine harvesting options within October 1 during the years 1991–2000 for 'Bamse' barley, at soil type area units in the Inderøy community and partly that of Steinkjer.

As may be seen from *Fig. 3*, much of the variation in number of calculated combining days is related to the distance from the sea. This is confirmed by *Fig. 4*, which shows a declining barley crop security with altitude. Up to 50 m a.s.l. on most of the soil type area units, one could expect six or seven years out of ten with at least five days with combining conditions within mid September. Very few area units came to eight, nine, and even ten years out of ten, whilst more units, though relatively few, reached only five, four, and three years. A large part of the arable land in the two communities is situated between 50 and 100 m a.s.l. (*Fig. 4*). In this altitudinal interval the distribution of soil type area units with varying crop security had a lower kurtosis, i.e., less peakish, than in the interval closer to sea level. The majority of field units could meet the requirement in four, five, or six years out of ten. However, equal numbers of area units fell under the classes three or seven years, and area units towards both ends of the entire range from nil to ten years were found.

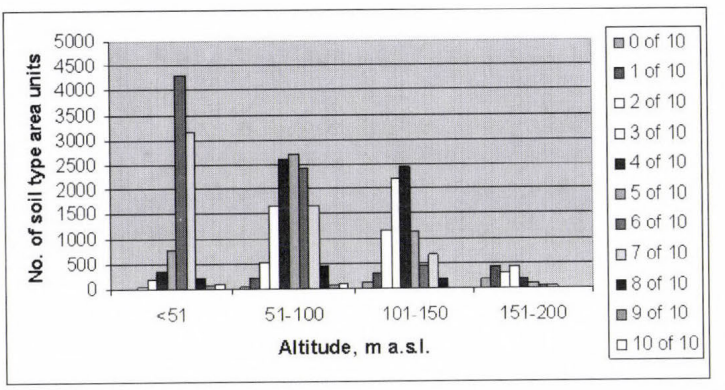

Fig. 4. Number of soil type area units with more than four combine harvesting options within September 15, in none to all years out of ten (1991–2000), in four altitudinal intervals.

In the interval 101 to 150 m a.s.l., the distribution of soil type area units was much similar to that of the interval below, but more than half of the number of field units fell into the categories in three and four years out of ten, and a clear majority in two to five. This shows the gradual decline in crop security with rising altitude. The picture is completed by proceeding to the higher elevation interval of 151–200 m a.s.l. In that height, most of the arable land could exhibit a probability that met the specified requirement in only one to three out of ten years.

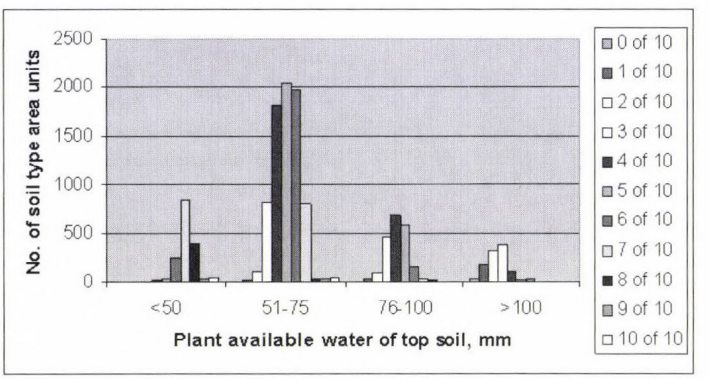

Fig. 5. Number of soil type area units in the altitude interval 51 to 100 m a.s.l., grouped according to intervals of topsoil moisture capacity, and their estimated classing with the requirement of more than 4 days suitable for combine harvesting within September 15, in none to all years during the period 1991–2000.

A certain part of the variation within altitude intervals in *Fig. 4* was due to differences in soil moisture capacity of the topsoil, and its implication for soil drying in spring. This is illustrated in *Fig. 2* with respect to sowing date. *Fig. 5* shows how an increasing soil moisture capacity of the topsoil was related to a declining ability to meet the requirement of at least five days of combine harvesting options within mid September. The median crop security classification of the four intervals of soil moisture capacity fell in class seven, five, four, and barely into three out of ten years, respectively.

4. Discussion

It is outside the scope of this short presentation to repeat a full discussion of methods, results, and possible applications as given by *Aune et al.* (2004) and *Tveito et al.* (2005). A coherent use of a series of disciplines creates many interfaces and needs for mutual adjustments, and only a few points may be emphasized. The approach depicts both the great annual variation in crop performance and also that originating from the interaction between soil type and weather.

Regional variation was included by use of the digital terrain model and the interpolation of weather elements. GIS has facilitated the use of all weather parameters and not only the simplest one, the temperature. However, the interpolation procedures have not yet included local effects of aspect, cold air drains, vicinity to open water, etc. The results are, therefore, more valid for somewhat larger areas than the individual soil type area units, and averages over larger areas, for instance altitude intervals, can easily be computed. Also on the agronomic side there are challenges. The sowing day estimates still lack a record of soil frost. Soil moisture capacity was calculated according to *Riley* (1996) on the basis of soil texture and content of organic matter. The functions are considered to be less precise for soils with a high content of organic matter. Sowing day is in practice dependent also on machine capacity, and all sowing can not be made on the very first day. The use of the same relative moisture level required for sowing day dryness of all soil types, is probably not optimal. On organic soils sowing may take place even with frost in deeper soil layers. In a rainy spring, when approaching the deadline for successful sowing time, farmers are expected to sow on a wetter soil than else preferred. Most of the various meteorological and agronomic shortcomings may be remedied, either by incorporating additional submodels or by strictly defining the preconditions specified for the calculations.

The phenological functions are considered to be fairly correct, and the same may be said about the grain moisture model. The logging of days suitable for combine harvesting needs improvement. Firstly, precipitation less than or equal to 2 mm is now recorded as a 24 h rainfall. It is very decisive, whether the

rain has fallen during the day or during the night. This may be improved by using more detailed rainfall records. Secondly, the requirement for grain moisture content at various times during the autumn is very differently evaluated by farmers. The required level of grain moisture should rather be strictly defined and given as a precondition for the calculations. However, for special use, the flexibility of the model tool easily opens for runs with various choices. Furthermore, inclusion of additional subroutines to remedy more of the mentioned shortcomings is fairly simple.

5. Conclusions

The combined use of GIS techniques with access to weather and soil data makes it possible to quantify the natural basis for crop production in agronomically meaningful terms. The key instruments to reach such a goal are models at a suitable resolution level of soil moisture conditions and crop growth and development. As field crop production is continuously subjected to the vagaries of weather, probabilities for crop failure or success are useful characteristics of conditions for plant production. The basis for the present probability estimates has been: (1) a wide range in soil conditions over numerous area sites within a geographically small area, (2) site specific interpolated weather estimates, and (3) the above mentioned model tools. Probability estimates of this or similar types may find applications in public administration, advisory service in agriculture and management of natural resources, and in research and development.

References

Angus, J.F., Kornher, A., and *Torssell, B.W.R.,* 1980: A systems approach to Estimation of Swedish ley production. *Progress report* 1979/80. *Report 85.* Department of Plant Husbandry, Swedish University of Agricultural Sciences, 29 pp.

Aune, B., Aurbakken, E.A., Bjørdal, I., Tveito, O.E., and *Skjelvåg, A.O.,* 2004: *Project Soil Resource Map.* Combined use of soil, climate, and plant data for quantification of production potential. Report from a working group established by NIJOS (in Norwegian). Norwegian Institute of Land Inventory. *Report No. 16/2004,* 51 pp.

Bleken, M.A., 2001: KONOR. A model for simulation of cereal growth. Documentation. Agricultural University of Norway, *Report* No. 2/220, 33 pp.

FAO, 1998: World Reference Base for Soil Resources. *World Soil Resources Reports 84.* FAO, ISRIC og ISSS, Rome, 88 pp.

Govasmark, E., 2000: Modeling of grain moisture content in barley after yellow ripeness (in Norwegian). *MSc Thesis.* Agricultural University of Norway, Department of Horticulture and Crop Sciences, 80 pp.

Hutchinson, M.F., Nix, H.A., and *McMahon, J.P.,* 1992: Climate constraints on cropping Systems. In *Field Crop Systems* (ed.: *C.J. Pearson*), *Vol. 18 of Ecosystems of the World* (ed.: *D.W. Goodall*). Elsevier, Amsterdam, pp. 37-58

Köppen, W., 1900: Versuch einer Klassifikation der Klimate, vorzugsweise nach ihren Beziehungen zur Pflanzenwelt. *Geogr. Z. 6,* 593-611 and 657-679.

Mischenko, Z.A., 1984: Agroclimatic mapping of the continents. World Meteorological Organization. Agricultural Meteorology. *CAgM Report No 2*, 109 pp.

Netherlands Scientific Council for Government Policy, 1992: Ground for choices. Four perspectives for the rural areas in the European Community. *Reports to the Government 42*, 144 pp.

Riley, H., 1996: Estimation of physical properties of cultivated soils in southeast Norway from readily available soil information. *Norw. J. Agr. Sci. Supplement 2*, 51 pp.

Ritchie, J.T., 1972: Model for predicting evaporation from a row crop with incomplete cover. *Water Resour. Res. 8*, 1204-1213.

Samnordisk planteforedling, 1992: Agroclimatic mapping of Norden (in Norwegian). *Skrifter och rapporter nr 5*, 97 pp.

Shaw, E., 1983: *Hydrology in Practice*. Van Nostrand Reinhold, Wokingham, UK. 569 pp.

Skjelvåg, A.O., 1986: Estimation of the first sowing date from weather recors (in Norwegian). *Forskning og forsøk i landbruket 37*, 295-301.

Stewart, D.W. and *Lievers, K.W.*, 1978: A simulation model for the drying and rewetting processes of wheat. *Can. Agr. Eng. 20*, 53-59.

Tveito, O.E. and *Førland, E.*, 1999: Mapping temperatures in Norway applying terrain information, geostatistics and GIS. *Norsk geografisk Tidsskrift 53*, 202-212.

Tveito, O.E. and *Schöner, W.*, 2002: Application of spatial interpolation of climatological and meteorological elements by the use of geographical information systems (GIS). *Met. no Report 28/02 KLIMA*.

Tveito, O.E., Bjørdal, I., Skjelvåg, A.O., and *Aune, B.*, 2005: A GIS-based agro-ecological decision system based on gridded climatology. *Meteorol. Appl. 12*, 57-68.

IDŐJÁRÁS
Quarterly Journal of the Hungarian Meteorological Service
Vol. 111, No. 2–3, April–September 2007, pp. 101–108

A diffusive Boussinesq plume

Peder A. Tyvand

Department of Mathematical Sciences and Technology,
Norwegian University of Life Sciences,
P.O. Box 5003, 1432 Ås, Norway; E-mail: peder.tyvand@umb.no

(Manuscript received in final form January 31, 2007)

Abstract—An axisymmetric Boussinesq plume in a uniform ambient fluid is considered. The classical similarity solution of *Morton et al.* (1956) is modified to account for diffusive losses of buoyancy flux and momentum flux. This leads to a buoyancy flux and a momentum flux that both tend to zero at infinite height. The mass flux at infinity will tend to a finite value that depends on the diffusion parameters for buoyancy and momentum.

Key-words: buoyancy, Boussinesq, diffusion, heat source, plume

1. Introduction

Plumes are relatively slender vertical flows rising above concentrated buoyancy sources. Fire disasters produce strong buoyant plumes. Plumes are important in local meteorology, especially in connection with formation of cumulus clouds. Some basic mathematical solutions for plumes can be found when a singular heat source is taken as the driving mechanism. The most important of these is the celebrated similarity solution of *Morton et al.* (1956), hereafter called the MTT solution.

The MTT solution with the Boussinesq approximation is mathematically compact. It accounts for mass balance, and it preserves momentum and energy within the plume. However, its obvious shortcoming is that it possesses no physical length scale. Any similarity solution will assume that the plume rises to infinite height. According to a similarity solution, the plume velocity will ultimately tend to zero, but the upward mass flux will increase indefinitely. In spite of its mathematical convenience, a similarity solution lacks physical consistency in that it implies an indefinite amount of mass entrainment, up to

infinite height. In reality, the entrainment of momentum from outside into the plume must vanish asymptotically at great heights, when the plume velocity slows down sufficiently. Opposing the entrainment, there will be diffusive losses of momentum and buoyancy, from the plume to the surrounding fluid. These diffusive losses introduce physical length scales in the vertical direction. A well-known example of such a length scale is the altitude of a cumulus cloud above the heated ground.

Convective flows in the atmosphere or ocean occur as recirculating convection cells. This means that a plume cannot be considered as an isolated phenomenon. All plumes in the atmosphere and ocean occur as parts of convection cells. This fact suggests another physical shortcoming of the MTT solution. It disregards the fact that a rising plume occupies only a narrow section of the convection cell that it belongs to. A narrow upwelling plume should therefore be surrounded by a broad and slow downwelling flow. However, in the course of this study it becomes clear that the present modifications of the MTT model are insufficient to construct a recirculating convection cell.

The MTT paper succeeded a seminal paper on plumes by *Batchelor* (1954), who also developed similarity solutions. After MTT a lot of papers have followed. To our knowledge, the physical validity of similarity solutions has not been addressed. A recent work by *Scase et al.* (2006) generalizes the axisymmetric MTT model in a fruitful way by starting from the basic hydrodynamic equations to take time-dependence into account.

2. *The MTT model*

We consider a rising axisymmetric plume in a fluid that would otherwise be at rest. The flow is generated by a singular heat source. The gravitational acceleration is denoted by g. The axisymmetric flow depends on the vertical coordinate z and the radial coordinate r. We define $z = 0$ by the concentrated heat source that drives the flow. We define the radial coordinate r as the horizontal distance from the vertical line through the heat source.

The classical MTT plume model assumes 'top-hat' profiles for the density $\rho(r,z)$

$$\begin{aligned} \rho(r,z) &= \rho(z), \quad r \le b(z), \\ \rho(r,z) &= \rho_\infty, \quad r > b(z), \end{aligned} \tag{1}$$

and the vertical velocity $w(r,z)$

$$\begin{aligned} w(r,z) &= w(z), \quad r \le b(z), \\ w(r,z) &= 0, \quad r > b(z). \end{aligned} \tag{2}$$

Here we have introduced the plume radius $b(z)$ and the density of the ambient fluid ρ_∞ We will consider only the simplest case, where ρ_∞ is taken constant so that the ambient fluid is assumed uniform. We take the Boussinesq approximation where density variation is included only in the buoyancy term of the momentum equation. The 'top-hat' description, Eqs. (1)–(2), assumes that the plume radius $b(z)$ can be sharply defined at each height z. Moreover, it replaces the density and velocity fields within the plume by their average values taken over the plume cross section at each given height z. In the MTT solution, the only communication with the fluid outside the plume is the entrainment of fluid by turbulent mixing into the plume. It is assumed that no loss of momentum or energy from the plume to the surrounding fluid will take place.

The entrainment constant α is introduced by the standard entrainment assumption

$$u_r\big|_{r=b(z)} = \alpha w, \tag{3}$$

where u_r is the inward radial velocity of the surrounding fluid at the boundary of the plume. This radial entrainment velocity u_r is thus assumed to be proportional to the vertical velocity in the plume at each vertical level z. In this theory, the radial velocity is significant only at the plume boundary. Once the entrained fluid has entered the plume, it is assumed to be thoroughly mixed so that the net average flow becomes vertical. In this averaging procedure one cannot include continuity in radial velocity across the plume boundary.

We introduce the mass flux πQ, the momentum flux πM, and the buoyancy flux πF for the steady plume. By definition we have

$$Q = b(z)^2 w(z)\rho(z), \tag{4}$$

$$M = b(z)^2 w(z)^2 \rho(z), \tag{5}$$

$$F = b(z)^2 w(z) g(\rho_\infty - \rho(z)). \tag{6}$$

This implies the relationships

$$w = M/Q,\ \ \rho = \rho_\infty gQ/(gQ+F),\ \ b = Q/\sqrt{M\rho},\ \ g' = g(\rho_\infty - \rho)/\rho = F/Q. \tag{7}$$

Here we have introduced the 'reduced gravity' g'. The conservation of mass, momentum, and energy in a steady plume is expressed by the equations

$$dQ/dz = 2\alpha\sqrt{\rho_\infty M}, \tag{8}$$

$$dM/dz = QF/M, \tag{9}$$

$$F = F_0 = constant, \tag{10}$$

respectively.

3. *Diffusive losses of buoyancy and momentum*

Since the buoyancy flux F_0 is constant in the MTT model described above, it parameterizes the singular hot spot in the origin. The energy equation is simply F = constant for a steady plume in homogeneous ambient fluid. Let us take into account a turbulent diffusive loss of energy by postulating the relationship

$$F(z) = F_0 \exp(-\gamma z), \tag{11}$$

where F_0 remains the buoyancy flux specified by the MTT solution, and a spatial decay parameter γ is introduced, assumed to be constant. With this modification, F_0 still parameterizes the hot spot in the origin. The energy equation that is implicitly assumed by the solution, Eq. (11) is

$$dF / dz = -\gamma F, \tag{12}$$

replacing the previous energy conservation equation dF/dz=0. The solution, Eq. (11) is a reasonable starting point, because it introduces a physical length scale $1/\gamma$. Since the MTT solution does not contain any length scale, γz immediately constitutes itself as a dimensionless vertical coordinate, which establishes a physical length scale.

A physically consistent description of a diffusive plume must also take into account a diffusive loss of momentum. We modify the momentum equation, Eq. (9) as follows

$$dM / dz = QF / M - \Gamma M, \tag{13}$$

where an additional spatial decay parameter Γ for momentum is introduced, assumed to be constant. Γ is introduced in analogy with the buoyancy decay parameter Γ introduced above. This is a simpler model of turbulent momentum loss than the averaged Navier-Stokes momentum equation with eddy viscosity. However, a Navier-Stokes equation cannot be formulated for the plume in the 'top-hat' description, since the relevant velocity gradients have already been eliminated by the averaging procedure.

We will now derive the plume solution following from the starting point of Eqs. (11) and (13). We still assume that mass is conserved within the plume, with the application of the entrainment hypothesis. We introduce dimensionless length, velocity, mass flux, momentum flux, and buoyancy flux, respectively, by the definitions

$$\hat{z} = \gamma z, \quad \hat{w} = w(\rho_\infty / (\gamma F_0))^{1/3}, \quad \hat{Q} = (\gamma^{5/3} Q) / (F_0^{1/3} \rho_\infty^{2/3}),$$
$$\hat{M} = (\gamma^{4/3} M) / (F_0^{2/3} \rho_\infty^{1/3}), \; \hat{F} = F / F_0 .$$

From now on, we work with dimensionless quantities and drop the hat superscripts. From Eqs. (8) and (13) the governing equations are

$$dQ/dz = 2\alpha\sqrt{M}, \qquad dM/dz = QF/M - \beta M, \tag{14}$$

expressing conservation of mass and a diffusive loss of momentum. Here we have introduced a dimensionless parameter β defined as

$$\beta = \Gamma/\gamma, \tag{15}$$

which may be considered as a turbulent Prandtl number, expressing the relative rate of momentum diffusion compared with buoyancy diffusion. For strong turbulence (large Reynolds numbers), it is plausible that β will be of order unity.

The postulated loss of buoyancy flux is given by

$$F(z) = \exp(-z). \tag{16}$$

In order to solve this set of governing equations we define

$$Q(z) = Q_S(z)\varphi(z), \qquad M(z) = M_S(z)\mu(z), \tag{17}$$

thereby introducing two unknown functions $\varphi(z)$ and $\mu(z)$ that represent the local relative deviations from the steady MTT solution. The MTT similarity solution is represented by $Q_S(z)$ and $M_S(z)$, given by

$$Q_S(z) = (6\alpha/5)(9\alpha/10)^{1/3} z^{5/3}, \quad M_S(z) = (9\alpha/10)^{2/3} z^{4/3}. \tag{18}$$

This is called a similarity solution since it assumes no other length scale than the vertical coordinate itself.

We will now compute the unknown functions $\varphi(z)$ and $\mu(z)$ in this diffusive plume problem. Their boundary conditions are simply

$$\varphi(0) = \mu(0) = 1, \tag{19}$$

since the solution coincides with the MTT solution near the source. The governing equations for $\varphi(z)$ and $\mu(z)$ are determined by inserting their definitions, Eq. (17) into Eq. (14). The resulting equations are

$$(3/5)z\varphi'(z) + \varphi(z) = \sqrt{\mu(z)}, \tag{20}$$

$$(3/4)z\mu'(z) + (1 + (3/4)\beta z)\mu(z) = \exp(-z)\varphi(z)/\mu(z). \tag{21}$$

Eqs. (20) and (21) valid for all $z>0$ with the spatial 'initial' conditions, Eq. (19). It is worth noting that Eqs. (20)–(21) are independent of the entrainment

constant α. The mathematical problem is thus a one-parameter problem in terms of the dimensionless momentum diffusion parameter β. The dependence of buoyancy diffusion is implicit through the definition of dimensionless variables.

This nonlinear system of two first-order Eqs. (20)–(21) will be solved numerically by MATHEMATICA. Because of the factor z accompanying the derivatives, we have to start the integration with a value of z slightly greater than 0. Some results are shown in *Fig. 1* and *2*. *Fig. 1* shows the functions $\varphi(z)$ and $\mu(z)$. *Fig. 2* gives the mass flux $Q(z)$ (upper graphs) and the momentum flux $M(z)$ (lower graphs). The case $\beta=1$ is represented by solid curves. The dotted curves represent $\beta=1/3$, while the dashed curves represent $\beta=1/3$. Since β is a kind of turbulent Prandt number, it should be of order unity.

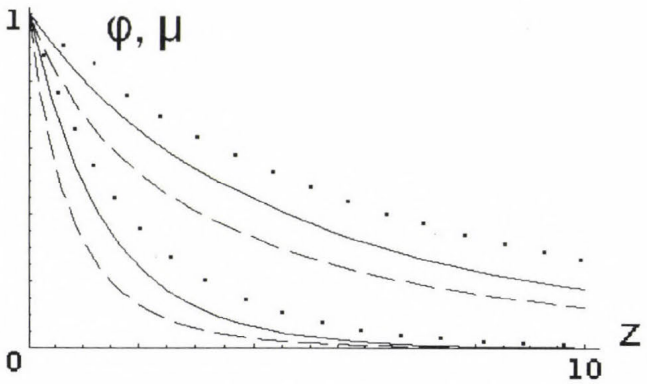

Fig. 1. The functions $\varphi(z)$ (upper curves) and $\mu(z)$ (lower curves). These functions are displayed for $\beta=1/3$ (dotted curves), $\beta=1$ (solid curves), and $\beta=3$ (dashed curves).

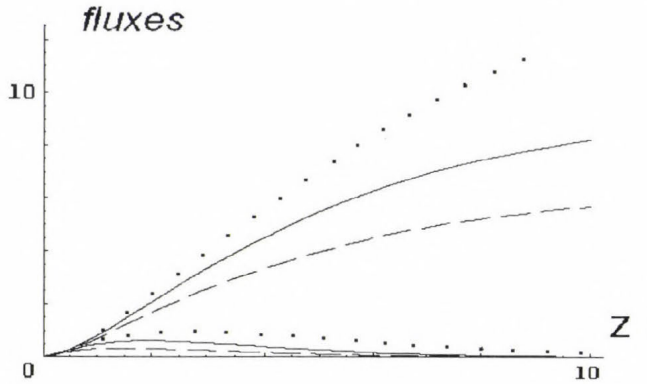

Fig. 2. The upper set of curves represent mass flux $(5/(6\ \alpha))(10/(9\ \alpha))^{1/3}Q(z)$. The lower set of curves represent momentum flux $(10/(9\ \alpha))^{2/3}M(z)$. The functions are displayed for $\beta=1/3$ (dotted curves), $\beta=1$ (solid curves), and $\beta=3$ (dashed curves).

From *Fig. 2* we see that the momentum flux $M(z)$ has a maximum value for a certain value of z, depending on β. On the other hand, there is no maximum value for the mass flux $Q(z)$. Further computations show that it increases with increasing z, and it reaches a constant asymptotic value, dependent on β when $z \to \infty$. In *Table 1* we show $Q(\infty)$ for various values of β, together with the maximal values for $M(z)$. There may be a certain amount of roundoff errors in this system where boundary conditions are specified only at $z=0$, and the numerical integrations for determining $Q(\infty)$ in *Table 1* have all been terminated at $z=50$. The present coupled system of first-order equations seems to defy analytical treatment, since the variables are not separable. *Table 1* shows that $z>1$ at the point of maximum momentum flux, even when the momentum diffusion is relatively strong. This is because the diffusive loss of momentum is compensated by the buoyancy source up to unit height above the heat source.

Table 1. The mass flux at infinite height and the maximum point for the momentum flux for various values of the dimensionless momentum diffusion parameter β

β	$(5/(6\alpha))(10/(9\alpha))^{1/3}Q(\infty)$	$(10/(9\alpha))^{2/3}M_{max}$	z at $M=M_{max}$
0.2	25.02	1.1237	3.141
0.5	12.77	0.8352	2.386
1	9.39	0.6188	1.926
2	7.34	0.4322	1.608
5	5.42	0.2523	1.356

The dimensionless expressions for the plume velocity and plume radius are

$$w(z) = (5/(6\alpha))(9\alpha/(10z))^{1/3}\,\mu(z)/\varphi(z), \tag{22}$$

$$b(z) = (6\alpha z/5)\varphi(z)/\sqrt{\mu(z)}\,. \tag{23}$$

In *Fig. 3* we show the radius of the plume as a function of the height, represented by $(5/(6\alpha))\,b(z)$, for some values of β. For comparison, the MTT solution is represented by an exact cone that gives the common tangent for these three curves at the apex in the origin.

Contrary to the motivation for this work, it proves impossible to construct an outer solution that gives a closed convection cell, since the mass flux does not tend to zero as $z \to \infty$. There is no balance between sources and sinks in the outer field, so the streamlines will not be closed curves.

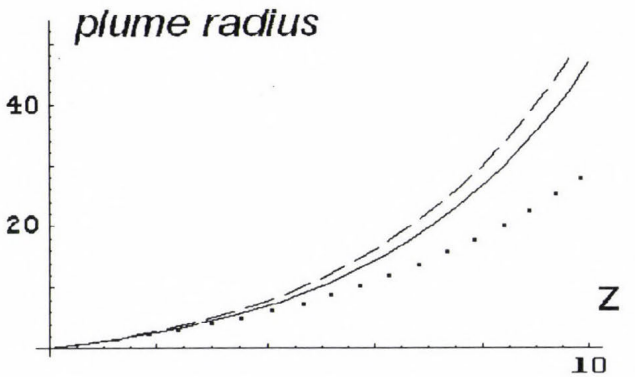

Fig. 3. The plume radius as a function of height represented by $(5/(6\ \alpha))b(z)$. It is displayed for $\beta=1/3$ (dotted curve), $\beta=1$ (solid curve), and $\beta=3$ (dashed curve).

4. Conclusions

An aim of the present work was to model consistently the inner and outer flow field of a plume. In order to achieve this, we included diffusive losses of momentum flux and buoyancy flux from the plume to the ambient fluid, which is assumed of constant density. In order to model the outer flow, it is necessary that the mass flux of the plume ultimately tends to zero with increasing height. The present work shows that this is impossible when the density of the ambient fluid is assumed to be constant. The mass flux in the plume will not tend to zero with increasing height, but it will settle at a constant value. Therefore, no recirculating convection cell can be described by the present type of modeling.

Any model of plume flow in a fluid must be irreversible in time. In the classical MTT solution, the only entropy producing mechanism is the mass entrainment into the plume. As a contrast, the present model takes into account three irreversible phenomena: (i) Turbulent entrainment from the ambient fluid, incorporated into the mass balance. (ii) Turbulent diffusive loss of momentum flux to the ambient fluid. (iii) Turbulent diffusive loss of buoyancy flux to the ambient fluid. While these three phenomena are still being modelled in a highly simplified way, their descriptions in the present work are mutually consistent.

References

Batchelor, G.K., 1954: Heat convection and buoyancy effects in fluids. *Q. J. Roy. Meteor. Soc. 80*, 339-358.

Morton, B.R., Taylor, G.I., and *Turner, J.S.*, 1956: Turbulent gravitational convection from maintained and instantaneous sources. *Proc. Roy. Soc. London A 234*, 1-32. (Herein referred to as MTT.)

Scase, M.M., Caulfield, C.P., and *Dalziel, S.B.*, 2006: Boussinesq plumes and jets with decreasing source strengths in stratified environments. *J. Fluid Mech. 563*, 463-472.

IDŐJÁRÁS

Quarterly Journal of the Hungarian Meteorological Service
Vol. 111, No. 2–3, April–September 2007, pp. 109–122

Curved free convection plume paths in porous media

Oliver J. Brambles and **D. Andrew S. Rees**

Department of Mechanical Engineering, University of Bath,
Claverton Down, Bath, BA2 7AY, U.K.; E-mail: D.A.S.Rees@bath.ac.uk

(Manuscript received in final form January 31, 2007)

Abstract—This short paper presents some numerical simulations of how free convection plumes in a porous medium are affected by the presence of a neighboring boundary or a neighboring plume. It is found that they are drawn towards a vertical boundary with the 'centreline' following a curved path from the source to the boundary. Thus the boundary entrains the plume in a manner which is reminiscent of the well-known Coandă effect in aerodynamics where a fluid jet is drawn towards a solid surface. When two plumes are present in a horizontally unbounded porous medium, the plumes are drawn towards one another before rising vertically. In many cases where one plume is weaker or lower than the other, the former is affected greatly by the latter, but not vice versa.

Key-words: porous media, free convection, plume, entrainment

1. Introduction

Free convection plumes usually rise vertically. However, this is true only in certain circumstances, namely, when the flow domain is symmetric about a vertical line through the heat source. This situation was assumed by *Afzal* (1985), where a line source of heat was placed at the intersection of two plane surfaces bounding a wedge-shaped region of porous medium, but where the boundaries are at equal but opposite inclinations away from the vertical. *Afzal* (1985) provided a detailed high order boundary layer theory to determine the manner in which such boundaries affect the strength of the plume, thereby extending the analysis of *Wooding* (1963). A more general situation was considered by *Bassom et al.* (2000), where a porous wedge was allowed to have a centreline which is no longer vertical. In this case the centreline of the plume remains straight, at least according to boundary layer theory, but it no longer remains vertical. In general, the direction of the plume is somewhere between the vertical and the direction corresponding to the centreline of the wedge, and it

is, therefore, a compromise between the effect of buoyancy (which induces vertical forces) and the need to entrain equal amounts of fluid from either side of the plume (which draws the plume towards the centreline of the wedge). *Bassom et al.* (2000) used boundary layer theory and presented an analytical expression for the direction taken by the plume in the terms of the inclinations of the bounding surfaces. Similar situations arise for anisotropic porous media (*Rees et al.*, 2002) and for clear fluids (*Rees* and *Storesletten*, 2002; *Kurdyumov*, 2006).

In the context of groundwater studies the presence of groundwater flow, together with other effects, such as heterogeneities and variable saturation, also serve to modify the path taken by contaminant plume in porous medium; see *Harter* and *Yeh* (1996a, b) for example. It is also a matter of common experience that a crosswind will modify the direction of chimney plumes. Deviations from straight path were also found by *Shaw* (1985) when considering plume flow in a cavity with an inlet and outlet at different horizontal locations.

In the present paper we consider (i) how a plume path is modified by presence of an adjacent insulated vertical surface and (ii) the merging of two plumes. This is a purely numerical study of the fully elliptic equations of motion, and it is, therefore, not a boundary layer study. Indeed, we regard this as an exploratory investigation into the behaviour which may be displayed by free convection plumes in porous media, and we intend to follow this work by a more detailed quantitative study in the near future.

As we have used a time-dependent solver to determine the eventual steady state solutions, we conclude that such plume flows are stable, at least to two-dimensional perturbations. We find that, when a localized heat source is placed away from a vertical surface, the plume curves towards the surface, and the point of attachment changes its location as the Rayleigh number varies. We also consider the interaction of two plumes, a situation which has been reviewed by *Gebhart* (1979) for plumes in clear fluids.

2. *Equations of motion and numerical scheme*

The equations governing two-dimensional convection in a porous medium are,

$$\frac{\partial \bar{u}}{\partial \bar{x}} + \frac{\partial \bar{v}}{\partial \bar{y}} = 0, \tag{1}$$

$$\bar{u} = -\frac{K}{\mu}\frac{\partial \bar{p}}{\partial \bar{x}}, \tag{2}$$

$$\bar{v} = -\frac{K}{\mu}\left[\frac{\partial \bar{p}}{\partial \bar{y}} - \rho g \beta (T - T_0)\right], \tag{3}$$

$$\sigma\frac{\partial T}{\partial \bar{t}}+\bar{u}\frac{\partial T}{\partial \bar{x}}+\bar{v}\frac{\partial T}{\partial \bar{y}}=\frac{k}{\rho C}\left(\frac{\partial^2 T}{\partial \bar{x}^2}+\frac{\partial^2 T}{\partial \bar{y}^2}\right)+\frac{q'''}{\rho C}, \tag{4}$$

where Darcy's law has been assumed to be valid for the momentum equation and the Boussinesq approximation holds. Here $\bar{x}$ and $\bar{y}$ are the horizontal and vertical coordinates, respectively, and the corresponding flux velocities are $\bar{u}$ and $\bar{v}$. In addition, $\bar{p}$ is the pressure and T is the temperature. Heat generation takes place within the porous medium with the rate q''', which represents a local source centreed at the horizontal distance L, from an insulated vertical surface. The other quantities, namely K, μ, ρ, g, β, k, C, and σ, take their usual meanings: permeability, dynamic viscosity, reference fluid density, gravity, coefficient of thermal expansion, thermal conductivity of the porous medium, specific heat of the fluid, and the ratio of thermal capacities of the porous medium and the fluid. Finally, T_0 is the ambient temperature of the porous medium.

Nondimensionalization takes place using the following transformations

$$(\bar{x},\bar{y})=L(x,y),\quad (\bar{u},\bar{v})=\frac{k}{L(\rho C)}(u,v),\quad \bar{p}=\frac{k\mu}{(\rho C)K}p,\quad T=T_0+\frac{QL^2}{k}, \tag{5}$$

where

$$Q=L^{-2}\int_0^\infty\int_0^\infty q'''\,d\bar{x}\,d\bar{y}. \tag{6}$$

On introduction of the streamfunction ψ, using

$$u=-\frac{\partial\psi}{\partial y},\qquad v=\frac{\partial\psi}{\partial x}, \tag{7}$$

the governing equations become

$$\frac{\partial^2\psi}{\partial x^2}+\frac{\partial^2\psi}{\partial y^2}=\mathrm{Ra}\frac{\partial\theta}{\partial y}, \tag{8}$$

$$\frac{\partial\theta}{\partial t}=\frac{\partial^2\theta}{\partial x^2}+\frac{\partial^2\theta}{\partial y^2}-\frac{\partial\psi}{\partial y}\frac{\partial\theta}{\partial x}+\frac{\partial\psi}{\partial x}\frac{\partial\theta}{\partial y}+S(x,y), \tag{9}$$

where the Darcy-Rayleigh number is given by

$$\mathrm{Ra}=\frac{\rho_0(\rho C)g\beta KL^3Q}{k^2\mu}, \tag{10}$$

and where $S(x,y)$ is a local heat source centred at $(x,y) = (x_c,y_c)$ which, given that $S = q'''/Q$ must satisfy

$$\int_0^\infty \int_0^\infty S(x,y)dx\,dy = 1. \tag{11}$$

When the plume is situated on the horizontal bounding surface at y=0, we use

$$S = \frac{c}{2\pi} e^{-c((x-x_c)^2+y^2)}, \tag{12a}$$

but when it is well above this surface we use

$$S = \frac{c}{\pi} e^{-c((x-x_c)^2+(y-y_c)^2)}. \tag{12b}$$

We use the value c=2 here.

The statement of the problem is completed by the boundary conditions. For the case of a single plume, the flow is bounded by surfaces at $x = 0$ and $y = 0$ with the porous medium contained in the quarter plane, $x, y \geq 0$. Each surface is a streamline and both are assumed to be insulated. Therefore, we set

$$\psi = 0, \quad \frac{\partial \theta}{\partial n} = 0 \quad \text{on} \quad x = 0 \quad \text{and} \quad y = 0. \tag{13}$$

Inflow occurs at $x = x_{\max}$, and we set

$$\frac{\partial^2 \psi}{\partial x^2} = \theta = 0 \quad \text{on} \quad x = x_{\max}. \tag{14}$$

Outflow occurs at the upper surface, and the conditions used here are

$$\frac{\partial \psi}{\partial y} = \frac{\partial \theta}{\partial y} = 0 \quad \text{on} \quad y = y_{\max}. \tag{15}$$

Outflow conditions are not as destructive for convective flows in porous media as they are for the flows of clear fluids. For the present problem it was found that the outflow conditions given by Eq. (15) cause small streamwise oscillations for only a few grid points upstream of the upper boundary which, given that the upper boundary is very far from where plume attachment takes place due to the use of a coordinate transformation, means that the results presented are essentially independent of the outflow conditions given by Eq. (15).

Eqs. (8) and (9) were solved using second order finite differences in space on a nonuniform grid and first order backward differences in time. The accuracy with respect to time is not of importance here since every simulation eventually yielded a steady state solution. The use of backward differences means that the system being solved is fully implicit and, therefore, we employed a Full Approximation Scheme multigrid methodology to the problem, where iterations on each grid were undertaken using the line Gauss-Seidel method. While this complicates the numerical coding, the fact that the method is implicit means that it is possible and indeed desirable to increase substantially the time steps towards the end of the calculation to enhance convergence to the steady state. Therefore, a crude timestep-changing methodology was employed. In many cases we determined steady state solutions on relatively coarse grids, interpolated these solutions onto finer grids and used this as an initial condition – this increased further the rapidity with which highly accurate solutions were obtained. The code used is a modified version of the one described in detail in *Rees* and *Bassom* (1993).

3. Results

The present paper is an exploratory work where, despite the complexity of the numerical code, we are solely interested in determining the qualitative nature of plume entrainment. Comments will be made later about planned improvements of the methodology.

In the numerical code we choose not to vary the value of the Rayleigh number from the chosen value of Ra = 200, rather we alter the location of the source. When the source is located at $x_c = d$, then the transformations

$$(x, y) = d(\hat{x}, \hat{y}), \quad \psi = \hat{\psi}, \quad \theta = \hat{\theta}, \quad \mathrm{Ra} = \hat{\mathrm{Ra}}\, d, \quad S = \hat{S} d^{-2} \tag{16}$$

mean that Eqs. (8), (9), and (11) are reproduced precisely in the new variables with the source at $\hat{x} = 1$. Therefore, the setting of Ra = 200 and $x_c = d$ is equivalent to setting $\mathrm{Ra} = 200d$ and $x_c = 1$. The only difference between the two cases is the size of the spatial region over which the source is defined. The principle reason we followed this route rather than simply increasing the value of Ra is that solutions were obtained much more quickly.

Fig. 1 shows some typical streamlines and isotherms for cases where the source is centred on the axis. We have taken $x_c = 3$, 5, 7, and 9, and, therefore, the effective Rayleigh numbers are $\hat{\mathrm{Ra}}$ = 600, 1000, 1400, and 1800. The streamlines show clearly that fluid is entrained from the far right, turns near the corner, and travels upward in the expected manner. In addition there is a small region of weak recirculation which is bounded by a dividing streamline which

may be regarded as 'centreline' of the plume from the point of view of fluid; this will be called the fluid centreline.

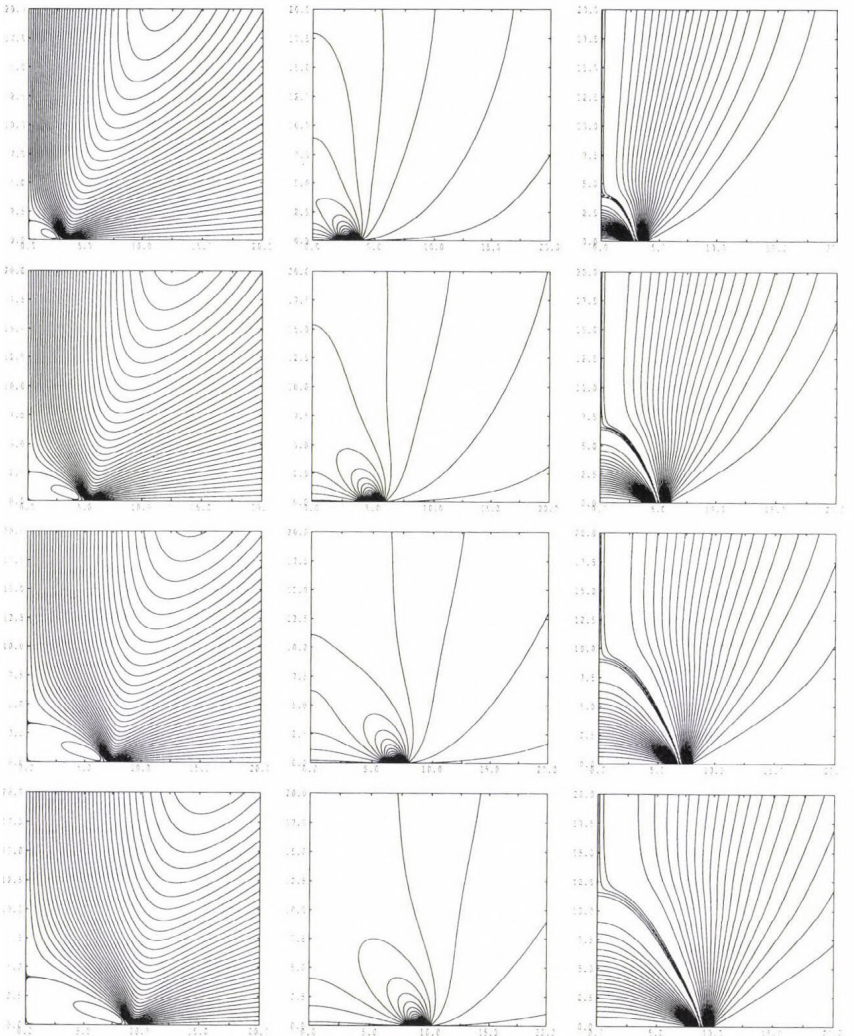

Fig. 1. Streamlines (left), isotherms (centre), and modified isotherms (right) for Ra = 200 with x_c=3, 5, 7, and 9 (from top to bottom) and y_c=0.

We have a situation where buoyancy forces cause the plume to rise, but the plume requires an equal amount of fluid to be entrained from each side for the plume to rise vertically. As the left side of the plume has only a finite amount of

fluid (in terms of x) which may be entrained, the plume curves to the left to fulfil its need for fluid to entrain, and it attaches onto the vertical surface thereafter to rise as a wall plume (or, given the boundary conditions, as one half of a standard plume).

It is interesting to see that the point of attachment on the vertical surface (which should be labeled as y_c) is closer to the origin than is the horizontal distance of the source from the origin. *Table 1* shows that this attachment point gradually gets lower as Ra increases. Therefore, the need to entrain fluid appears to be a stronger effect than that due to buoyancy forces, which cause vertical motion.

Table 1. Attachment points for the plume; y_ψ and $\hat{y}_\psi$ correspond to where the dividing streamline joins onto the vertical surface, and y_θ and $\hat{y}_\theta$ to where thermal centreline joins

Râ	y_ψ	$\hat{y}_\psi$	y_θ	$\hat{y}_\theta$
600	1.60	0.53	2.43	0.81
1000	2.50	0.50	6.60	0.94
1400	3.35	0.48	9.10	1.30
1800	4.05	0.45	11.75	1.31

The second column of subfigures in *Fig. 1* shows the corresponding isotherms, but this is not particularly instructive, since the temperature of a free convection line plume in porous media decays roughly as $y^{-1/3}$ as y increases, and this masks the thermal behaviour of the plume that we wish to present. Therefore, the third column of subfigures has been prepared where the temperature at any point has been scaled with respect to the maximum temperature at that value of y. Thus, the contour plots show clearly where the maximum temperature is located and the path taken by this thermal centreline. *Table 1* gives the detailed values of where the thermal attachment point is as a function of Ra, and it is clear that this location (labeled as y_θ) increases slightly as Ra increases. However, we feel that further computation needs to be undertaken on this aspect as the position of the attachment point has not increased greatly between Ra = 1400 and Ra = 1800; it may be that this represents the large-Ra asymptotic limit, or it could presage a lowering of the attachment point following that of the dividing streamline. Further numerical work is needed to determine which of these scenarios is correct.

Fig. 2 shows how the plume reacts to changes in the location of its source, where $x_c = y_c$, or, equivalently, to changes in Ra. Here the source is above the horizontal surface and, therefore, fluid passes beneath the plume in order to feed the entrainment on the left side of the plume. It is important to note that the abscissa and ordinates of the subframes in *Fig. 2* have been scaled in such a way that each represents $0 \le \hat{x}, \hat{y} \le 4$. Given that computations were performed in terms of x and y with the source defined in Eq. (12), the increasing concentration of the isotherms around the source region as x_c increases is a direct consequence of the fact that the source has a diameter of roughly 1 in terms of x and y.

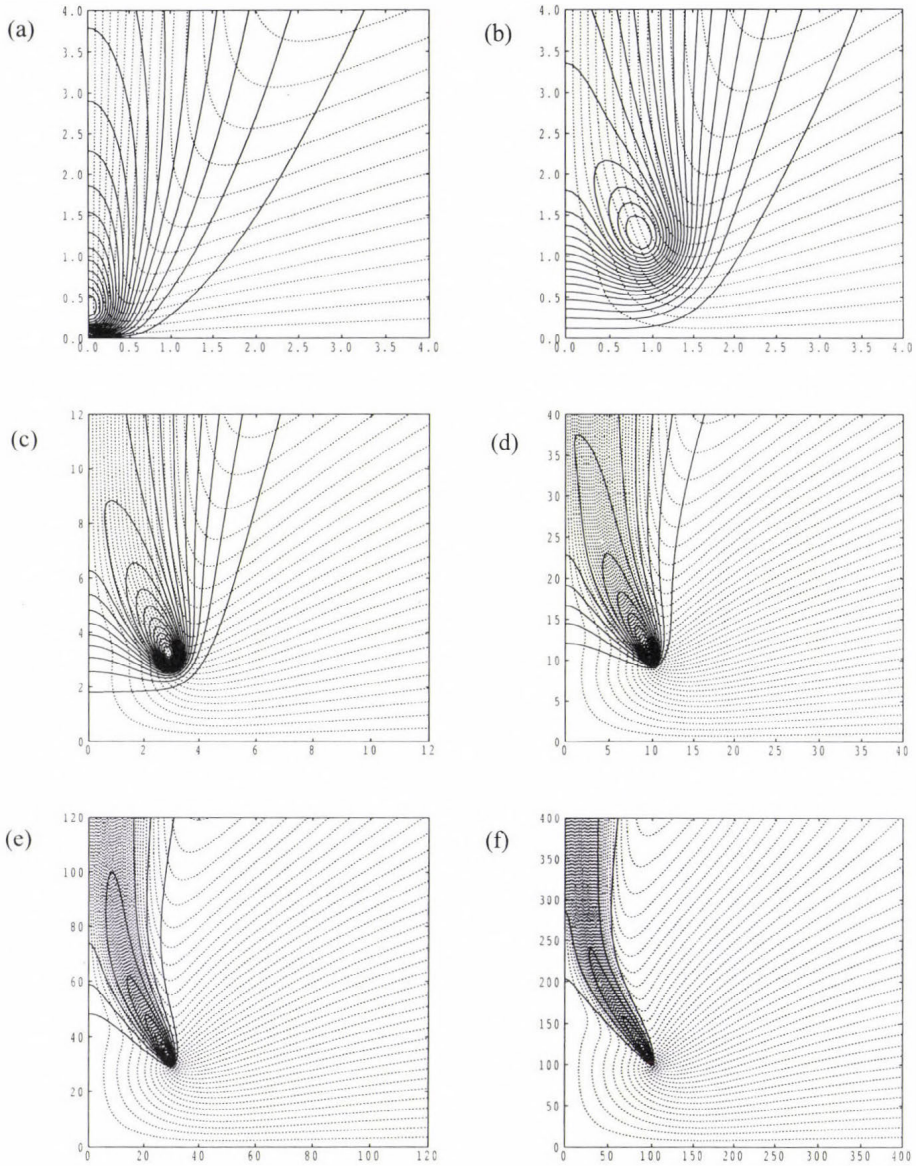

$$x_{\text{source}} = \begin{matrix} 0 & 1 \\ 3 & 10 \\ 30 & 100 \end{matrix} \quad \Rightarrow \quad \text{Ra} = \begin{matrix} 100 & 100 \\ 900 & 10^4 \\ 9 \times 10^4 & 10^6 \end{matrix}$$

Fig. 2. Streamlines (dashed) and isotherms (continuous) for Ra = 200 with $x_c = y_c$, where x_c takes the values (a) 0, (b) 1, (c) 3, (d) 10, (e) 30, and (f) 100.

The chief effect of raising the source above $y = 0$ is to delay the attachment of the plume onto the vertical surface. The concept of an attachment point in terms of the streamfunction now no longer exists since there is no recirculation, and the only places where $\psi = 0$ are the two bounding surfaces. However, the concept of thermal attachment still applies, and the presence of a strong upward flow past the plume source means that thermal attachment is delayed substantially. This is seen most clearly in *Fig. 2c* which corresponds to Râ = 600, which is the same as the case represented by the first row of *Table 1.* For the sake of comparison we shall define $\hat{y}_\theta$ to be based on the vertical distance between the attachment position and the location of the source: $\hat{y}_\theta = (y_\theta - y_c)/x_c$. As the maximum temperature at any value of y will correspond to that isotherm which has a turning point there, *Fig. 2c* shows clearly that y_θ is well above $y = 9$. Hence $\hat{y}_\theta$ is greater than 2, which is substantially further downstream than the value $\hat{y} = 0.81$ shown in *Table 1.* The attachment point in *Fig. 2d* is close to $\hat{y}_\theta = 3$, which is even greater.

Figs. 3, 4, and *5* show how two plumes interact, and each represents a different type of situation. The computational domain is now a half-plane. *Fig. 3* represents cases where two plumes have sources centred on $y_c = 0$, but where their horizontal locations are $x_c = \pm 4$; therefore, these correspond to cases where Ra = 800 and $\hat{x}_c = \pm 1$. The strength of the right and left hand plumes are given by the expressions given in Eq. (12), but where the right and left hand sides are multiplied by S_r and S_l, respectively. We take $S_r = 1$ and vary S_l between 0 and 1.

Fig. 3a depicts an isolated plume for comparison, while *Fig. 3b* shows that the presence of a weak second source nearby has little effect on the overall flow field and isotherm pattern, except for close to the horizontal bounding surface. We see that the plume generated by the weaker source exists independently for only a small distance above the surface before being absorbed into the main plume. As S_l increases, the left hand plume becomes stronger, and it begins to deflect the main plume towards itself, until, when $S_l = 1$ we are left with a perfectly symmetrical flow pattern.

Fig. 4 represents the same situation as *Fig. 3* except that both sources are placed at $y_c = 4$. The scenario described for *Fig. 3* in the above paragraph also occurs here, apart from the fact that the increased upward flow due to the positioning of the sources allows the weaker plume to exist for longer before being captured by the stronger plume. In this regard the behaviour is similar to that represented by *Fig. 2.*

Finally, two plumes of equal strength, but whose source heights are different, are depicted in *Fig. 5.* In *Fig. 5a* the lower plume is affected very strongly by the flow induced by the upper plume, although the upper plume is hardly affected by the presence of the lower plume, at least in terms of the part it takes. Indeed it is only when the source of the lower plume is as large as $y_c = 0.5$, which is shown in *Fig. 5c,* that the thermal centreline of the combined plume

changes from being close to $x = 4$. When $y_c = 0.75$ for the lower plume, the centreline of the combined plume is now very close to $x = 0$, and symmetry is obtained when $y_c = 1$.

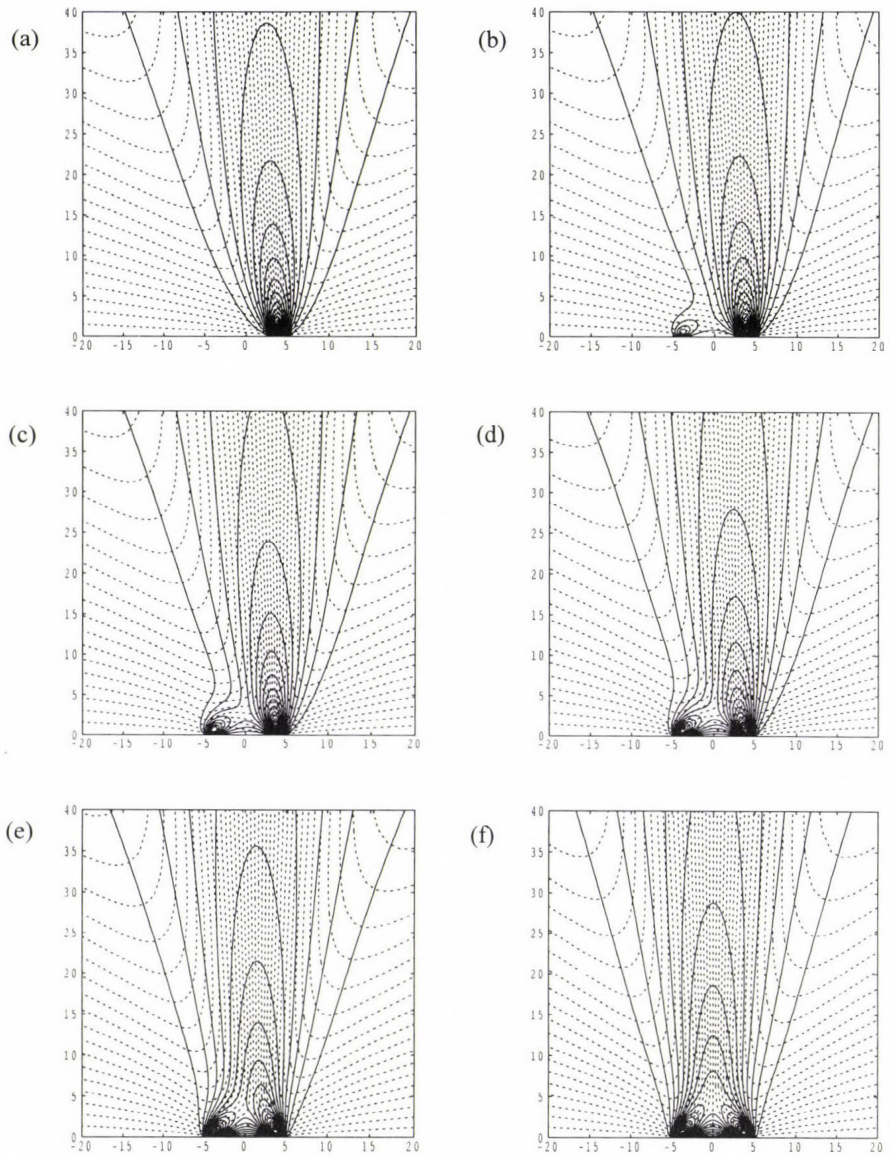

Fig. 3. Streamlines (dashed) and isotherms (continuous) for a situation with two plumes with Ra = 200 and $y_c = 0$. The strength of the right hand plume is S_r, and it is centred at $x_c = 4$. The strengths of the left hand plume are (a) $S_l = 0$, (b) 0.2, (c) 0.4, (d) 0.6, (e) 0.8, and (f) 1. The source of the left hand plume is centred at $x_c = -4$.

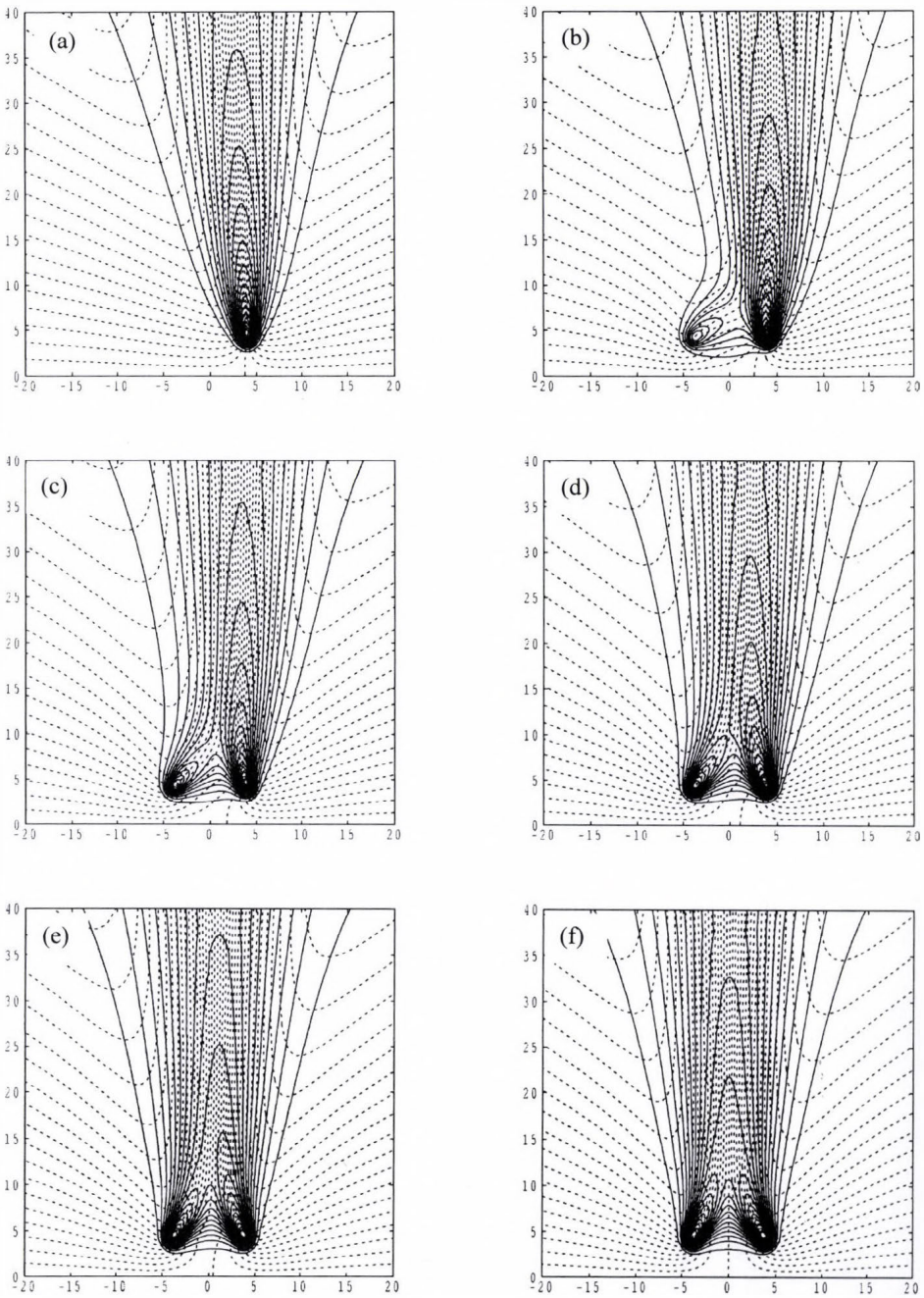

Fig. 4. As Fig. 3 but where the source of each plume is above the lower surface at $y_c = -4$.

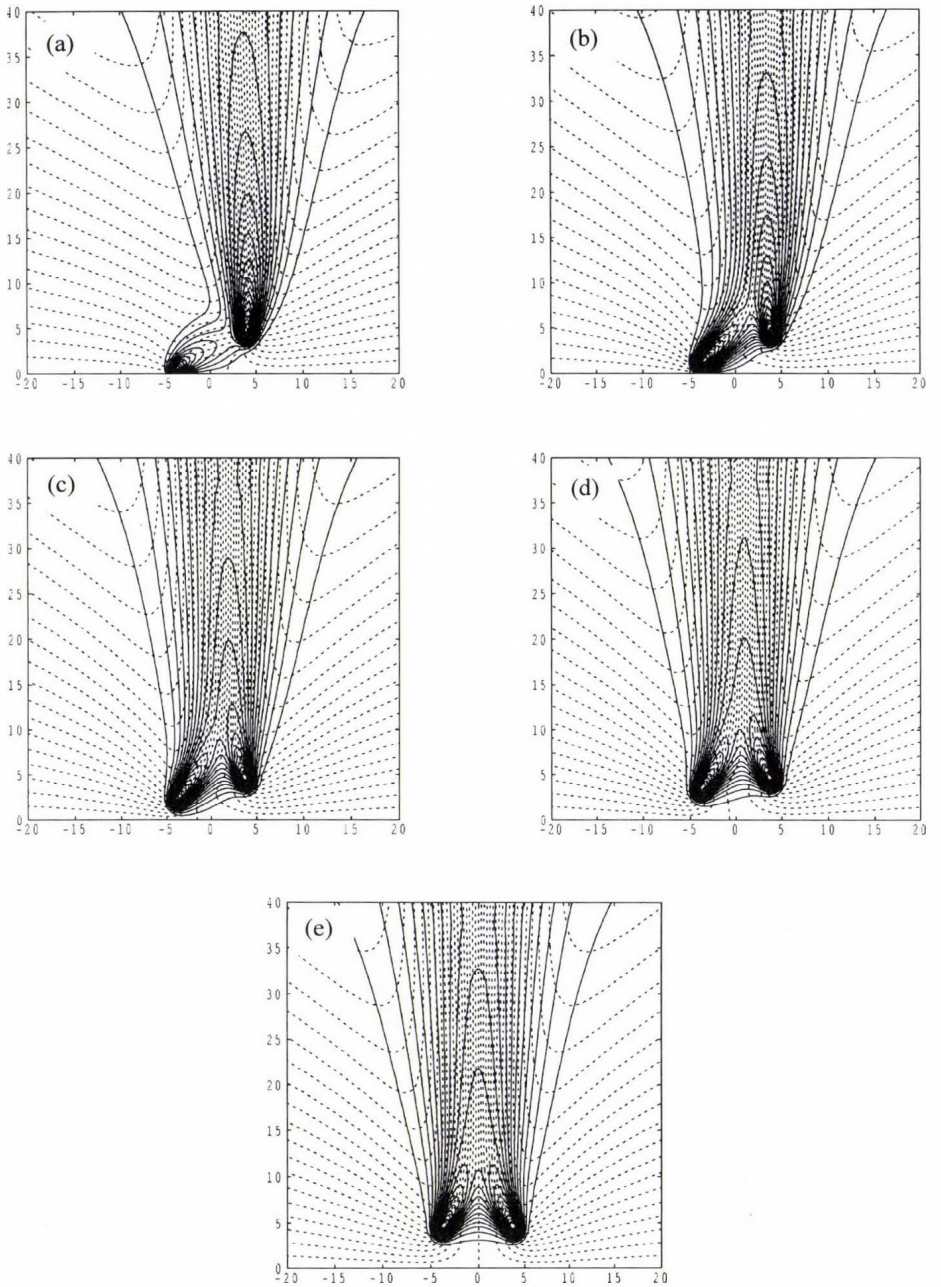

Fig. 5. Interaction of two plumes of equal strength ($S_r = S_l = 1$), where the source of the right hand plume is at $x_c = y_c = 4$, while the source of the left hand plume is at $x_c = -4$ with (a) $y_c = 0$, (b) 0.25, (c) 0.5, (d) 0.75, and (e) 1.

4. Conclusions

The main conclusion of this qualitative paper is that plumes are highly sensitive to their external environment. This was shown analytically by *Bassom et al.* (2000) where plumes in a wedge-shaped domain have a centreline which is straight, but not vertical, in general. In the present numerical study we have found that plumes will exhibit curved centrelines, although, in those cases where a fluid centreline may be defined, the fluid centreline does not coincide with the thermal centreline. In fact, within the parameters covered here, we find that the fluid attachment point descends as Ra increases, while the thermal centreline rises slightly. In addition, the restriction afforded by the placing of a source on a horizontal surface, means that there are substantial differences in both the flow field and the position of the thermal attachment point when the source is raised above the horizontal surface.

When two sources are present, the weaker one or the lower one is assimilated into the stronger one or the upper one, in some cases with little obvious qualitative effect on the latter.

It is our intention to perform further and more detailed computations, but given the sensitivity to domain shape and the need to keep the source region of constant size while the Rayleigh number is increased, it will be necessary to employ more sophisticated coordinate transformations than those employed here. In particular (i) the grid will need to be concentrated near the source region, as the whole flow field depends strongly on this, and (ii) the effective size of the computational domain in terms of the physical variables will need to be very large indeed in order to minimize the effects on the behaviour of the plume of the size and geometry of the computational domain and the inflow and outflow boundary conditions used.

Finally, we believe it to be true that the speed of migration of the plume towards the vertical wall, shown in *Figs. 1* and *2*, will be reduced substantially when point sources are considered. The flow that is induced in the y direction in these cases should provide some of the fluid for entrainment that is necessary to delay attachment.

References

Afzal, N., 1985: Two-dimensional buoyant plume in porous media: high-order effects. *Int. J. Heat Mass Tran. 28,* 2029-2041.

Bassom, A.P., Rees, D.A.S., and *Storesletten, L.*, 2000: Convective plumes in porous media: the effect f asymmetrically placed boundaries. *Int. Comm. Heat Mass Tran. 28,* 31-38.

Gebhart, B., 1979: Buoyancy induced fluid motions characteristic of applications in technology. *Trans. A.S.M.E. J. Fluids Eng. 101,* 4-29.

Harter, T. and *Yeh, T.-C.J.*, 1996a: Stochastic analysis of solute transport in heterogeneous, variably saturated soils. *Water Resour. Res. 32,* 1585-1595.

Harter, T. and *Yeh, T.-C.J.*, 1996b: Conditional stoastic analysis of solute tansport in heterogeneous variably saturated soils. *Water Resour. Res. 32,* 1597-1609.

Kurdyumov, V.N., 2006: Thermal plume induced by line source of heat in asymmetrical environment. *Z. Angew. Math. Phys. 57*, 269-284.

Rees, D.A.S. and *Bassom, A.P.*, 1993: The nonlinear nonparallel wave instability of free convection induced by horizontal heated surface in fluid-saturated porous media. *J. Fluid Mech. 253*, 267-296.

Rees, D.A.S. and *Storesletten, L.*, 2002: Convective plume paths from a line source. *Q. J. Mech. Appl. Math. 55*, 443-455.

Rees, D.A.S., *Storesletten, L.*, and *Bassom, A.P.*, 2002: Convective plume paths in anisotropic porous media. *Transport Porous Med. 49*, 9-25.

Shaw, D.C., 1985: The asymptotic behaviour of a curved line source plume within an enclosure. *I.M.A. J. Appl. Math. 35*, 71-89.

Wooding, R.W., 1963: Convection in a saturated porous medium at large Rayleigh number or Peclet number. *J. Fluid Mech. 15*, 527-544.

IDŐJÁRÁS

Quarterly Journal of the Hungarian Meteorological Service
Vol. 111, No. 2–3, April–September 2007, pp. 123–132

Discussing certain features of the transfer of wave energy in stationary gravity waves and stationary gravity-inertia waves in the atmosphere

Tor Håkon Sivertsen

Norwegian Institute for Agricultural and Environmental Research, Høgskoleveien 7, N-1432 Ås, Norway; E-mail: thsivert@online.no

(Manuscript received in final form January 29, 2007)

Abstract—The topography of Earth influences the movements of parcels of air in the atmosphere. Wind systems blowing across mountain ridges sometimes excite stationary gravity wave systems behind and above ridges with a breadth of about 10 km. The conceptual discussion in this paper is connected to the transport of wave energy in stationary gravity waves and stationary gravity inerta waves, where there are discontinuities in the parameters describing the vertical stratified atmosphere. The discussion is closely connected to two theorems deducted by *Eliassen* and *Palm* (1961) showing that the vertical flux of wave energy is conserved throughout the atmosphere for a great class of systems. But the boundary conditions, used by *Eliassen* and *Palm* (1961) in the gravity wave systems connecting the vertical layers in situations with discontinuities, do not cover all possible physical situations of interest. It is shown how the boundary conditions may be modified to cover most situations of interest.

Key-words: stationary gravity waves, stationary gravity-inerta waves, wave energy

1. Introduction

The influence of the topography on the movements of the parcels of air in the atmosphere is an important theme of dynamic meteorology. In a vertically stratified atmosphere gravity waves or inertia-gravity waves are excited by mountains and mountain ridges on different spatial and temporal scales.

The classical physics of Newtonian mechanics, thermodynamics, and fluid dynamics contains several basic principles, called 'laws of nature', like the conservation of energy, the conservation of mass, the conservation of momentum, and the second law of thermodynamis telling something about the allowed direction of certain physical processes. Sometimes useful results of

dynamics are derived, but it is not possible to show exactly how some of the physical laws' are contained in the system of equations.

Examples of this you find in the theory of turbulence. It is not possible to derive theoretically by using the Reynolds equations how the energy and momentum are transferred from the mean flow through the turbulence and to the molecular system, see *Tennekes* and *Lumley* (1987). When using the Navier-Stokes equations, this transfer of energy and momentum is fully described from the flow to the molecular scale. The reason is that the dissipation may be neatly defined, but we have got no theory giving us the components of the Reynold stress tensor.

In this paper certain features of the following concepts are considered: Wave energy of stationary mountain waves, flux densities of wave energy in the horizontal and vertical directions, and reflection of wave energy in the vertical direction. *Eliassen* and *Palm* (1961) did show that the vertical flux of wave energy is conserved throughout the atmosphere in these stationary systems of gravity waves. They also did look theoretically at stratified systems with discontinuities of the parameters in the vertical direction. Below theoretical situations with discontinuities of the mean flow, U is discussed in some details. The theoretical treatment of *Eliassen* and *Palm* (1961) did not cover this physical situation.

2. The landscape studied and the physical situation considered

We consider a landscape containing a mountain ridge with a breadth of about 10 km, and the atmosphere is considered stratified in the vertical direction. The landscape and the physical phenomena are modeled in a Cartesian coordinate system with the origin placed under a mountain ridge, the x-axis is normal to the ridge, and the y-axis is parallel with the ridge. The z-coordinate is used to model the height above the (x,y)plane. The fluid-dynamical macrophysical description of the atmosphere is used, by considering the physics to be described by the Navier-Stokes equations, or more precisely by the Euler equations, while the viscosity of the air parcels is not included in this study.

We are using a macrophysical description of the atmosphere. At a moment of time t and at a coordinate point (x,y,z) we have got a parcel of air described by the pressure $p(x,y,z,t)$, temperature $T(x,y,z,t)$, density of the air $\rho(x,y,z,t)$, and wind velocity $\mathbf{v}(x,y,z,t)$. Furthermore, the parcels of air are considered not to exchange heat with the surroundings by conduction or radiation. Also the chemical content of each parcel is considered not to change in time.

We then may consider the thermodynamic processes of each parcel of air as adiabatic. *Eliassen* and *Palm* (1961) is describing the adiabatic process by using the coefficient of piezotropy, γ. In adiabatic thermodynamic processes in the air, the corefficient of piezotropy is given in this manner:

$$\gamma = 1/ C_L^2, \tag{1}$$

where C_L denotes the velocity of sound .

3. *The perturbation equations and the concept of wave energy*

Then we get the mathematical description of the perturbation of the basic flow (only in the (x,z)dimensions):

the horizontal wind velocity is $U(z) + u(x,z)$,

the vertical wind velocity is $w(x,z)$,

the pressure is $p_0(z) + p(x,z)$,

the density of the air is $\rho_0(z) + \rho(x,z)$.

By putting these expressions into the Navier-Stokes equations and the equation of continuity and linearizing, *Eliassen* and *Palm* (1961) obtains the following expression of the wave energy equation:

$$(EU + pu)_x + (pw)_z = -\rho U_z uw, \tag{2}$$

where the indices x and z indicates partial differentiation in x- and z-directions.

$$E = \tfrac{1}{2}\rho_0(u^2 + w^2 + v_0{}^2\zeta^2 + \gamma\rho_0{}^{-2}p^2) \tag{3}$$

is defined as the total wave energy per unit volume. The unit of wave energy is J m^{-3}. ν_0 denotes the Väisälä-Brunt frequency, and $\zeta = \zeta(x,z)$ denotes the vertical displacement of the particles in the disturbed flow.

The wave energy E is made up by

a kinetic part: $\tfrac{1}{2}\rho_0(u^2 + w^2)$,

an available potential part: $\tfrac{1}{2}\rho_0(v_0{}^2\zeta^2)$,

an internal part: $\tfrac{1}{2}\rho_0(\gamma\rho_0{}^{-2}\rho^2)$.

The kinetic part is the kinetic energy connected to the velocity perturbations of the air parcel. The available potential energy is connected to the buoyancy of the air parcel and the distance from the undisturbed equilibrium position. The internal energy is connected to the compressibility of the air parcel.

The horizontal flux density of wave energy is given by the expression $EU + pu$. The vertical flux density of wave energy is denoted by pw, and Eq. (2) is expressing the divergence of wave energy.

If all perturbation quantities tend towards zero as x tends to $\pm\infty$, the following statement is valid concerning the vertical flux of wave energy see *Eliassen* and *Palm* (1961):

$$(1/U)\int pw\,dx = -\rho_0 \int uw\,dx\,. \tag{4}$$

This flux is conserved throughout the atmosphere in systems of stationary gravity waves in the atmosphere on local scales (possible to study by the linearized equations).

4. A situation containing discontinuity of the parameters

We assume that the basic flow, U, the density, ρ_0, or the gradient of the density is discontinuous at a height $z=H$. The kinematic boundary condition is then given by

$$\zeta_1 = \zeta_2 \quad \text{at} \quad z = H \qquad \text{or} \qquad (\zeta_1)_x = (\zeta_2)_x \quad \text{at} \quad z = H\,. \tag{5}$$

The physical content of this statement is that the vertical displacement, ζ, is the same for the parcels of each side of the surface of discontinuity. The indices 1 and 2 denotes the upper and lower side of a surface of discontinuity.

The linearized vertical velocity is given by $w = U\zeta_x$. Eq. (5) is then transformed into

$$w_1 / U_1 = w_2 / U_2 \quad \text{at} \quad z = H\,. \tag{6}$$

We get the dynamic boundary condition by requiring that the individual perturbation of the pressure shall be the same on each side of the surface of discontinuity. This condition, linearized, is given by

$$(p_{01})_z \zeta_1 + p_1 = (p_{02})_z \zeta_2 + p_2 \quad \text{at} \quad z = H\,. \tag{7}$$

By multiplying the right and left sides of Eq. (7) with the right and left sides of the kinematic boundary condition, and integrating along the x-axis we get

$$\int (p_1 w_1 / U_1)dx = \int (p_2 w_2 / U_2)dx\,. \tag{8}$$

This equation tells us that by using the boundary conditions mentioned, the vertical flux of wave energy is conserved also through the discontinuities of the internal boundaries.

5. Mesoscale mountain waves

We then look at a mountain ridge with a breadth of 100–500 km. This ridge is oriented towards north-south. The Cartesian coordinates x and y are directed eastward and northward, respectively. Pressure p is used as a vertical coordinate. The mountain is situated in an eastward flow, U (p, y). All the physical properties in the atmosphere are functions of y and p, but they are independent of x. The basic flow is in hydrostatic and geostrophic balance.

Behind the mountain ridge we assume the occurrence of a stationary lee wave, which can be described by the linearized equations of motion and continuity. The scale is so large that the flow can be regarded as quasi-static, but the Coriolis parameter, f, is assumed to be constant. *Eliassen* and *Palm* (1961) has then shown the following theorem to be valid

$$\frac{\partial}{\partial \rho}\left(\frac{\overline{\phi\omega}}{U}\right)+\frac{\partial}{\partial \gamma}\left(\frac{\overline{\phi v}}{U}\right)=0, \tag{9}$$

where

$$\overline{(\,)}=\int_{-\infty}^{\infty}(\,)dx.$$

Here ϕ is the local perturbation of the geopotential, ω is the individual time derivative of pressure, v is the velocity in the y-direction. It is assumed that the perturbation disappears for large positive and negative values of x. $\phi\omega$ and ϕv are the vertical and horizontal components of the flux of wave energy. We use the following notation

$$\begin{aligned}\frac{\overline{\phi\omega}}{U}&=-\frac{\partial\psi}{\partial\gamma}=-\psi_y,\\ \frac{\overline{\phi v}}{U}&=\frac{\partial\psi}{\partial\psi}=\psi_p,\end{aligned} \tag{10}$$

where subscripts indicate partial derivatives.

We then define a vector function

$$\mathbf{G}=\mathbf{i}\times\nabla\psi, \tag{11}$$

where

$$\mathbf{i}=\nabla x.$$

The flux of wave energy is then given by

$$\mathbf{F}=U\,\mathbf{G}. \tag{12}$$

ψ is the stream function of the solenoidal vector $\mathbf{F}/U$. The curves ψ = constant are the stream functions of the flux of wave energy in the meridional plane. The flux of wave energy in a channel between two adjacent streamlines varies along the channel in proportion to U.

We then assume the occurence of a surface of discontinuity in the atmosphere. Both the density and the basic flow velocity may be discontinuous along this surface.

The slope of the surface is expressed in the formula of Margules, which in pressure coordinates is given by

$$\frac{dp}{dy} = -f\frac{(U_1 - U_2)}{\alpha_1 - \alpha_2} = K. \tag{13}$$

The flow is perturbed by the mountain ridge, and it is assumed that the perturbation can be approximated by linear expressions. In this case the particles move along the surface of discontinuity, and it is assumed that the slope of the surface is not affected.

Let $\eta(x, p)$ represent the particle displacement in the y-direction and π the change of pressure for a particle from its upstream value. The displacements in the (y, p)plane are assumed to take place along straight lines. The kinematic boundary condition is given by

$$\frac{\pi_1 - \pi_2}{\eta_1 - \eta_2} = -f\frac{U_1 - U_2}{\alpha_1 - \alpha_2} = K, \tag{14}$$

or

$$K\eta_1 - \pi_1 = K\eta_2 - \pi_2, \tag{15}$$

where $\pi_i, \eta_i, (i = 1,2)$ represent the displacement of the particles on each side of the surface of discontinuity which were adjacent upstream.

The requirement, that the geopotential shall vary continuously on the surface of discontinuity, constitutes the dynamic boundary condition. Upstream the boundary condition then is given by

$$\phi_1(y, p) = \phi_2(y, p). \tag{16}$$

Downstream the geopotential on each side of the surface at the point $(y + \eta_1, p + \pi_1)$ is given by

$$\phi_1(y, p) + \phi_{i1}(y, p) = \phi_2(y + \eta_1 - \eta_2, p + \pi_1 - \pi_2) + \phi_{i2}(y + \eta_1 - \eta_2, p + \pi_1 - \pi_2), \tag{17}$$

where $\phi_{ij}\ (y, p), (j = 1,2)$ is the individual change of geopotential for a particle from its upstream value along the streamline (y, p). Thus, the particles at the point $(y+\eta_1, p+\pi_1)$ on each side of the surface downstream come from the points (y, p) and $(y+\eta_1-\eta_2, p+\pi_1-\pi_2)$ upstream. The linearized individual perturbation is given by

$$\phi_{ij} = \phi_{jp}\,\pi_j + \phi_{jy}\,\eta_j + \phi_j, (j = 1,2). \tag{18}$$

By using Eqs. (15)–(17) and retaining only the first order terms, we get

$$\phi_2 - \phi_1 + \eta_1(\phi_{2y} - \phi_{1y}) + \eta_1(\phi_{2p} - \phi_{1p}) = 0. \tag{19}$$

We then use the hydrostatic relation, $\phi_p = -\alpha$, and the geostrophic relation, $\phi_y = -fU$, thus, Eq. (19) is alternatively given by

$$\phi_1 - \phi_2 + \eta_1(U_2 - U_1)f + \pi_1(\alpha_2 - \alpha_2) = 0. \tag{20}$$

By noting from Eq. (16) that $f(U_2 - U_1) = K(\alpha_2 - \alpha_1) = 0$ and by using Eq. (15), Eq. (20) becomes

$$\phi_1 - \phi_2 = (K\eta_1 - \pi_1)(\alpha_2 - \alpha_1) = (K\eta_2 - \pi_2)(\alpha_2 - \alpha_1). \tag{21}$$

Using Eq. (15) and multiplying Eq. (20) on each side by $(K\eta_1 - \pi_1)_x = (K\eta_2 - \pi_2)_x$ we get

$$\phi_1(K\eta_1 - \pi_1)_x - \phi_2(K\eta_2 - \pi_2)_x = (K\eta_1 - \pi_1)(K\eta - \pi_1)_x(\alpha_2 - \alpha_1), \tag{22}$$

where α_1 and α_2 are independent of x. Integration along the x-axis then gives

$$K\overline{\phi_2 \eta_{2x}} - \overline{\phi_2 \pi_{2x}} = K\overline{\phi_1 \eta_{1x}} - \overline{\phi_1 \pi_{1x}}. \tag{23}$$

We suppose for the sake of argument that there is only one surface of discontinuity in the space. Above the surface we define a vector $\mathbf{G}_2 = \mathbf{i} \times \nabla \Psi_2$ and below the surface a vector $\mathbf{G}_1 = \mathbf{i} \times \nabla \Psi_1$. The surface of discontinuity is (for each value of x) represented in a (y, p)plane by a line. Let $d\mathbf{l}$ denote a vector element of this line.

A vector element of the surface of discontinuity is then defined by

$$d\boldsymbol{\sigma} = \mathbf{i} \times d\mathbf{l}. \tag{24}$$

Since $\mathbf{G}_1$ and $\mathbf{G}_2$ are solenoidal, we have

$$\oint_{\Omega j} \mathbf{G}j \cdot d\boldsymbol{\sigma}_j = 0, \quad (j = 1,2). \tag{25}$$

The domains Ω_j, (j = 1,2) are not cut by the surface of discontinuity. The theorem corresponding to this on the surface would be

$$\mathbf{G}_1 \cdot d\boldsymbol{\sigma} = \mathbf{G}_2 \cdot d\boldsymbol{\sigma}. \tag{26}$$

From the preceding we get

$$\mathbf{G}_1 \cdot d\boldsymbol{\sigma} = \mathbf{i} \times \nabla\Psi \cdot (\mathbf{i} \times d\mathbf{l}) = d\mathbf{l} \cdot \nabla\psi_j = d\psi_j, \quad (j = 1,2). \tag{27}$$

If Eq. (26) is valid, then $d\psi_1 = d\psi_2$ on the surface of discontinuity, and it is possible to define a scalar function, the equilines of which are continuous on this surface.

Eq. (13) gives

$$d\psi_j = \psi_{jp}dp + \psi_{jy}dy = (\psi_{jp}K + \psi_{jy})\,dy, \quad (j = 1,2). \tag{28}$$

The linearized ω and v are given by

$$\omega = U\pi_x \quad \text{and} \quad v = U\eta_x. \tag{29}$$

Eqs. (10) and (29) give

$$\psi_{jp} = \frac{\overline{\phi_j v_j}}{U_j} = \overline{\phi_j \eta_{jx}}, \quad (j = 1,2) \tag{30}$$

$$\psi_{jy} = \frac{\overline{\phi_j \omega_j}}{U_j} = \overline{\phi_j \pi_{jx}}.$$

From Eqs. (28) and (30) we have

$$d\psi_1 = \left(K\overline{\phi_1\eta_{1x}} - \overline{\phi_1\pi_{1x}}\right)dy,$$

$$d\psi_2 = \left(K\overline{\phi 2\eta_{2x}} - \overline{\phi_2\pi_{2x}}\right)dy. \tag{31}$$

By comparing (31) and (23) we notice that Eq. (23) is equivalent to the assertion $d\psi_1 = d\psi_2$ on the surface of discontinuity.

According to *Eliassen* and *Palm* (1961), the flux of wave energy, $\mathbf{F} = U\mathbf{G}$, in a stationary quasi-static wave in a non-uniform basic current varies between adjacent streamlines, ψ = constant, in proportion to the basic current U. The preceding shows that this is also the case when there is a surface of discontinuity in the atmosphere. Along this surface both the basic flow U and the density ρ may be discontinuous, see also *Sivertsen* (1976).

6. *Fourier-transformation of the equations and the idea of vertical transmission and reflection of wave energy*

The system of linear equations for this stationary situation on local scale is manipulated and we arrive at the following equation for w (the vertical wind velocity):

$$w_{zz} + w_{xx} - l^2(z)w = 0.$$

$l^2(z)$ is called the Scorer-parameter, and with good approximation we get:

$$l^2(z) = {v_0}^2 U^{-2} - U_{zz} U^{-1}.$$

By Fourier-transforming this equation we arrive at the following formula:

$$\hat{w}_{zz} - (l^2 - k^2)\hat{w} = 0,$$

where k is the wave number in this transformation.

In a layered atmosphere, each layer with a constant Scorer-parameter; the analytical solutions in each layer may be linked by the knowledge of the boundary conditions between each layer.

Eliassen and *Palm* (1961) invoked an analogy with the theory of electromagnetism when discussing reflection and transmission of energy in an atmosphere with layers of constant Scorer-parameter. In order to maintain this analogy, they are using something they call 'pure mathematical boundary conditions':

$$w_1 = w_2 \tag{32}$$

and

$$w_{1z} = w_{2z}. \tag{33}$$

Nevertheless, they sometimes violate their own main result, Eq. (4), that the vertical flux of wave energy always is conserved through the atmosphere in a stationary system. Their theory is not valid in situations with discontnuities in the main stream, U.

When using the ordinary kinematical and dynamical boundary conditions Eqs. (6) and (7), we get other results in calculating the coefficient of reflection than according to the analogy with electromagnetism, see *Sivertsen* (1972). When studying other aspects of the phenomenon of stationary gravity waves in the atmosphere, like calculation of the pressure drag on the mountains in a layered atmosphere with discontinuity of the parameters connecting to the different layers, using boundary conditions Eqs. (32) and (33) sometimes will give the wrong results.

References

Eliassen, A. and *Palm, E.*, 1961: On the transfer of energy in stationary mountain waves. *Geofysiske Publikasjoner*, Oslo.

Sivertsen, T.H., 1972: About stationary mountains waves (in Norwegian). *Thesis Master of Science.*University of Oslo.

Sivertsen, T.H., 1976: On the transfer of energy in stationary mountain waves in an atmosphere with discontinuous parameters. *Meteorologiske annaler 7*, No. 3. Det norske meteorologiske institutt, Oslo, 9 pp.

Tennekes, H. and *Lumley, J.L.*, 1987: *A First Course in Turbulence.* MIT Press Cambridge Massachusetts, London, England.

IDŐJÁRÁS

Quarterly Journal of the Hungarian Meteorological Service
Vol. 111, No. 2–3, April–September 2007, pp. 133–148

Internal waves and internal boundary currents
In memoriam Fridtjof Nansen

Yuli D. Chashechkin

Laboratory of Fluid Mechanics,
Institute for Problems in Mechanics of the Russian Academy of Sciences
101/1 prospect Vernadskogo, Moscow, 119526, Russia; E-mail: chakin@ipmnet.ru

(Manuscript received in final form February 5, 2007)

Abstract—Re-reading of books written by Fridtjof Nansen after his great travels and humanitarian feats shows that his precise observations as well as deep thoughts are still rich source of inspiration. He gave clear description of the behavior of this ship *Fram* in dead waters of Siberian seashores and invited Vagn Ekman to clarify the phenomenon in laboratory experiments. Laboratory studies of stratified flows is now performed in many laboratories around the globe. The first part of this paper is a memorial talk of Nansen. In the second part a classification of infinitesimal periodic motions including waves and singular components of motions is presented. Singular solutions describe a set of linear periodic boundary layers. Approximation of a 3D homogeneous fluid results in merging boundary layers and degeneration of the governing equations set. Structure of 2D attached internal waves is visualized numerically.

Key-words: viscous stratified fluids, exact regular singular solutions, periodic motions

1. Introduction — life in the service of science and humanity

Fridtjof Nansen was born in Norway, on October 10, 1861 in aristocratic family. His father, Baldur Fridtjof Nansen, a prosperous lawyer, was a religious man with a clear conception of personal duty and moral principle. His mother, baroness Adelaide Johanna Tekle Isidore Belling formerly Wedel Jarlsberg was a strong-minded, athletic woman. She owned a farmstead near Christiania (now Oslo) where Fridtjof Nansen, together with his brother Alexander and a number of older half-brothers and half-sisters, had a privileged childhood. Mother had introduced children to outdoor life and encouraged them to develop physical skills. Not massively built, F. Nansen was tall, supple, strong, and possessed the physical endurance to ski fifty kilometers in a day and then to win a skiing competition.

Preferring physics and mathematics he, nevertheless, selected zoology to spend more time in the open air, when in 1880 he entered the University of Christiania. Even during student days, in 1882, when, at a tutor's suggestion, he took passage aboard a sealer *Viking* to the Arctic Ocean, he used thermometers, bathometers, and different nets for scientific observations of winds, ocean currents, ice movements, and animal life. He firstly found that warm salty Atlantic waters were placed below cold and fresh Arctic waters and rightly described freezing of polar seas. He landed on a floating iceberg and collected stones. Thinking about the patterns of the frozen in ice ship drift, he recognized that the effect of complex vortex currents caused by the bottom topography dominate, over a wind impact. He wrote extended diaries and published papers about his expeditions in newspapers and scientific journals that were illustrated by his own excellent sketches. After the travel he firmly decided to study cold Arctic Ocean and crossed Greenland icecap on skies.

On his return Nansen was offered the post of curator at the Bergen Museum. During six years he performed intensive laboratory study mostly with the microscope that was a gift of his father. The transition from the rugged days aboard the Arctic sealer to study minute animals through microscopes was productive. He wrote his thesis *The Structure and Combination of Histological Elements of the Central Nervous System* in English language in 1887, accepted by the examining board with a degree of skepticism. He could obtain his doctorate only four days before leaving for Greenland in view of his future dangerous travel. In the course of two years he published abbreviated version of his thesis in four different languages and today his thesis is regarded as a classic. He visited the international biological station in Naples (Italy) in 1886 and was so impressed that recommended to construct similar stations in Norway. The idea was supported and two biological stations were built on Nansen's projects. Constructions were so good that the station in Drobak is still operating today, in the same building.

In 1887 Nansen embarked on the preparations for the journey to cross the Greenland icecap. The six-man expedition was financed by a wealthy Danish businessman A. Gamel and Nansen himself. The expedition started in June on the east coast and going to the inhabited west coast. The ice drift delays the beginning of the journey as it took 12 days to row to land in open boats instead of expecting 2–3 hours. Nansen, still only 27 years of age, had led his team firmly and finally reached the west coast in late September. Throughout the journey the team made careful records of meteorological conditions when the temperature fell to 50 °C below zero. Data were analyzed later by the known meteorologist H. Mohn (1835–1916). No boats were due to leave Greenland until the following spring, so Nansen spent the enforced winter in Greenland studying the Inuits and returned to Norway in May 1889. After the expedition he published many articles and books, like *The First Crossing of Greenland* (1890) and *Eskimo Life* (1891).

Meanwhile, he started planning an another great expedition by ship over the Polar Sea hoping to reach the North Pole. He read a lot of lectures in different countries discussing his plans and construction of the ship. When – in 1892 – he outlined his plan for a North Pole expedition in the Royal Geographic Society of London, he met a lot of criticism and opposition by the most experienced Arctic explorers. But the idea received a great support in Norway. The Storting (the Norwegian Parliament) granted a large part of the necessary expenses, subscriptions from the King, private individuals and own payment of Nansen provided the rest.

The primary task was to build a ship that could withstand the pressure of the ice. Nansen collaborated with famous shipbuilder Colin Archer to design it. The government provided by the best oak and timber for the ship construction from the state stock. The hull of the vessel *Fram* was made exceptionally strong, and her lines below the waterline were far rounder than customary. As a result, when the pack became jammed hard together, the ship slipped free and was lifted clear instead of being crushed.

In June 1893 the *Fram* left Christiania with provisions for six years and fuel oil for eight. Nansen believed the trip would take from two to three years. After having sailed the nothern Siberian coast, the expedition reached the area around New Siberian Islands where the *Fram* had been frozen fast in the drifting ice. However, it became evident soon, that the ship root was too far from the North Pole. Then Nansen with Hjalmar Johansen left the *Fram* on February 1895 to ski to the North Pole with dog sledges. Despite the incredible difficulties they reached 86°14'N when the drifting ice and lack of food forced them to turn back. The travelers had no idea of *Fram's* whereabouts, so they decided to spend the winter in Franz Josef Land, and they survived in a stone hut by shooting walruses and polar bears. After the long winter they started to go to south, and by an incredible stroke of luck, they met a British expedition, headed by Frederick George Jackson, which took them back to Norway. Just after Nansen had arrived in Norway, the *Fram* came in, too. Nansen described the history of the expedition in a two-volume work *Farthest North* (1897). The successful outcome of the North Pole expedition made Nansen a national hero and gave him a world-wide reputation.

The most important results of Nansen's *Fram* expedition were

- the discovery of the deep Arctic Ocean completely devoid of islands,
- the confirmation of the existence of the trans-polar current,
- existence of intermediate warm and salty waters,
- thickening pack ice from below due to freezing of melting fresh water.

Furthermore, Nansen recognized that the *Fram* and the ice pack drifted approximately 30° to the right of the wind direction. This fact he interpreted as the effect of the Earth's rotation, which laid the concept for the Ekman spiral and the foundation for the modern wind-driven ocean circulation. Nansen descibed in details the misterious "dead water" phenomen which the *Fram* met

in Bergen fjord and Siberian coast waters. Scientific results of expedition were published in a six volumes collection of papers. Later Nansen decided to hand the *Fram* over to Roald Amundsen for an expedition to the South Pole. Nansen and Captain Otto Sverdrup shared their rich experience on ship motion in ice with the Russian Admiral S.O. Makarov, who decided to built the first large icebraker with iron hull .

As a scientist, Nansen was much aware of the need for precise and exact measurements. Leaving the ship in March 14, 1895 he wrote in a letter to Sverdrup: "Besides foods, weapons, clothes, and equipment, take off scientific materials, diaries, and collections, but not so heavy, ...photos and plates... It is good to take off Oderman's densimeter for measuring of sea water density...". Later Nansen found that some of the oceanographic measurements on the *Fram* were not of sufficient precision. He wrote: "I understood that future studies in physical oceanography would have small impact or even no sense if they will not produced by more exact methods than current methods or used before". At that time, when densimeters were the most precise instruments in physical oceanography, Nansen exchanged his experience of methods of calibrations with the known Russian oceanographer Admiral S.O. Makarov (1848–1904), who made round-the-world expedition on the corvette *Vityaz* (1886–1889, 903 days of travel and 526 days of sailing and steaming) and wrote the famous book *Vityaz and the Pacific Ocean*. Nansen was able to remarkably improve methods and instruments, and he invented the bottle for sampling ocean water at various depths and different types of current meters. He supported the international cooperation in oceanography, and he was one of the founding fathers of the International Council for the Exploration of the Sea (ICES) in 1902.

Nansen's books were soon translated into Russian (first in 1897) making his name extremely popular. He was honored by the Prince Konstantin Gold Medal of the Russian Geographic Society in 1897. He visited Russia first in 1898, when he was awarded by the State Stanislav insignia and was elected Honor Member of St. Petersberg Academy of Science.

The success of the *Fram* expedition stimulated Norwegians to act for state independence, and Nansen involved himself in the political debates. He played an important role in the actions in 1905 when the union with Sweden was dissolved and Norway declared its full independence. Reportedly, he was also secretly requested to become either president or king but declined both offers, on the grounds that he was "a scientist and explorer". However, he played a personal part in bringing to the vacant Norwegian throne the Danish Prince Carl, who took the Norwegian name Haakon VII and was appointed as Norway's first ambassador in London.

After two years in London, he returned to scientific work for some years and had some good years studying the oceanography of the Norwegian Sea and the way of formation of bottom water in the Greenland Sea. His results were published jointly with Professor B. Helland-Hansen in the classic book *The Norwegian Sea.*

In 1913 he traveled to Siberia and Far East with a diplomat I.G. Loris-Melikov and the deputy of the State Duma (Parliament), S.V. Vostrotin from Tromsoe to Krasnoyarsk. They followed the only working way from Far East to Europe up to the still mouth of the river Enisey on a cargo ship *Correct*, then up along the river Enisey on a motor boat to Krasnoyarsk. Then he took a rail car and went to Vladivistok on the just constructed Transsiberian railway, where one of the stations was named by him. The Eastern Siberian railroad is the longest continuous railway of the world. His impressions of the environment, common people life, and seeing of future development of these extended but almost unhabitated lands are expressed in his excellent book *Into the country of Future (Fremtidens Land) – Great North Marine way from Europe to Asia through Kara Sea* with a supplement *Shipping in Kara Sea*. The book contains right prognosis of future economic development of this outermost land and was reprinted in Russia (*Nansen*, 1992).

The further life of Fridtjof Nansen is an illustration of his deep thinking, efficiency, and humanism. He did save the lives of millions of people. In 1917–1918 Nansen negotiated in Washington, USA an agreement for a relaxation of the blockade of the allies to permit shipments of essential food to neutral Norway.

In June 1921 the Council of the League of Nations, spurred by the International Red Cross and other organizations, instituted its High Commission for Refugees and asked Nansen to administer it. For the stateless refugees under his care Nansen invented the "Nansen Passport", a document of identification, which was eventually recognized by fifty-two governments. In the nine-year life of this office, Nansen ministered to hundreds of thousands of refugees – Russian, Turkish, Armenian, Assyrian, Assyro-Chaldean – utilizing the methods that were to become classic.

A heavy drought in the Russian grain growing areas in 1921 brought famine to millions of people. Nansen responded on appeal of Maxim Gorky and opened in Moscow Kremlin an office of the International Russian Relief Executive. But his appeals to the League of Nations for funds to finance the work met deaf ears. As Nansen was sure that even a small food parcel can save a life, he appealed to common people and succeeded in raising finances. Norwegian pensioners, peasants, and charity organizations collected 3,225,295 Norwegian crowns, and the government added 770,000 crowns to this sum. Nansen was proud that the small populated Norway gave more for struggle with famine in Russia than great states. Although this amount was not sufficient to save all of the starving people and many of them died, thousands received help and survived, particularly in Ukraine and the Volga districts (the figures quoted are ranging from 7 to 22 millons). Nansen was made an honorary member of the Moscow Soviet and honored by Thanking Letter of the Russian Supreme Soviet. Together with Maxim Gorky he wrote the book *Russia and Peace* (Russland og freden), where he defended Lenin's harsh methods and argued that they were necessary in order to build up the country.

In recognition of his work for refugees and the famine-stricken, the Nobel Committee in Oslo decided to honor Fridtjof Nansen with the 1922 Nobel Prize for Peace. A Danish publisher, Christian Erichsen, presented him with the same sum. Half of the total amount Nansen spent to create two agricultural stations: one in the Saratov region and the second in Ukraine. Idea of machinery stations and rural agricultural institutes was reborn in the 1930's, when kolkhoses replaced the individual rural economy.

Nansen arranged an exchange of about 1,250,000 Greeks living on Turkish land for about 500,000 Turks living in Greece, with appropriate indemnification and provisions. Nansen's fifth great humanitarian effort was to save the remnants of the Armenian people from extinction. He drew up a political and financial plan for creating a national home for the Armenians in Erivan, which was not accepted by the League of Nations. By personal efforts he settled later some 10,000 Armenians in Erivan and 40,000 in Syria and Lebanon. Impressed by Armenian history and fortune, Nansen wrote the books *Armenia and the Middle East* (1927), *Along Armenia* (1929), and *Across Caucas to Volga*, and the made money-raising tours in USA for the Armenian people.

During all these years Nansen remained interested in Arctic studies. He initiated the creation of the Aeroarctic Society, was elected as its Permanent President in 1924, and took part in the Second Aeroarctic Congress in St. Petersburg in 1928. In 1930 he planned to take part in an Arctic expedition on the dirigible balloon *Count Zeppelin* when he died from a heart attack on May 13, 1930. Nansen was buried on May 17, on the national celebration day of Norway.

The world lost a great humanist, scientist, traveller, and writer. The memory of his humanitarian actions is still alive in different countries and especially in Russia in the hearts of the descendants of millions of saved people.

2. *Discovery of internal waves*

Although mathematical studies of waves on an interface between fluids of different densities was initiated by *Stokes* (1847), physical significance of the phenomenon as well as their existence inside a continuously stratified fluid were not recognized up to the *Fram* expediton. The pioneering paper of *Rayleigh* (1880), containing the definition of buoyancy frequency was not properly written up to the late twentieth of the next century, when *Väisälä* (1925) and *Brunt* (1927) rediscovered this principle parameter for a stratified atmosphere.

Nansen gave a picturesque descriprion of the "dead water" (*Ekman*, 1906) and later interpreted the semidiurnal variation of the ocean temperature as the manifestation of internal waves. The deepness of his understanding is illustrated by a letter to the Russian polar explorer Barony E.V. Tall, in which he recommended to register the lost of the ship velocity, to measure thickness of upper fresh layer, and to measure the difference in salinities below the the ship and under the boat which is towed on different distances from the ship

(*Pasetskii*, 1986). He discussed the problem with V. Bjerknes, who asked his former student to model the "dead water" phenomenon in a laboratory. Nansen provided money for organizing the experiment, Bjerknes found a grant for the work, Ekman performed a comprehensive study of forces acting on the model of *Fram* and visualized the patterns of waves on the interface. Unfortunately, the resulting paper (*Ekman*, 1906) did not receive continuation up to the late fifties of the last century, when *Lighthill* (1978) started to study anisotropic waves and collected theoreticians and experimenters for cooperative studies on the internal waves in a continuously stratified liquid. Results were also applied for qualitative explanation of mysterious phenomena like "turbulence of the clean sky" caused by overturning of internal waves, "mountain lee waves" in the atmosphere and waves behind moving vehicles in the ocean. The number of work increased greatly and setups for internal waves modeling were created in diffent countries. As the results of the studies based of different approaches were in general in agreement while not fitting completely, the classification of infinitesimal periodic motions was done (*Chashechkin* and *Kistovich*, 2004) and its results were used for construction of exact solutions of some inernal wave generation problems (*Chashechkin et al.*, 2004; *Bardakov* and *Chashechkin*, 2004).

3. Classification of infinitesimal periodic motions

Periodic motions are studied on rotating with angular velocity Ω spherical planet with the gravity field characterized by gravity acceleration g. The density profile $\rho(z)=\rho_o\exp(-z/\Lambda)$ is defined by the total salinity $S=\Sigma S_n$ that is of concentration of dissolved or dispersed matter S_n and is characterized by a scale $\Lambda=(d\ln\rho(z)/dz)^{-1}$ and frequency $N=\sqrt{g/\Lambda}$ of buoyancy, which can be supposed to be constant and by $N_c=\sqrt{(N^2c_s^2-g^2)/c_s^2}$ where c_s is sound velocity. Disturbances of density $\rho=\rho(p,S_n,|\mathrm{v}|)$ depend on velocity $\mathbf{v}=(u,\mathrm{v},w)$ pressure p, and S_n.

The set of governing equations in the linear approximation has the form

$$
\begin{aligned}
&\frac{\partial\overline{\rho}}{\partial t}-\frac{\mathrm{w}}{\Lambda}+\nabla\cdot\mathbf{v}=0,\quad \frac{\partial\overline{S}}{\partial t}-\frac{\mathrm{w}}{\Lambda}-\kappa\Delta\overline{S}=0\\
&\frac{1}{c^2}\frac{\partial\overline{p}}{\partial t}-\frac{\mathrm{w}g}{c^2}+\nabla\cdot\mathbf{v}+\kappa\Delta\overline{S}=0\\
&\frac{\partial\mathrm{u}}{\partial t}=-\frac{\partial\overline{p}}{\partial x}+2\Omega\left(\mathrm{v}\sin\varphi-\frac{1}{\sqrt{2}}\mathrm{w}\cos\varphi\right)+\nu\Delta\mathrm{u}+\left(\mu+\frac{\nu}{3}\right)\frac{\partial}{\partial x}\nabla\cdot\mathbf{v}\\
&\frac{\partial\mathrm{v}}{\partial t}=-\frac{\partial\overline{p}}{\partial y}+2\Omega\left(\frac{1}{\sqrt{2}}\mathrm{w}\cos\varphi-\mathrm{u}\sin\varphi\right)+\nu\Delta\mathrm{v}+\left(\mu+\frac{\nu}{3}\right)\frac{\partial}{\partial y}\nabla\cdot\mathbf{v}\\
&\frac{\partial\mathrm{w}}{\partial t}=-\frac{\partial\overline{p}}{\partial z}+\sqrt{2}\Omega(\mathrm{u}-\mathrm{v})\cos\varphi+\nu\Delta\mathrm{w}+\left(\mu+\frac{\nu}{3}\right)\frac{\partial}{\partial z}\nabla\cdot\mathbf{v}-\overline{\rho}g
\end{aligned}
\qquad (1)
$$

where $\bar{\rho}$, $\bar{p}$, $\bar{S}$ are the pressure minus hydrostatic pressure, medium-density perturbation normalized to the density at the reference level $z=0$, and normalized on salinity profile perturbation, φ is the latitude of the observation point, and ν and μ are the first and second kinematic viscosities.

In particular cases the set (1) had to be supplemented by initial and no-slip and no-flux boundary conditions $\mathbf{v}=\mathbf{I}_n\cdot\mathbf{n}=0$ where $\mathbf{n}$ is local normal to the contact solid boundary Σ. In the present study the scale of stratification is large and dissipative coefficients of kinematic viscosity ν and salt diffusion κ_s are small. Axis z of the Cartesian coordinate frame (x,y,z) is directed to zenith and the x- and y-axes are taken so that the corresponding projections of the angular velocity are equal to each other.

For periodic flows $\mathbf{v}=\mathbf{v}_0\,\mathrm{f}_p(\mathbf{k},\omega)$, $P=P_0\,\mathrm{f}_p(\mathbf{k},\omega)$, $\rho=\rho_0\,\mathrm{f}_p(\mathbf{k},\omega)$ where $\mathrm{f}_p(\mathbf{k},\omega)=\exp(i\mathbf{kr}-i\omega t)$ with real positive frequency ω and wave vector $\mathbf{k}=(k_x,k_y,k_z)$, the general solution of to system Eq. (1) can be written as a superposition of elementary waves

$$A=\sum_j\int_{-\infty}^{+\infty}\int_{-\infty}^{+\infty}a_j(k_x,k_y)\exp\Big(i\big(k_{zj}(k_x,k_y)z+k_xx+k_yy-\omega\,t\big)\Big)\,dk_xdk_y\,, \qquad (2)$$

where A is a velocity component, pressure, or density. The summation must be performed over **all** roots of the dispersion equation that are obtained from the condition of non-trivial solvability of the equation set Eq. (1). Coefficients $a_j(k_x,k_y)$ are defined from the boundary conditions. For stationary periodic waves, frequency ω is fixed, and the dispersion equation describes the relation between the wave number components that is expressed $k_{zj}(k_x,k_y)$ for given k_x and k_y values and has a form

$$\begin{aligned}
&D_\kappa\{\omega D_\nu(k)\Big[\omega D_\nu(k)\tilde{D}_\nu(k)+2\sqrt{2}\omega\Omega\big(k_x-k_y\big)\cos\varphi\Big]\\
&-\omega D_\nu(k)N^2\Big[D_\nu(k)+i\big(\mu+\nu/3\big)k_\perp^2\Big]+\\
&+4\omega\Omega^2\Big[N^2\sin^2\varphi-\omega\Big(D_\nu(k)+i\big(\mu+\nu/3\big)f^2(k)\Big)\Big]+\\
&+\frac{\kappa c^2k^2}{\Lambda}\times\Big[\omega k_zD_\nu^2(k)-2\sqrt{2}\omega\Omega^2f(k)\sin\varphi-iD_\nu(k)\Big(gk_\perp^2+\sqrt{2}\omega\Omega\big(k_y-k_x\big)\cos\varphi\Big)\Big]\Big\}=0,
\end{aligned} \qquad (3)$$

where $\tilde{\nu}=4\nu/3+\mu$, $k^2=\Sigma k_i^2$, $k_\perp^2=k_x^2+k_y^2$, $f(k)=\big(k_z\sin\varphi+\big(k_x+k_y\big)\cos\varphi\big)/\sqrt{2}$, $D_\nu(k)=\omega+i\nu k^2$, $\tilde{D}_\nu(k)=\omega+i\tilde{\nu}k^2$, $D_\kappa(k)=\omega+i\kappa k^2$.

The power of the singularly perturbed dispersion equation (the leading, k^8, term involves a small factor $\nu^2\,\tilde{\nu}\,\kappa$) defines the number of roots. When all

dissipative coefficients equal to zero, Eq. (3) becomes a second order equation. So two of eight roots of Eq. (3) are regular in dissipative factors and describe propagating waves. The remaining six roots characterize the set of singular components including coexisting boundary layers. The question what components of motions propagate in the fluid body (only regular or regular and singular components which looks like interfaces in a fluid interior) is still open. The boundary of domains of propagating waves with the real frequency ω existence depends on the ratio of wave and intrinsic rotation and buoyancy frequencies, the compressibility of the medium, and the geometry of the problem.

Solutions of Eq. (3) are further analyzed in the spherical coordinate system (k,Ψ,Θ) introduced in the wave number space (k_x,k_y,k_z) by the relations $k_x = k\sin\Theta\cos\Psi$, $k_y = k\sin\Theta\sin\Psi$, $k_z = k\cos\Theta$. Regular in dissipative factors solutions are written in a power series

$$k_z^{(r)} = k_0 + \sum_{i,j,k=0}^{\infty} b_{ijk}\,\kappa^i \nu^j \mu^k . \tag{4}$$

In the zero approximation all kinetic coefficients in Eq. (4) are equal to zero and solution for k_0 has a form

$$\begin{aligned} k_0 &= \frac{\beta \pm \sqrt{\beta^2 - 4\alpha\gamma}}{2\alpha};\ \alpha = c^2\left(N_c^2\sin^2\theta - \omega^2 + 4\Omega^2 F^2\right) \\ \beta &= 2\sqrt{2}\,\omega\,\Omega g\left(\sin\psi - \cos\psi\right)\cos\theta\cos\varphi; \\ \gamma &= \omega^2\left(\omega^2 - N^2\right) + 4\Omega^2\left(N^2\sin^2\theta - \omega^2\right) \end{aligned} \tag{5}$$

and the domain of existence of propagating waves of frequency ω is defined by condition $\beta^2 - 4\alpha\gamma \geq 0$ and determined by the inequality

$$\begin{aligned} &2\omega^2\Omega^2 g^2 \sin^2\theta\cos^2\varphi\left(\sin\psi - \cos\psi\right)^2 \geq \\ &\geq \frac{c^2\left(4\Omega^2\left(N^2\sin^2\varphi - \omega^2\right) - \omega^2\left(N^2 - \omega^2\right)\right)}{N_c^2\sin^2\theta - \omega^2 + 4\Omega^2 F^2}. \end{aligned} \tag{6}$$

More detailed calculations show that complete regular solution at the first approximation can be written as sum $k_z^{(r)} = k_0 + k_1$ that is phase correction term depends on diffusivity only. Boundaries of frequency ranges depend on many

factors, such as the ratio of wave and intrinsic rotation and buoyancy frequencies, the compressibility of the medium and geometry of the problem.

4. Singular components of periodic motions

Singular components are analyzed on the plane whose direction of the normal is defined by the above mentioned angles ψ and θ in local coordinate frame. Solution of the dispersion equation is a function, describing the dependence of the normal component of the wave number k_n on two components, which are parallel to the plane. Approximate form of the dispersion equation, Eq. (3), defining only the main parts of the singular solutions in the local coordinate frame is

$$\begin{aligned}&\omega\kappa\nu^2 k_n^6 - i\nu\left[\omega^2\nu - \kappa\left(\left(N_c^2 - N^2\right)\sin^2\theta - 2\omega^2\right)\right]k_n^4 + \\ &+\omega\left[\nu\left(N_c^2\sin^2\theta - 2\omega^2\right) + \kappa\left(\left(N_c^2 - N^2\right)\sin^2\theta - \omega^2 + 4\Omega^2F^2\right)\right]k_n^2 - \\ &-i\omega^2\left(N_c^2\sin^2\theta - \omega^2 + 4\Omega^2F^2\right) = 0\end{aligned} \qquad (7)$$

There are no components of wave number, which are parallel to the contact plane in Eq. (7). Thus near the contact surface only solenoidal motions exist with $\mathrm{div}\,\mathbf{v} = 0$. Eq. (7) has three solutions with respect to variable k_n^2

$$\begin{aligned}k_{n\kappa}^2 &= -\frac{\omega}{\kappa}\left[1 + \varepsilon\frac{N^2\sin^2\theta}{\omega^2} - \varepsilon^2\frac{N^2\sin^2\theta\left(N_c^2\sin^2\theta - \omega^2\right)}{\omega^4}\right], \\ k_{n\nu\pm}^2 &= \frac{1}{\nu}\left[\omega_\pm - \omega + \varepsilon\frac{N^2\sin^2\theta}{\omega^2}\frac{N_c^2\sin^2\theta - \omega^2}{N_c^2\sin^2\theta - 2\omega\omega_\pm}\right]\end{aligned} \qquad (8)$$

where $\varepsilon = \kappa/\nu = Sc^{-1}$ is the inverse Schmidt number (typically in a real fluid $\varepsilon << 1$) and

$$\omega_\pm = \frac{N_c^2\sin^2\theta}{2\omega}\left[1 \pm \sqrt{1 + \frac{16\omega^2\Omega^2F^2}{N_c^4\sin^2\theta}}\right]. \qquad (9)$$

Solution $k_{n\kappa}^2$ in Eq. (8) describes density boundary layer of a thickness $\delta_\kappa \approx \sqrt{2\kappa/\omega}$. The two other expressions $k_{n\nu\pm}^2$ in Eq. (9) describe two different viscous boundary layers with transverse scales $\delta_{\nu\pm} \approx \sqrt{2\nu/|\omega_\pm - \omega|}$. All three singular components exist at the same time and their relative thickness depends

upon parameter ε. When the rotation frequency is small $\Omega << N_c^2 \sin\theta/4\omega F$ the viscous boundary layers have essentially different thickness as in this case $\omega_+ \approx N_c^2 \sin^2\theta/\omega$, $\omega_- \approx 4\omega\Omega^2 F^2/N_c^2$ and $\delta_{v+} = \delta_N \sqrt{2\omega^*/\left|N_c^2 \sin^2\theta - \omega^2\right|}$, $\delta_{v-} = \delta_N \sqrt{2/\omega^* \left|1 + 4\Omega^2 F^2/N_c^2\right|}$, where $\delta_N = \sqrt{\nu/N}$ is universal microscale. One of the velocity boundary layers with the thickness δ_{v+} is defined by viscosity, buoyancy frequency and compressibility effects. Parameters of the second layer with thickness δ_{v-} additionally depend upon the rotation frequency Ω. In high frequency limit ($\omega^2 >> N_c^2 \sin^2\theta$) thickness of both boundary layers tends to the Stokes scale $\delta_{v+} \approx \delta_v \approx \sqrt{2\nu/\omega}$.

Taking compressibility into account and disregarding rotation effects ($\Omega = 0$), we conclude from Eq. (6) that propagating three-dimensional acoustic gravity waves exist in two frequency bands $\omega \le N_c$ and $\omega \ge N$. At the low frequency ($\omega \le N_c$) they exhibit the properties of internal gravity waves. Their properties for $\omega \ge N$ approach the isotropic sound. Simultaneously with waves, two types of boundary layers with the characteristic thickness

$$\delta_{St} = \delta_N \sqrt{2/\sin\Theta_\omega}, \quad \delta_i = \delta_N \, 2\sin\Theta_\omega \Big/ \left|\sin^2\Theta - \sin^2\Theta_\omega\right|, \tag{10}$$

where $\delta_N = \sqrt{\nu/N}$, $\Theta_\omega = \arcsin(\omega/N)$, are formed on rigid boundaries. The first of them is similar to the periodic Stokes flow in a homogeneous fluid (*Stokes*, 1847), and the second, whose parameters depend both on the buoyancy frequency N and on the speed of sound c, is specific for stratified media. The universal microscale $\delta_N = \sqrt{\nu/N}$ is common for both boundary layers. The thicknesses of the boundary layers also depend on the slopes of the waves and bounding surfaces.

The frequency band $\omega_- < \omega < \omega_+$ of the existence of inertial gravity waves in stratified rotating incompressible media is limited by the values

$$2\omega_\pm^2 = N^2 + 4\Omega^2 \pm \sqrt{\left(N^2 + 4\Omega^2 \cos 2\varphi\right)^2 + 16\Omega^4 \sin^2 2\varphi},$$

which depend on the latitude of the observation point. Simultaneously with 3D inertial gravity waves, there are two types of boundary layers with the scales

$$\delta_{b\pm} = \delta_N \sqrt{\frac{2}{\left|\omega_\pm - \omega^*\right|}}, \quad \omega_\pm = \frac{\sin^2\Theta}{2\omega^*}\left[1 \pm \sqrt{1 + \frac{16\omega^2\Omega^2 F^2}{N^4 \sin^4\Theta}}\right] \quad \omega^* = \frac{\omega}{N}. \tag{11}$$

Inertial acoustic waves in homogeneous fluid (N = 0) coexist with two separated boundary layers with the thickness

$$\delta_{b\pm} = \sqrt{\nu/\Omega|F \pm \cos\Theta_\omega|}\ , \tag{12}$$

where $\Theta_\omega = \arccos(\omega/2\Omega)$ is the slope of the propagation lines of the inertial acoustic waves to the horizon. One of these waves with thickness δ_{b+} is an analogue of the known Ekman layer. Periodic flows have the properties of inertial and acoustic waves for $\omega << \Omega$ and the opposite case, respectively.

Three-dimensional acoustic waves in a homogeneous fluid ($N = \Omega = 0$) are characterized by the dispersion $\omega^2 = k^2\left(c^2 - i\omega\left(4\nu/3 + \mu\right)\right)$. In this case two sets of boundary layers are joined in the united doubly degenerate Stokes layer with the thickness $\delta_b = \sqrt{2\nu/\omega}$. Perturbations within this layer are transverse with zero divergence of the velocity; i.e., the fluid within it behaves as incompressible.

From the form of the dispersion of three-dimensional periodic perturbations in a homogeneous incompressible fluid, $k^2\left(\omega + i\nu k^2\right)^2 = 0$, when $\left(N = \Omega = \nabla \cdot \mathrm{u} = 0\right)$, it follows that this medium is free of developed propagating waves. Doubly degenerated viscous boundary layer consisting of two periodic Stokes flows with thickness $\delta_b = \sqrt{2\nu/\omega}$ is formed on the rigid oscillating boundary. It means that classical 3D Navier–Stokes equations both for compressible and incompressible fluids form ill-posed problem due to merging of boundary layers. The degeneration of Navier–Stokes equations for homogeneous fluids is removed by specific boundary conditions abolished one of the boundary layers (2D or axial-symmetric problems).

5. Attached internal waves past horizontally moving strip

Calculation of periodic waves beams show that singular components manifest itself near the contact rigid surface as set of boundary layers and inside the wave beam as fine components with their intrinsic spatial and temporal scales (*Chashechkin et al.*, 2004). Here attached internal waves produced by a horizontally moving strip are discussed as example of 2D Navier–Stokes equations exact solution. In this case both the boundary conditions and governing equations are linearized.

In the simplest case when the source of disturbances is uniformly moving horizontal strip the set of governing equations, Eq. (1), is transformed into standard internal wave equation for stream function Ψ defining components of velocity $u_x = \partial\Psi/\partial z$, $u_z = -\partial\Psi/\partial x$

$$\left[\frac{\partial^2}{\partial t^2}\left(\frac{\partial^2}{\partial x^2} + \frac{\partial^2}{\partial z^2}\right) + N^2\frac{\partial^2}{\partial x^2} - \nu\frac{\partial}{\partial t}\left(\frac{\partial^2}{\partial x^2} + \frac{\partial^2}{\partial z^2}\right)^2\right]\Psi = 0 \tag{13}$$

with no-slip boundary conditions at the plane and on the strip of length a

$$\left.\frac{\partial\Psi}{\partial z}\right|_{z=0} = U\,\vartheta\left(x+\frac{a}{2}-Ut\right)\vartheta\left(\frac{a}{2}+Ut-x\right),$$
$$\left.\frac{\partial\Psi}{\partial x}\right|_{z=0} = 0. \tag{14}$$

and attenuation of all disturbances at infinity.

The solution of Eq. (13) is represented as the Fourier integral expansion:

$$\Psi(x,z,t) = \int_{-\infty}^{\infty} e^{-i\omega t}\int_{-\infty}^{\infty}\left[A_w(\omega,k)e^{ik_w(\omega,k)z} + B_i(\omega,k)e^{ik_i(\omega,k)z}\right]e^{ikx}\,dk\,d\omega \tag{15}$$

The roots of the dispersion equation, corresponding Eq. (13) are

$$\omega^2\left(k^2+k_z^2\right) - N^2k^2 + i\omega\,\nu\left(k^2+k_z^2\right)^2 = 0 \tag{16}$$

and include both regular in viscosity (corresponding to waves)

$$k_w^2(\omega,k) = -k^2 + \frac{i\omega}{2\nu}\left[1-\sqrt{1+\frac{4i\nu k^2N^2}{\omega^3}}\right],$$

and singular in viscosity characterizing boundary layers

$$k_i^2(\omega,k) = -k^2 + \frac{i\omega}{2\nu}\left[1+\sqrt{1+\frac{4i\nu k^2N^2}{\omega^3}}\right].$$

Substitution of Eq. (15) into the boundary conditions Eq. (14) leads to a system of algebraic equations for spectral component of amplitude

$$A_w(w,k) = -A_i(\omega,k) = \frac{iU}{\pi k\left(k_w-k_i\right)}\sin\frac{ka}{2}\delta(\omega-kU). \tag{17}$$

Substitution of the solution of Eq. (17) into Eq. (15) and integration give the resultant expression for the stream function

$$\Psi(x,z,t)=\frac{iU}{\pi}\int_{-\infty}^{\infty}\frac{1}{k}\sin\frac{ka}{2}e^{ik(x-Ut)}\frac{e^{ik_w(kU,k)z}-e^{ik_i(kU,k)z}}{k_w(kU,k)-k_i(kU,k)}dk\,. \qquad (18)$$

From Eq. (18), it follows that the field of lee waves is transient ahead and stationary behind the source in the local reference frame (*Bardakov* and *Chashechkin*, 2004).

Visualization of exact solution, Eq. (18), for the vertical component of velocity and vorticity by the modified method of isopleths makes it possible to reveal not only the complete structure of transient leading and stationary attached internal waves, but also details of the fine structure of the boundary layer. Wave perturbations near the plate are more contrasting for the horizontal velocity than for the vertical one (*Fig. 1*). Moreover, the number of perturbation peaks in a single wave field turns out to be different for different wave components (one peak band for the horizontal component and two bands for the vertical one). The phase surface slope to the horizon is characterized by local frequency values.

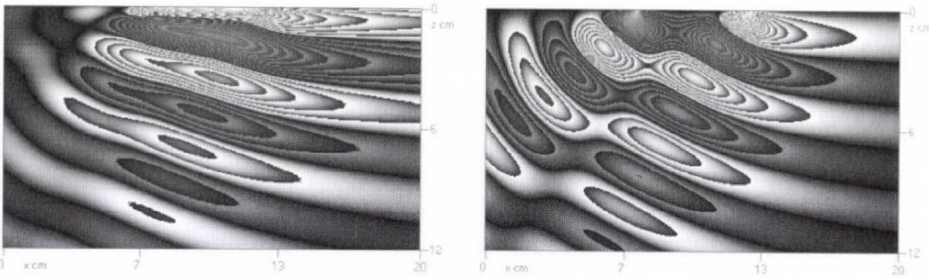

(a) (b)

Fig. 1. Pattern of attached internal waves for horizontal (a) and vertical (b) components of velocity. Bright points on upper horizontal line indicate edges of the strip moving from left to right (T_b = 6.28 s, a =5.5 cm, U = 1 cm/s, λ = 6 cm, Fr = 0.18, Re = 550).

The detailed structure of the module of field velocity within the boundary layer is shown as a magnified continuous-tone image in *Fig. 2*. Both leading and trailing edges of the plate incorporate singular perturbations with the vertical velocity oriented at first toward the fluid and, then, toward the plate. The edge singularities of the horizontal velocity are much less prominent. The thickness of Prandtl's boundary layer (with a typical length scale of $\delta_u = \nu/U$) monotonously increases with distance from the leading edge the same way as in laminar flow of a homogeneous liquid. The boundary layer is detached from the trailing edge into the liquid. The complicated structure of boundary layers at a horizontally moving plate indicates that it is impossible to model the formation

of attached internal waves near a real obstacle in terms of a set of singular mass or force sources.

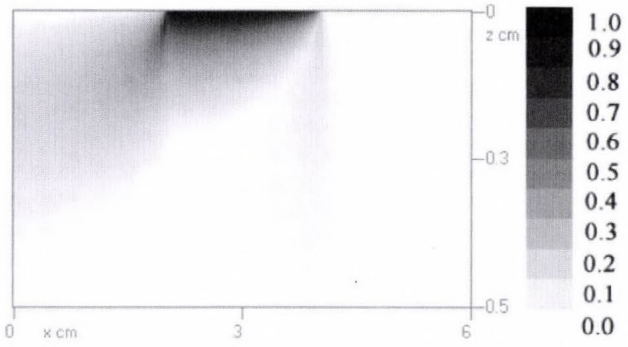

Fig. 2. Module of field velocity within the boundary layer on the strip (T_b = 14 s, a = 2 cm, U = 1 cm/s, λ = 14 cm, Fr = 1.12, Re = 200.

The complex structure of a calculated flow pattern indicates that even on the strip a drag is produced due to emission of waves and viscous lost of energy. Calculated flow pattern fit in laboratory experiments when sensitive Schlieren instrument and markers are used for flow observation.

6. Conclusion

Analysis of complex questions put by F. Nansen shows that internal wave fields have a complex structure and include transient and attached waves and boundary singularities. Therefore, molecular effects play an important role in a stratified flow fine structure formation. Presented classification of 3D periodic motions in fluids generalizes classical Stokes scheme for the wave and accompanying periodic boundary layer. Two different types of viscous boundary layers on rigid boundaries supplement all kinds of waves. The first of them is similar to the periodic Stokes flow, the second one has no analogue in homogeneous fluid. Diffusivity effects are resposible for the formation of new kinds of boundary layers.

In the general case, the dynamics of hydrodynamic systems is determined by nonlinear interaction between all structural elements of flows including both regular (waves, vortices) and singular types (boundary layers and singular components in a fluid interior). In particular, variations in thickness and nonlinear interactions of boundary layers make the generation of internal waves possible even in the cases when the direct excitation is forbidden by the linear theory. Owing to large vorticity, interacting boundary layers may be effective generators of vortex motions. Instruments for experimental studies of fluid dynamics must resolve the fine structure of the smallest elements of flows.

Acknowledgements—The work is supported by the Russian Foundation for Basic Research (Grant 05-05-64090).

References

Bardakov, R.N. and *Chashechkin, Yu.D.*, 2004: Calculation and visualization of two-dimensional joined internal waves in viscous exponentially stratified fluid. *Atmospheric and Oceanic Physics 40*, 470-482.

Brunt, D., 1927: The period of simple vertical oscillations in the atmosphere. *Q. J. Roy. Meteor. Soc. 53*, 30-32.

Chashechkin, Yu.D. and *Kistovich, A.V.*, 2004: Classification of Three-Dimensional Periodic Fluid Flows. *Doklady Earth Science 397*, 667-681.

Chashechkin, Yu.D., Vasiliev, A.Yu., and *Bardakov, R.N.*, 2004: Fine structure of Beams of Three-Dimensional periodic internal wave. *Doklady Earth Sciences 397A*, 816-819.

Ekman, V.W., 1906: On dead water: Being a description of the so-called phenomenon often hindering the headway and navigation of ships in Norwegian Fjords and elsewhere and an experimental investigation of its etc. *The Norwegian North Polar expedition 1893–1896. Scientific Results* (ed.: *F. Nansen*). Vol. 5, 1-152.

Lighthill, J., 1978: *Waves in Fluids.* University Press, Cambridge.

Nansen, F., 1992: Into the country of Future – Great North Marine way from Europe to Asia through Kara Sea (*Fremtidens Land*) (in Russian). Krasnoyarsk, kn. Izdat.

Pasetskii, V.M., 1986: *Fridtjof Nansen* (in Russian). Nauka, Moscow, 336 pp.

Rayleigh, Lord, 1980: Investigation of the character of the equilibrium of an incompressible heavy fluid of variable density. *Proceeding of the London Mathematical Society*. 1883. Vol. 14, 170-177 (Papers V.2, 200).

Stokes, G.G., 1847: On the theory of oscillatory waves. *Transactions of Cambridge Philosophical Society 8*, 441-455. (*Mathematical and Physical Papers 1*, 1880. University Press, Cambridge, 197-229).

Väisälä, V., 1925: Über die Wirkung der Windschwankungen auf die Pilotbeobachtungen. *Soc. Sci. Fenn. Commentat. Phys.-Math. 2*, 19-37.

IDŐJÁRÁS

Quarterly Journal of the Hungarian Meteorological Service
Vol. 111, No. 2–3, April–September 2007, pp. 149–159

A new model for boundary layer flows interacting with particulates in land surface on complex terrain

Kirill Karelsky, Arakel Petrosyan* and **Igor Smirnov**

Space Research Institute of the Russian Academy of Sciences,
*Profsoyuznaya 84/32, Moscow 117997, Russia; E-mail: *apetrosy@iki.rssi.ru*

(Manuscript received in final form January 29, 2007)

Abstract—This paper presents a model describing three-dimensional atmospheric flows with solid particles or aerosols. The model uses the Nigmatulin equations for two-phase atmosphere, which describes lifted atmosphere by ideal gas equations with variable equation of state. The Godunov numerical method based on solution of the one dimensional initial discontinuity decay problem on an interface of two cells of computational grid is applied in this work.

Key-words: boundary layer, Curant-Friedrichs-Levy condition, discontinuity decay problem, Godunov method, grid-scale function, Nigmatulin equations, scheme viscosity, single-velocity model, relaxation, two-phase atmosphere

1. Introduction

In the present work a new physical model of transport of atmospheric impurities (solid particles or heavy gases) by the wind in regions over non-homogeneous or variable in time surfaces is realized. This task is very important for solving the problems linked with preservation and optimal using of the nature. It is necessary to discuss fundamental difficulties, which prevent constructive solution of this problem. Essentially this task can be divided into two subtasks:

- Description of an atmospheric flow in planetary boundary layers under non-homogeneous and/or non-stationary conditions.
- Prediction of the space-time distribution of transported particulates concentration.

* Corresponding author

Well-known traditional theories of boundary layers are applied to atmospheric flows along plane, homogeneous, and stationary surfaces. Along such ideal surfaces, atmospheric boundary layer is also horizontally homogeneous and it is in state of equilibrium. The problem of impurity transport reduces to solving the equation of passive scalar for turbulent flow in boundary layer in this simple situation. However, concentration of particulates or external factors can be beyond the limits of applicability of the passive scalar approximation (*Barenblatt* and *Golitsin*, 1974). In these cases the full system of thermo-hydrodynamic equations of boundary layer with parameterization of sub-grid scale turbulent flows in large eddy simulations method or in Reynolds averaged equations approach fails. Non-homogeneity of the Earth surface and its variations in time change the picture of the flow considerably. When flowing around various obstacles (mountains, buildings, and street canyons), the flow may change both dramatically and gradually. Usually, different space-time variations of planetary surface may appear simultaneously. In such situations it is impossible to create an adequate model of turbulent boundary layer.

The complicated topology of flows in such complex terrain may change the character of the impurity. In such a situation the initially passive impurity may be transformed into active one (affecting the hydrodynamic flow). A well-known example, which should be mentioned, is the origination of dust vortexes (devils) in domains with valleys. Moreover, an initially homogeneous cloud of particulates is transforming to complex non-homogeneous structure. Such structure includes regions with high concentration of impurities, which have its own dynamic behavior. As a result, besides the possibility of changing of impurity character, which was stated above, we face the necessity to analyze the interaction of such formations with the entire cloud of particles, and to predict duration of their life.

In the present work we develop the method describing the transport of particulates in atmospheric boundary layer over complex surface. This method is directed to overcome the difficulties of traditional methods, described above. Besides, it practically expands the opportunity of predictions of transportation of solid particles onto cases when it is impossible to use the approximation of passive scalar or in changes of impurity character in particular domains of cloud. Our model also permits to analyze phenomena, which are driven by complex topology of the flow above obstacles and can describe processes on interface between cloud of solid particles and pure atmosphere. In our model we use Nigmatulin equations (*Nigmatulin*, 1987) describing two-phase medium "gas-particles" by equations of ideal gas with variable equation of state. Effective equation of state for such medium depends upon characteristic size and concentration of spherical particles, and in the limit of absence of solid phase it is converted to usual equations of the ideal gas. Practically, the task to analyze the transport of particles in the atmosphere is reduced to solving equations of ideal gas with variable in space and time equations of state.

It provides the opportunity of describing the loaded and pure atmosphere by the same set of equations with different thermodynamic properties. In fact it means that this system of equations can be applied for modeling the boundary of clouds of solid particles and pure atmosphere. The use of the system of equations of ideal gas with a variable equation of state provides a direct dependence of hydrodynamic flow velocity upon the concentration of solid phase. Practically, it means that there is a possibility of overstepping the limits of applicability of passive impurity approximation.

The main idea of the suggested method is to use the non-viscous equations for modeling the transport of solid particles near a complex surface (*Kulikovskii et al.*, 2001). For free atmospheric flows the Reynolds number, which characterizes the ratio of inertial force to viscosity force in hydrodynamic equations, is very large. That is why nonlinear inertial terms exceed significantly the molecular viscosity terms. The opposite situation appears for atmospheric flows near a surface, where viscosity mechanisms play the main role.

Flows in a viscous atmosphere with arbitrarily small viscosity coefficient have to satisfy non-slip conditions, which demand the full velocity of flow on solid surface to be zero. Undoubtedly, the hypothesis of Prandtl is satisfied (*Schlichting*, 1955). This means that the terms describing dissipation of energy in atmospheric flows are comparable with inertial force for a wide range of conditions in a layer boundering a solid surface. Thus, according to the Prandtl hypothesis, atmospheric flows, characterized by a high Reynolds number, formate a boundary layer. Within this layer a necessary transition from zero value of wind velocity to finite value on external side of a boundary layer is provided. In this case such values on external side of the boundary layer are very similar to the values that appear in an ideal atmospheric flow (*Zilitinkevich*, 1970). Within this layer, the high gradients of velocity field lead to the situation when viscosity effects are comparable to inertial force effects.

Thus, first we have to conciliate the concept of high gradients of wind in a boundary layer, and second, we have to ignore molecular viscosity in equations of the two-phase atmosphere. In this work we suggest to provide the high wind field gradients by means of the scheme viscosity of the numerical algorithm for modeling phenomena near a surface.

We use Godunov method (*Godunov*, 1976) for numerical solution of equations of the two-phase atmosphere. The main idea of Godunov method is to use the generalized solutions of initial discontinuity decay problem with discretization of impulse, mass, and energy conservation laws in each cell of the computational domain. These solutions include local tangential gaps, which do not appear on outer scales, and none the less provide dissipation of kinetic energy, as it is necessary for flows in a boundary layer. Thus, the structure of the used finite difference scheme provides diffusion of ranges with high entropy on all space coordinates and represents qualitatively effects of molecular viscosity. It should be mentioned that influence of the scheme

viscosity is shown more considerably in the situation when boundary layer is loaded with solid particles and in regions with considerable variations of surface relief. In such cases the influence of molecular viscosity also increases in reality. The value of molecular viscosity depends on gradients of sub-grid flows and has a finite limit as the grid of discretisation decreases. Thus, it can be regulated by a choice of the size of the grid. It is clear that for a turbulent flow, the scheme viscosity exceeds one for laminar flows, demonstrating a well-known relation between the turbulent and laminar viscosity.

2. Model of the effective ideal gas for atmosphere with solid particles

The effects of inhomogeneities seriously complicate the investigations of the processes in the atmospheric boundary layers. If we suppose that the size of particles is much smaller than the characteristic scale of those of atmospheric flows, we may describe macroscopic processes in such atmosphere with averaged parameters. We will use the same mass, impulse, and energy conservation equations for the atmosphere lifted by solid particles as for a single-phase medium. In this case it is necessary to take into account boundary conditions on the interface between the phases.

We suppose that volume concentration of solid phase is small enough. Let α_i $(i = 1,2)$ be the part of particulates volume which is occupied by each phase: $\alpha_1 + \alpha_2 = 1$ $(\alpha_i \geq 0)$. Hence, ${\alpha_2}^2 \leq 1$. The solid phase is represented by spherical particles of the radius a. In our model ${\rho_1}^0$ and ${\rho_2}^0$ are the density of the atmosphere and the solid particles, respectively, n is the number of particles of dispersed phase in a unit volume of particulates. Thus, according to our assumption, we have $\alpha_2 = \frac{4}{3}\pi a^3 n$, $\alpha_1 = 1 - \alpha_2$. Weights of phases in a unit volume of the atmosphere are denoted as $\rho_i (i = 1,2)$, and $\rho_1 = {\rho_1}^0 \alpha_1$, $\rho_2 = {\rho_2}^0 \alpha_2$, $\rho = \rho_1 + \rho_2$. We ignore the effects of inertia for moving solid particles, their interactions and collisions, and the process of subdivision and sticking of particles. Viscosity and heat-conduction of fluid and solid phase do not appear in the macroscopic transport of impulse and energy. The values of viscosity and heat-conduction are needed only to describe processes in inter-phases interaction. It allows using non-slip boundary conditions near the solid surface to find parameters of the fluid phase. The density of the atmosphere with solid particles is much less than the density of the substance of solid particles.

Under these conditions the atmosphere with solid particles allows hydrodynamic description. If velocities, **v**, and temperatures of these phases are equal to each other, we can describe such impurity by equations of nonviscous and non-heat-conducting medium of ideal gas. For three-dimensional atmosphere, these equations can be written as:

$$\frac{\partial \rho}{\partial t}+\frac{\partial(\rho v_x)}{\partial x}+\frac{\partial(\rho v_y)}{\partial y}+\frac{\partial(\rho v_z)}{\partial z}=0,$$
$$\frac{\partial(\rho v_x)}{\partial t}+\frac{\partial(p+\rho v_x^2)}{\partial x}+\frac{\partial(\rho v_x v_y)}{\partial y}+\frac{\partial(\rho v_x v_z)}{\partial z}=0,$$
$$\frac{\partial(\rho v_y)}{\partial t}+\frac{\partial(\rho v_x v_y)}{\partial x}+\frac{\partial(p+\rho v_y^2)}{\partial y}+\frac{\partial(\rho v_y v_z)}{\partial z}=0, \qquad (1)$$
$$\frac{\partial(\rho v_z)}{\partial t}+\frac{\partial(\rho v_x v_z)}{\partial x}+\frac{\partial(\rho v_y v_z)}{\partial y}+\frac{\partial(p+\rho v_z^2)}{\partial z}=0,$$
$$\frac{\partial e}{\partial t}+\frac{\partial(e+p)v_x}{\partial x}+\frac{\partial(e+p)v_y}{\partial y}+\frac{\partial(e+p)v_z}{\partial z}=0.$$

Here e is the total energy per unit volume of mixture: $e=\rho(\varepsilon+\frac{v_x^2+v_y^2+v_z^2}{2})$, $\varepsilon(\rho,p)$ is the internal energy determined by the equation of state. In accordance with Nigmatulin's model (*Nigmatulin*, 1987), rheology of mixture can be described by the equation of state of ideal gas with the effective gas constant R:

$$\varepsilon=cT,\ p=\rho RT,\ \text{ where } R=x_1R_1,\ c=x_1c_1+x_2c_2,\ x_i=\rho_i/\rho,\ x_1+x_2=1,$$

R and R_1 are the specific ratios of atmosphere gas mixture and solid particles, respectively, and c, c_1, c_2 are the heat capacities of the atmospheric gas mixture and solid phase under constant pressure accordingly. Thus, to close the system Eq. (1), we add a complimentary equation of change of mass of solid particles:

$$\frac{\partial \rho_2}{\partial t}+\frac{\partial(\rho_2 v_x)}{\partial x}+\frac{\partial(\rho_2 v_y)}{\partial y}+\frac{\partial(\rho_2 v_z)}{\partial z}=0. \qquad (2)$$

The described model of the atmosphere with solid particles is especially useful for modeling processes near a solid surface, because it formally coincides with classic hydrodynamic equations of ideal gas with the recalculated adiabatic index γ (*Ovsyannikov*, 1981): $\gamma=(c+R)/c\le\gamma_1$, and with the recalculated velocity of sound wave: $C_s=\sqrt{\frac{\gamma p}{\rho}}=C_{1s}\sqrt{\frac{\gamma x_1}{\gamma_1}}\le C_{1s}$. The formal coincidence of the equations of clear and lifted atmosphere provides a possibility of modeling nonstationary processes of the particle transport in the atmosphere and motion of dust clouds. In particular, it allows to investigate stability and dynamics of the propagation of a dust cloud and its boundary.

The main limitation of the model is related to ignoring the two-speed effects due to relative motion of the solid phase. It is interesting that the decreasing of the size of solid particles and retaining the same parameters of the atmosphere naturally result in a decrease of relaxation time of velocity and temperature of each phase. If characteristic time scale of the investigated flow is much smaller than the velocity inter-phase relaxation time, we can use a one-speed scheme. According to *Nigmatulin* (1987), for small characteristic Reynolds numbers (Re_1, $2 \leq 1$), describing the atmospheric stream flow over the individual particle, the relaxation time is determined only by viscosity of flowing phase μ_1, by the size and density of the particles substance ${\rho_2}^0$: $t_1 = \frac{2a^2 {\rho_2}^0}{9\mu}$. In the other limit case of high Reynolds numbers (Re_1, $2 \geq 50$), the relaxation time is determined by the density of the ambient atmosphere phase ${\rho_1}^0$, its flow velocities v_0, and the velocities of particles v_2: $t_2 = \frac{16a}{3} \frac{{\rho_2}^0}{{\rho_1}^0} \frac{1}{|v_0 - v_2|} << t_1$.

3. Computational method

To build the finite difference scheme, we use a cubic orthogonal grid with constant step. Initially we have calculation domain size (X + 2) (Y + 2) (Z + 2) with given cell size L. The internal part of the calculation region has the size XYZ and is filled with gas and solid particles with arbitrary initial conditions.

Internal part of the calculation region is surrounded by a layer of gas with arbitrary boundary conditions. We suppose that boundary cells are "infinite" – if any part of the ambient gas or gas with solid particles flow in or flow out from the cell, the thermodynamic parameters of the boundary conditions do not change. Inside of any internal cell, all thermodynamic parameters are isotropic through one time step.

Procedure of digitization of the computational domain consists of putting the space grid with constant step on this domain. In this case, for a cell, which contains elements of relief we set in the following criterion:

- If a volume filled with gas is less than one half of the total volume of the cell, we suppose that this cell completely consists of relief, otherwise we suppose that this cell is completely filled by gas or gas with admixture. In latter case, values of thermodynamic parameters for all cells are supposed to be equal to thermodynamic parameters in real range.

Calculation of all thermodynamic parameters in studied region is carried on the base of integral form of the equations, which in this case looks as follows:

$$
\begin{aligned}
&\iiint \rho_1 dxdydz + \rho_1 v_x dydzdt + \rho_1 v_y dxdzdt + \rho_1 v_z dxdydt = 0,\\
&\iiint \rho_2 dxdydz + \rho_2 v_x dydzdt + \rho_2 v_y dxdzdt + \rho_2 v_z dxdydt = 0,\\
&\iiint \rho_1 v_x dxdydz + (p + \rho_1 v_x^2) dydzdt + \rho_1 v_x v_y dxdzdt + \rho_1 v_x v_z dxdydt = 0,\\
&\iiint \rho_1 v_y dxdydz + \rho_1 v_x v_y dydzdt + (p + \rho_1 v_y^2) dxdzdt + \rho_1 v_y v_z dxdydt = 0,\\
&\iiint \rho_1 v_z dxdydz + \rho_1 v_x v_z dydzdt + \rho_1 v_y v_z dxdzdt + (p + \rho_1 v_z^2) dxdydt = 0,\\
&\iiint e dxdydz + (e + p) v_x dydzdt + (e + p) v_y dxdzdt + (e + p) v_z dxdydt = 0.
\end{aligned}
\tag{3}
$$

Suppose that the integration can be implemented on any close surface in four-dimensional space (x,y,z,t). We consider integrals in expressions of Eq. (3) as surface integrals of the second type, i.e., as integrals on oriented surface. Using the mean theorem we obtain the following equations:

$$
\begin{aligned}
R_1^* &= R_1 + \frac{\tau}{S}(R_1^{(1)} v_x^{(1)} - R_1^{(3)} v_x^{(3)} + R_1^{(2)} v_y^{(2)} - R_1^{(4)} v_y^{(4)} + R_1^{(5)} v_z^{(5)} - R_1^{(6)} v_z^{(6)}),\\
R_2^* &= R_2 + \frac{\tau}{S}(R_2^{(1)} v_x^{(1)} - R_2^{(3)} v_x^{(3)} + R_2^{(2)} v_y^{(2)} - R_2^{(4)} v_y^{(4)} + R_2^{(5)} v_z^{(5)} - R_2^{(6)} v_z^{(6)}),\\
R_1^* v_x^* &= R_1 v_x + \frac{\tau}{L}((P^{(1)} + R_1^{(1)} {v_x^{(1)}}^2) - (P^{(3)} + R_1^{(3)} {v_x^{(3)}}^2)),\\
R_1^* v_y^* &= R_1 v_y + \frac{\tau}{L}((P^{(2)} + R_1^{(2)} {v_y^{(2)}}^2) - (P^{(4)} + R_1^{(4)} {v_y^{(4)}}^2)),\\
R_1^* v_z^* &= R_1 v_z + \frac{\tau}{L}((P^{(5)} + R_1^{(5)} {v_z^{(5)}}^2) - (P^{(6)} + R_1^{(6)} {v_z^{(6)}}^2)),\\
E^* &= E + \frac{\tau}{L}((E^{(1)} + P^{(1)}) v_x^{(1)} - (E^{(3)} + P^{(3)}) v_x^{(3)} + (E^{(2)} + P^{(2)}) v_y^{(2)},\\
&\quad - (E^{(4)} + P^{(4)}) v_y^{(4)} + (E^{(5)} - P^{(5)}) v_z^{(5)} - (E^{(6)} + P^{(6)}) v_z^{(6)}).
\end{aligned}
\tag{4}
$$

The obtained formulas have simple physical meaning and they determine the stream of flowing phase and solid particles, impulse, and energy through a plane surface. In the set of equations of Eq. (4) symbols with superscripts are used to denote the values of thermodynamic parameters at corresponding sides of the cell. Symbols with asterisk denote the values of parameters inside the cells after time τ.

Starting from the initial conditions, our task consists of computing the value of all parameters inside the computational domain after a fixed time τ. Common computation scheme of the single time step, i.e., transition from the state of task on time moment t_0 to the state on time moment $t_0 + \tau$, in general consists of three parts:

- We have to compute the values of thermodynamic parameters on all sides of all cells in our computational domain, as a solution of the corresponding Riemann problem.
- It is necessary to find the maximum value of time step τ, which satisfies the Courant-Friedrich-Levy condition of stability (*Rogdestvenskiy* and *Yanenko*, 1987).
- Finally, we have to compute the values of thermodynamic parameters inside all cells in our computational domain at the next time step, which guaranties the stability of computation.

To finish the description of this method, we describe an algorithm of computation of flux values. The value of hydrodynamic parameters in neighbor cells is assumed to be an initial condition for one-dimension Cauchy problem for two infinite domains of gas. The concentration of dispersion phase in each of the gases is constant during one step of time and accordingly, effective value of polytrophic constant also stays constant during a computation step of time. Thus, our task is to solve the initial discontinuity decay problem for two polytrophic gases with different polytrophic constants. This task is Cauchy problem with constant initial conditions or Riemann problem. The solution of this task is well-known (*Landau* and *Lifshic*, 1988; *Kochin et al.*, 1963; *Billett* and *Toro*, 1997).

4. Modeling results

To illustrate the capabilities of the developed theory, we have carried out numerical computations. These model computations are directed to show main effects, described by the model. We have created a computer code, which computes the problem with any complex relief. It demonstrated strong influence of admixture on the character of flow and formation of the boundary layer due to scheme viscosity on non-homogeneous surface. The computations are carried out for two different types of obstacles and for conditions characteristic for earth winds: the wind velocity is 10 m/s, the pressure is 100 000 Pa, the tdensity of medium and density of admixture are equal to 1.2 kg/m^3 and 0.01 kg/m^3, accordingly. In all cases, the size of the computational domain is chosen in such a way, that the number of cells within the relief or obstacles is about 10% of all cells in the computational domain. Boundary conditions are the following:

- Non-slip condition on solid surface,
- Constant values of stream on boundaries far from obstacle.

Nontrivial influence of particulates (which was taken to be SiO_2, i.e., sand in the experiments) has been obtained and graphically shown in the following figures of distribution of impurity and velocity field. As *Figs. 1* and *2* show, in the region of particulates, there is a zone with increasing and decreasing, horizontal component of the velocity compared to the average value. This fact is explained by the influence of admixture, because admixture has an active influence on forming boundary layer. *Figs. 1* and *2* show two-dimension visualization of moving steam of admixture over different kind of reliefs. Digits mean:

1. stream of particulates,
2. elements of relief,
3. wind direction,
4. domain of turbulence.

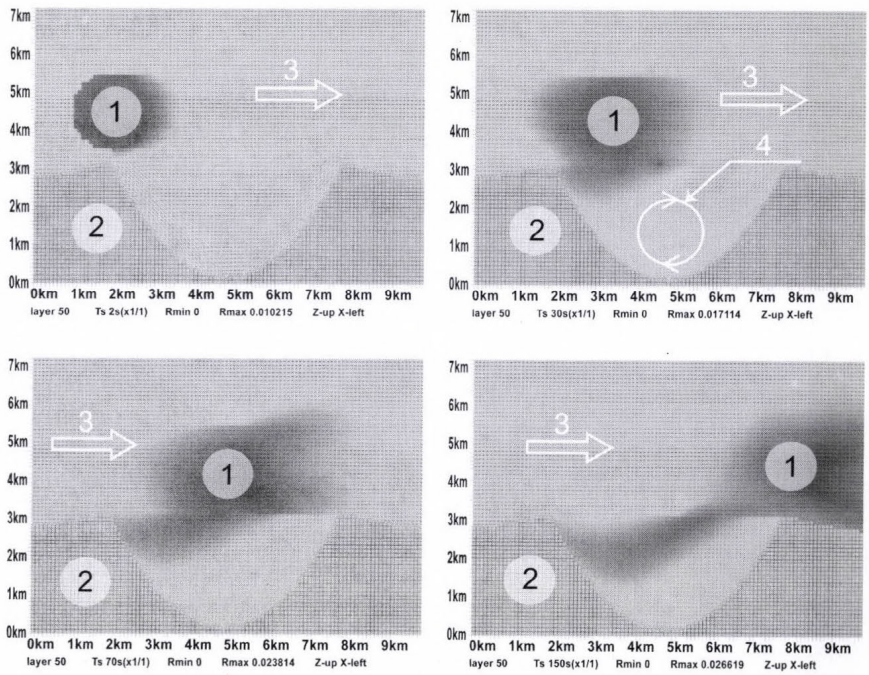

Fig. 1. Dynamics of the particulate cloud moving over a "crater". Tcomp = 2, 30, 70, 150c.

Fig. 3 shows the profiles of the x-component of the velocity at the different grids of computational domain near a surface. It clearly represents the gradients of wind velocity due to scheme viscosity.

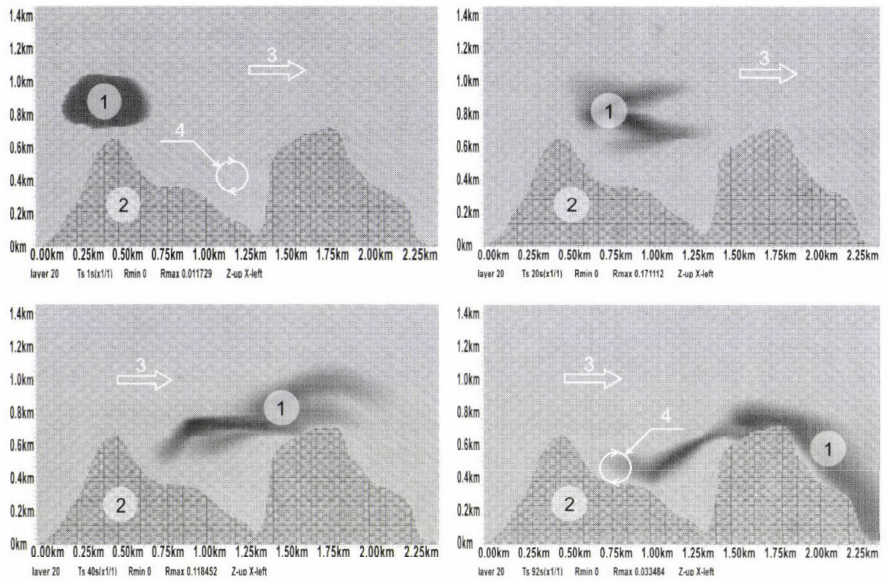

Fig. 2. Dynamics of the particulate cloud moving over "mountains". Tcomp = 1, 20, 40, 92c.

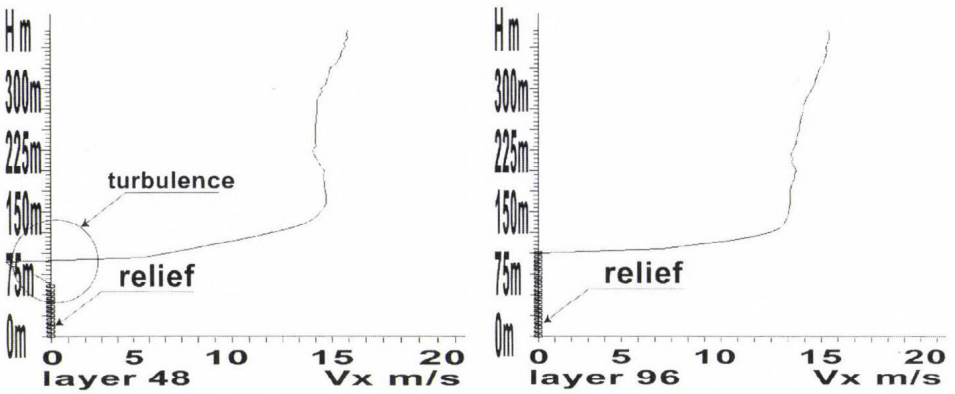

Fig. 3. Profile of the x-component of the velocity (v_x) in different layers.

5. *Conclusions*

At present work a three-dimension model of transport of solid particles and aerosols near a solid surface is proposed. This model is based on two main physical ideas:

- Description of two-phase atmospheric flows on the base of Nigmatulin equations (equations for perfect gases with renormalized equation of state),
- Use of the Godunov method, which has a scheme viscosity, for numerical solution of model equations.

The main advantage of our model the possibility of modeling of two-phase atmospheric flows in a range, where the vertical scale of inhomogeneousness is much higher than the horizontal scale. This is because of using initial fluid equations in integral form, and the idea of scheme viscosity provides good conditions for the stability of computations. As usual, in this case traditional modeling methods as LES and method based on Reynolds averaging face difficulties due to the modeling of turbulence in fractional grids, and these methods are still in the beginning of development. We will provide results of such computations with our method in subsequent papers. We showed, the that presence of two mechanisms of scheme viscosity in the created algorithm, namely, presence of homogeneities of surface and gradients of concentration of solid admixture, allows reproducing dynamic transport of admixture in boundary layer.

References

Barenblatt, G.I. and *Golitsin, G.S.*, 1974: On the local structure of developed dust storms. *J. Atmos. Sci. 31.*

Billett, S.J. and *Toro, E.F.*, 1997: WAF-Type schemes for multidimensional hyperbolic conservation laws. *J. Comput. Phys.*

Godunov, S.K., 1976: *Numerical Solve Multidimensional Tasks of Gas Dynamics*. Nauka, Moscow.

Kochin, N.E., Kibel, I.A., and *Rose, N.V.*, 1963: *Theoretical Hydromechanics*. Phismatgis, Moscow.

Kulikovskii, A.G., Pogorelov, N.V., and *Semenov, A.U.*, 2001: *Mathematic Questions of Numerical Solve of Hyperbolic Systems of Equations*. Phismatlit, Moscow.

Landau, L.D. and *Lifshic, E.M.*, 1988: *Theoretic Physics*. Nauka, Moscow.

Nigmatulin, R.I., 1987: *Dynamics of Multiphase Medium*. Nauka, Phismatlit, Moscow.

Ovsyannikov, L.V., 1981: *Lectures by Base of Gas Dynamics*. Nauka, Moscow.

Rogdestvenskiy, B.L. and *Yanenko, N.N.*, 1978: *Systems of Quasylinear Equations and Their Application in Gas Dynamics*. Nauka, Moscow.

Schlichting, H., 1955: *Boundary-Layer Theory*. McGraw-Hill, New York.

Zilitinkevich, S.S., 1970: *Dynamics of the Atmospheric Boundary Layer*. Gidrometeoizdat, Leningrad.

IDŐJÁRÁS

Quarterly Journal of the Hungarian Meteorological Service
Vol. 111, No. 2–3, April–September 2007, pp. 161–169

Numerical simulation of cross-flow ventilation of farm buildings in a cold, windy coast climate

Thomas K. Thiis, Willy K. Jeksrud† and **Andreas S. Flø**

Department of Mathematical Sciences and Technology,
Norwegian University of Life Sciences,
P.O. Box 5003, N-1432 Ås, Norway; E-mail: thomas.thiis@umb.no

(Manuscript received in final form February 2, 2007)

Abstract—New demands in farming industry in Norwegian sub-arctic regions has caused a need for larger animal buildings. To minimize the cost of the buildings, they are built without insulation. Uninsulated animal buildings in cold climates raise many new engineering challenges. One challenge is to maintain the animal welfare. Because of the lack of insulation, the walls of the buildings are exposed to a high risk of condensation. This is met with a high ventilation rate to remove the excess moisture. The present study is performed on a farm on the coast in northern Norway. Numerical simulations of cross-flow ventilation for animal housing are performed for several wind directions and different openings. Both the internal and external air movements are simulated in the same simulation domain. The ventilation openings in the walls are varied to assure that the animals are not exposed to draught in periods of cold weather and high wind speed. The study results in a graph showing the relationship between wind velocity, temperature, and porosity of the walls of the building.

Key-words: cross-flow ventilation, numerical simulations

1. Introduction

Animal welfare of cattle has been studied by several authors. A useful parameter for assessing animal exposure to climate is the Lower Critical Temperature (LCT). "LCT is the temperature below which the animal will increase its rate of heat production above normal in order to maintain a constant body temperature" (*Gregory*, 1995). LCT varies according to wind speed, the condition of the coat of the animal, and the feeding level. For cattle LCT is reported in *Table 1* (*Holmes* and *Sykes*, 1984)

Table 1 presents the air velocity in two steps, 0.3 m/s and 3.9 m/s, for dry cattle. This is usually the condition of the cattle in the houses in the study. The upper threshold value is probably also an upper practical limit inside the animal

building. If the air velocity should exceed 3.9 m/s, a number of other problems would arise, such as flying debris or dust. In this study, the preferred air velocity inside the animal housing is therefore set to maximum 3.9 m/s in 0.7 m height.

Table 1. Lower critical temperatures (°C) for cattle (*Holmes* and *Sykes*, 1984)

	Maintenance feed				**2 × Maintenance feed**			
	Dry coat		**Wet coat**		**Dry coat**		**Wet coat**	
Wind speed [m/s]	**0.3**	**3.9**	**0.3**	**1.1**	**0.3**	**3.9**	**0.3**	**1.1**
Calves with 40 kg liveweight								
Coat depth 2 cm	9	17	16	24	-9	4	3	16
Adults with 400 kg liveweight								
Coat depth 2 cm	-2	7	6	16	-19	-13	-14	1
Coat depth 3 cm	-7	3	2	11	-36	-20	-22	-5

The climate in Norway varies from cold to polar climate according to the Köeppen climate classification index. The wind climate is also very different in the costal areas compared to the interior of the country. The combination of cold climate and the large moisture emission from the cattle increase the risk of condensation of water on the cold interior surfaces of the animal building. This risk increases even further when the buildings are built without insulation, which is the case for several new animal buildings in Norway. To avoid condensation on interior surfaces, the ventilation rate of the building must be high. To avoid the installation cost of a ventilation system, parts of the walls of the buildings are made permeable, thus the ventilation of the buildings is driven by the wind. The internal climate and the comfort of the animals are thus directly linked to the surrounding climate. The local-scale climate is therefore an important design criterion in the design of new animal buildings. The large differences in local climate will introduce a variety of climate-adapted designs.

Computational Fluid Dynamics (CFD) is a well-known tool determining climate loads on building constructions. It has been used in studies of driving rain, blowing snow, and natural ventilation. *Shklyar* and *Arbel* (2004) performed a study of flow pattern inside and around greenhouses utilizing a similar approach as in the present study.

The indoor temperature should not fall below the LCT at the given feeding level and indoor air velocity. One can assume that the animal coat is dry when the animals are indoors. For high ventilation rates one can also assume that the outside and inside air temperatures are equal. However, measurements of indoor air temperature together with outside air velocity shows that for lower ventilation rates, there is a close correlation between the indoor/outdoor temperature difference and the wind velocity.

1.1. The building in the study

The building in the study is 29 meters long and 18 meters wide. Inside the building, there is a section consisting of the milking area, which is ventilated separately and not included in the calculations. There is also a 1.4 meters high fence dividing the building in two long rows, where the cattle can walk freely around. The longest outer walls of the building consist of a permeable, slotted wall from the eaves and 1 m down. The rest of the wall is non permeable to air. *Fig. 1* shows a sketch of the building.

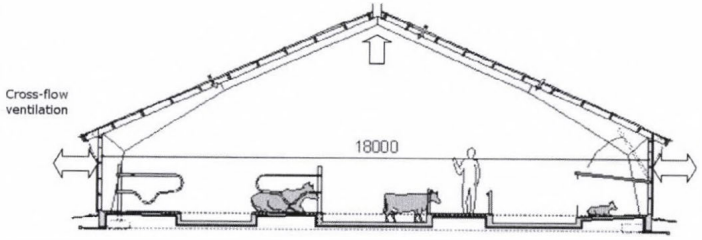

Fig. 1. Section of the building in the study.

2. Methods

2.1. Numerical method

To simulate the air flow around and inside the building, a general-purpose finite volume CFD code was applied. The CFD code solves the well-known incompressible, time averaged Navier-Stokes equations.

The standard k-ε turbulence model is used to close the equations. The turbulence model is known to compute excessive turbulence near the edges of the windward walls, which also can affect the downwind wakes. It is however widely used, and it is capable of producing realistic wind patterns around buildings. The total number of grid cells in the simulations is around 3.6 million with grid refinement near the surfaces.

The simulation of the wind pattern around and inside the building is performed for 12 wind directions: 0, 30, 60, 90, 120, 150, 180, 210, 240, 270, 300, and 330 degrees. These simulations are performed with an inlet wind velocity of 15 m/s at 10 meters height outside the building. It is assumed that the flow pattern inside the building remains independent of the wind velocity. Based on this assumption, the air velocity inside the building is normalized to the wind velocity at 10 meters height. The normalized air velocity is used to determine the indoor air velocity at different wind velocities. To verify that the flow pattern inside the building remains independent of the wind velocity, a range of

simulations has been performed with inlet wind velocity varying according to *Table 1*. In these simulations, the permeability of the wall and the wind direction is kept constant. *Fig. 2* shows the numerical simulation domain.

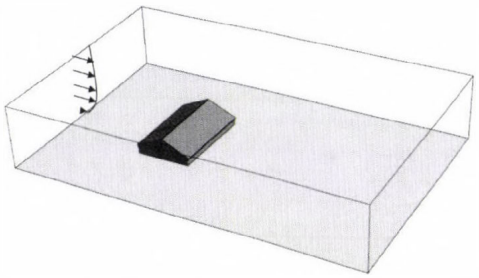

Fig. 2. Numerical simulation domain.

The permeable walls are considered as porous media, and the drag effect is included in the simulations as the source term S_i

$$S_i = C_{R1} u_i - C_{R2} |u| u_i \tag{1}$$

Here C_{R1} and C_{R2} are the linear and quadratic resistance coefficients, respectively. The resistance coefficients are found from solving the flow through the slotted wall with varying slot space, using the CFD solver. *Fig. 3* shows the numerical grid applied in the simulation with 33% porosity, i.e., 33% of the wall is open to air flow.

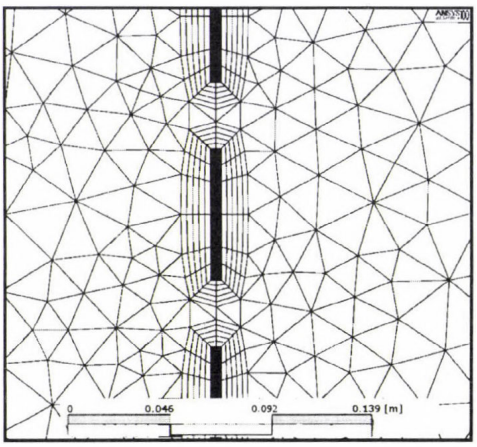

Fig. 3. Numerical grid in the simulation of a 33% slotted wall.

The inlet wind profile follows the logarithmic expression

$$u(z) = \frac{u*}{\kappa} \ln\left(\frac{z}{z_0}\right), \tag{2}$$

where $u(z)$ is the wind speed at height z, z_0 is the roughness of the surface, set to 0.1 m, u^* is the friction velocity set according to *Table 2*, and κ is the von Karman constant, equal to 0.4.

Table 2. Friction velocities used in Eq. (1)

$u(10)$	5	10	15	25
u^*	0.43	0.87	1.30	2.17

The turbulence intensity, i.e., the ratio of the root-mean-square of the turbulent velocity fluctuations and the mean velocity, at the inlet boundary is set to 5%. The outlet boundary is continuative, meaning that the normal derivatives of all quantities are set to zero. On the wall surface boundaries,the boundary conditions are set to "no-slip", i.e., the velocity at the surface is zero. The lateral and top boundaries of the simulation domain have symmetry conditions.

2.2. Permeable wall

To avoid excessive use of grid cells, the slotted walls were modeled as permeable walls with a pressure drop. The pressure drop over slotted walls of different porosity was found simulating the air flow trough the wall, using the CFD solver. The fraction of the wall open to flow and the air velocity were varied to produce the velocity-dependent pressure loss curves. *Miguel* (1998) used a similar procedure on physical measurements of the pressure loss over insect screens.

A section of 3.4 meters of the permeable wall was simulated to minimize any eventual end effects. An example of the numerical grid used in the 33% porosity wall simulation is shown in *Fig. 3*.

3. Results and discussion

3.1. Pressure loss in permeable wall

Fig. 4 shows the results of the simulations of pressure loss in the slotted wall at different air velocities and different porosities. The resistance coefficients used in Eq. (1) are found from these simulations and is shown in *Table 3*.

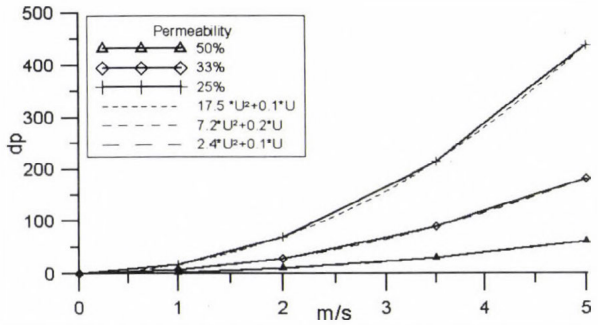

Fig. 4. Pressure loss in slotted walls with different porosity.

Table 3. Linear and quadratic resistance coefficients used in Eq. (1)

50%		33%		25%	
C_{R1}	C_{R2}	C_{R1}	C_{R2}	C_{R1}	C_{R2}
17.5	0.1	7.2	0.2	2.4	0.1

3.2. Air flow around and inside the building

It is assumed that the air inside the building is well mixed and the inside temperature equals to the outside temperature. The air velocity inside the building has a large spatial variability. Therefore, a residential zone is defined, where the climatic conditions should be better than outlined in *Table 1*. The residential zone, where the cattle rests, is indicated in *Fig. 5a* with three lines positioned 0.7 meters above the floor. *Fig. 5b* shows the air velocity along these lines for different wind velocities and a 50% porosity of the wall section.

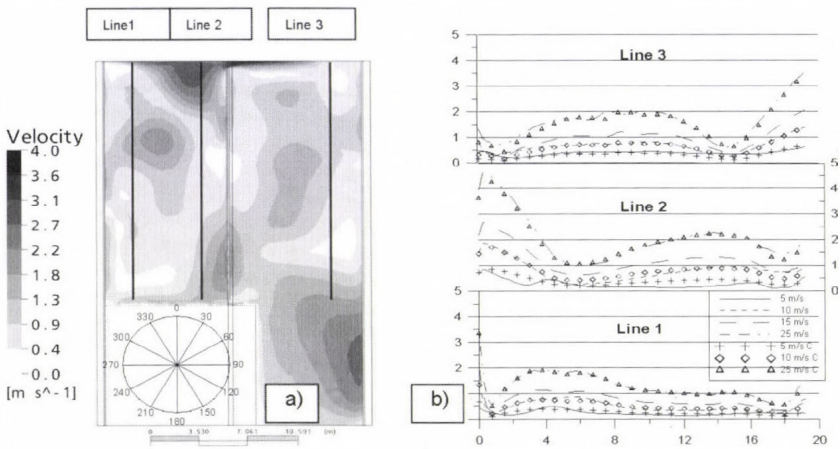

Fig. 5. (a) Position of the residential zone in the building and example of air velocity distribution at 0.7 meters height. (b) Air velocity in the residential zone.

Fig. 5b also shows the validation of the assumption, that the indoor air velocity is independent of the outdoor wind velocity. Points marked with letter C indicate the predicted air velocity along the lines when 15 m/s is used as reference velocity. The correlation between the simulated and predicted velocity with 15 m/s as basis is very good for 25 m/s and 10 m/s, and somewhat poorer for 5 m/s. This means that the indoor flow pattern is nearly independent of the wind velocity, and that it is adequate to use only the simulation with a velocity of 15 m/s at 10 meters height to assess other wind velocities as well.

Fig. 6 shows the maximum allowed wind velocity at 10 meters height outside of the building, above which the air velocity in the residential zone exceeds 0.3 m/s. An interesting feature of the results is that the air velocity in the residential zone is closest to the outdoor wind velocity, when the wind direction is normal to the shorter walls of the building. The reason for this is that the wind velocity is increasing near the upwind edges of the building, and this high speed jet is reattached near the middle of the building with an angle up to 90 degrees. This jet creates a wind environment inside the building, which is poorer than in the case of a wind direction perpendicular to the long wall.

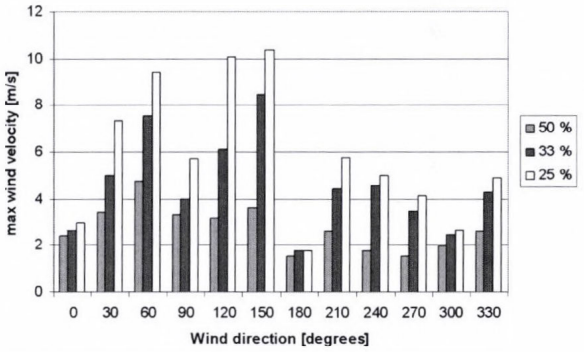

Fig. 6. The maximum allowed wind velocity at 10 meters height.

When the wind direction is normal to the long wall (90° an 270°), the air jet coming trough the air vents is directed above the cattle, driving a low-velocity recirculation flow in the residential zone. When the wind direction is normal to the gable wall, the vortices encircling the building provide a different direction to air entering the building. Air is entering trough the ridge and the sides of the building and a lot of the air is directed towards the floor. As a result, despite the lower air exchange rate for wind directions 0° and 180° found by *Shylar* and *Arbel* (2004), the animal comfort is lower than for wind approaching normal to the longer walls (90° an 270°).

Fig. 7 shows the wind pattern around the building in the case of wind approaching the shortest walls. A similar graph, as showed in *Fig. 6*, is produced for the 3.9 m/s threshold given in *Table 1*. Combining the two graphs produces *Fig. 8*, which shows the allowed combinations of wind velocity (u_{10}), porosity of the wall, and outdoor temperature (T) for wind direction 270°. This is the predominant wind direction at the site, therefore, it is regarded as a "design wind direction". The figure can be used to assess, which porosity the wall should have, based on climatic data.

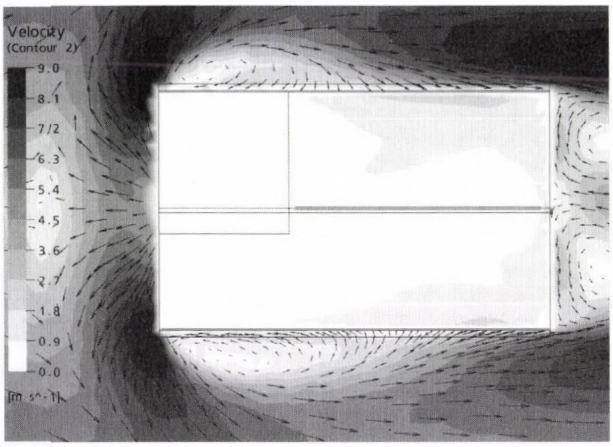

Fig. 7. Exterior wind vectors around the building, and wind velocity contours outside and inside the building.

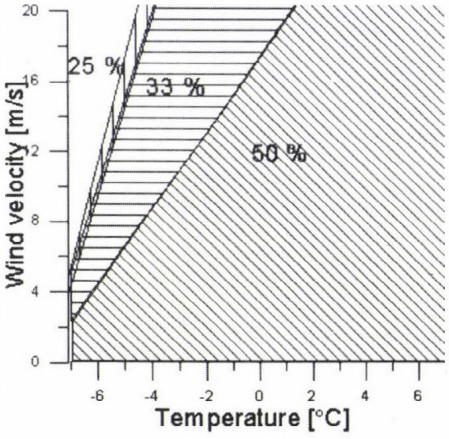

Fig. 8. Allowed combinations of wind velocity, porosity of the wall, and outdoor temperature for wind direction 270°.

4. Conclusions

The method outlined in the paper is capable of calculating the porosity needed to maintain a satisfactory animal comfort in a naturally ventilated animal building with permeable walls. The indoor wind velocity in the animal residential zone is strongly dependent on the outdoor wind direction. This is because the building itself modifies the air-flow pattern creating zones with high and low wind velocities. In some cases the permeable walls are placed in such high velocity zones, which will decrease the indoor animal comfort. This is the reason why the indoor animal comfort is poorest when the wind approaches the shorter walls in the present building design. The knowledge of this mechanism should be included in future designs of naturally ventilated animal buildings.

References

Gregory, N.G., 1995: The role of shelterbelts in protecting livestock: A review. *New Zeal. J. Agr. Res. 38*, 423-450.

Holmes, C.W. and *Sykes, A.R.*, 1984: Shelter and climatic effects on livestock. In *Shelter Research Needs in Relation to Primary Production* (ed.: *J.W. Sturrock*). Water and Soil Misc. Publ. No. 59, 19-35.

Miguel, A.F., 1998: Airflow through porous screens: from theory to practical considerations. *Energ Buildings 28*, 63-69.

Shklyar, A. and *Arbel, A.*, 2004: Numerical model of the three-dimensional isothermal flow patterns and mass fluxes in a pitched-roof greenhouse. *J. Wind Eng. Ind. Aerod. 92*, 1039-1059.

IDŐJÁRÁS

Quarterly Journal of the Hungarian Meteorological Service
Vol. 111, No. 2–3, April–September 2007, pp. 171–183

Surface patterns on thin liquid films, reduced 2D-descriptions. Part I. Perfect fluids

Michael Bestehorn

Department of Theoretical Physics II, Brandenburg Technical University Cottbus, Erich-Weinert-Str 1, 03046 Cottbus, Germany; E-mail: bes@physik.tu-cottbus.de

(Manuscript received in final form February 13, 2007)

Abstract—In this paper we show, how reduced equations for thin fluid layers can be systematically derived from the basic hydrodynamic equations. In this part we consider perfect fluids with zero viscosity. The shallow water equations are derived and extended to the case of a bistable pressure. Numerical solutions show instabilities, coarsening and relaxational behavior versus stationary states. Finally, parametric excitation is included, and a rich spatio-temporal behavior of the surface structures is obtained.

Key-words: hydrodynamic waves, shallow water equations, reduced description

1. Introduction

More or less regularly structured surfaces on fluids or interfaces separating liquids (or a gas and a liquid) are found in nature as well as in technological applications on a large variety of length and time scales. Far from being complete, we mention some examples:

- Water waves caused by wind or sea quakes and land slides (tsunamis) (*Kundu*, 2004; *Faber*, 1995; *Ward* and *Day*, 2001).
- Localized excitations of the surface (solitons), i.e., on shallow water (*Drazin* and *Johnson*, 1989).
- Shear instabilities in clouds or multi-layer systems like the Kelvin-Helmholtz instability or the Rayleigh-Taylor instability (*Kundu*, 2004; *Faber*, 1995; *Chandrasekhar*, 1981).
- Surface deflections in the form of holes or drops of thin fluid films in coating or wetting processes (*Bestehorn* and *Neuffer*, 2001; *Reiter*, 1992).

- Creation and controlled growth of ordered structures in (nano-) technological applications (*Kargupta* and *Sharma*, 2001).
- Biological applications: Behavior of liquid films on leaves or of the tear film on the cornea of the eye; dynamics of thin blood layers; blood clotting.
- Films on the walls of combustion cells.
- Lubrication films in mechanical machines.

Surface patterns may occur due to several mechanisms. One mainly can distinguish between two cases: Patterns excited and organized by some external forces or disturbances (e.g., tsunamis), and those formed by instabilities. The latter may show the aspects of self-organization and will be in the focus of the present contribution (*Haken*, 2004; *Cross* and *Hohenberg*, 1993).

Complicated systems are controlled by a certain set of parameters, which can be accessed from outside. They are named "control parameters". The states of the systems under consideration are described by state variables like temperatures, concentrations, velocity fields, etc. Changing one or more control parameters, the system may reach a certain critical point and an instability may occur. Then the old solution gets unstable and gives way to a qualitatively new behavior. Those instabilities can be regular (periodic) in space and/or time. In that way, new typical length or time scales are created by self-organization (*Haken*, 2004). On the other hand, they can also be homogeneous, stationary, or, the other extreme case, turbulent or chaotic.

The mathematical description of the systems listed above is more or less well known for a long time. Fluid motion is described by the Euler or Navier-Stokes equations, temperature fields by the heat equation, and chemical concentrations by some nonlinear reaction-diffusion equations. The location and spatio-temporal evolution of surfaces or interfaces can be computed by the kinematic boundary conditions, if the velocity of the fluid near the interface is known. All these equations can be coupled and provided with suitable boundary and initial conditions. In that way, rather complicated systems of nonlinear partial differential equations result. Even nowadays, in the age of supercomputers, their further treatment, especially in three room dimensions, remains still a challenge.

On the other hand, solving directly the basic equations, can be considered merely as another experiment. For these reasons, we wish to explore here other methods. In this and in the next contribution we shall describe how to derive reduced 2D descriptions of the fully 3D problems.

2. The shallow water equations

In this section we wish to derive briefly the equations describing the motion of a thin layer of a perfect fluid. They are called *shallow water equations*. Although

the derivation is standard (see, for instance, the textbooks (*Kundu*, 2004; *Faber*, 1995; *Bestehorn*, 2006), we wish to present it here, because it serves as a good example of how 2D equations can be found systematically from a 3D basic problem.

2.1. Potential flow

We consider an incompressible fluid. Its velocity field $\mathbf{v}(\mathbf{r},t)$ is ruled by the Euler equations and the incompressibility condition:

$$\rho\left[\frac{\partial \mathbf{v}}{\partial t}+(\mathbf{v}\cdot\nabla)\mathbf{v}\right]=-\nabla p+\mathbf{f}, \tag{1a}$$

$$\nabla\cdot\mathbf{v}=0, \tag{1b}$$

where $p(\mathbf{r},t)$ is the pressure, ρ is the (constant) density, and $\mathbf{f}(\mathbf{r},t)$ denotes some external forces like gravity, etc. If the fluid is free of vorticity, $\nabla\times\mathbf{v}=0$, the velocity can be expressed by a scalar potential $\Phi(\mathbf{r},t)$:

$$\mathbf{v}(\mathbf{r},t)=\nabla\Phi(\mathbf{r},t). \tag{2}$$

From Eq. (1b) we get the Laplace equation:

$$\Delta\Phi(\mathbf{r},t)=0, \tag{3}$$

which determines the velocity field along with suitable boundary conditions.

2.2. Kinematic boundary conditions

We assume the surface to vary on a large lateral scale compared to the liquid depth. In addition it should be writable as a (smooth) function $h(x,y,t)$. If the fluid moves, the location of the surface is changed according to the *kinematic boundary condition* (*kbc*) (*Fig. 1*):

$$\partial_t h=\mathbf{n}\cdot\mathbf{v}=(1+(\nabla h)^2)^{-1/2}(v_z-v_x\partial_x h-v_y\partial_y h)\approx v_z-v_x\partial_x h-v_y\partial_y h,$$

or, in terms of the potential

$$\partial_t h=\partial_z\Phi-\partial_x\Phi\partial_x h-\partial_y\Phi\partial_y h. \tag{4}$$

Here, $\mathbf{v}$ (and Φ) have to be evaluated at the surface $z = h$, and a small surface slope $(\nabla h)^2 << 1$ is assumed. Inserting Eq. (2) into the Euler equations Eq. (1a) and evaluating them at the surface lead to the other *kbc*:

$$\partial_t \Phi|_{z=h} + \frac{1}{2}(\nabla\Phi)^2{}_{z=h} = -g(h-h_0) - \frac{p(h)}{\rho}, \tag{5}$$

where we consider a constant gravity field in z-direction as external force, and a certain given pressure $p(h)$ at the surface that will be specified later.

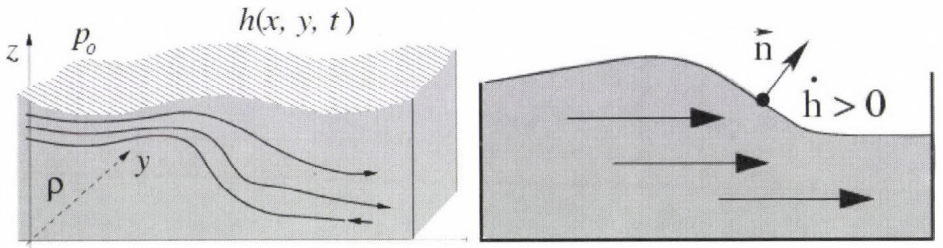

(a) **(b)**

Fig. 1. (a) An (incompressible) fluid with a free and deformable surface located at $z = h(x,y,t)$, on which a constant external pressure p_0 is applied. (b) The location of a certain point of the surface changes if the fluid is in motion.

2.3. Scaling and small parameter

The crucial point in the derivation of the reduced equations is the different scaling used for the vertical and horizontal coordinates. Let h_0 be the uniform depth of the motionless layer and ℓ a certain horizontal length scale (wave length, spatial extension of a front, etc.), then we introduce the dimensionless variables

$$x = \tilde{x}\ell\,,\ y = \tilde{y}\ell\,,\ z = \tilde{z}h_0\,,\ t = \tilde{t}\,\tau\,, \tag{6}$$

and

$$h = \tilde{h}h_0\,, \qquad \Phi = \tilde{\Phi}\frac{\ell^2}{\tau}\,, \tag{7}$$

where τ is a certain time scale that is left arbitrary for the moment. The different length scales define a small parameter

$$\delta = \frac{h_0}{\ell} << 1\,, \tag{8}$$

which can now be used for a systematic expansion. In the dimensionless quantities the basic equations and boundary conditions read (we drop all tildes):

$$(\delta^2\Delta_2 + \partial_{zz})\Phi = 0\,, \tag{9a}$$

$$\partial_t h - \delta^{-2}\partial_z\Phi|_{z=h} = -(\partial_x h)(\partial_x\Phi)_{z=h} - (\partial_y h)(\partial_y\Phi)_{z=h}\,, \tag{9b}$$

$$\partial_t\Phi|_{z=h} + G(h-1) = -p(h) - \frac{1}{2}\left((\partial_x\Phi)^2 + (\partial_y\Phi)^2 + \delta^{-2}(\partial_z\Phi)^2\right)_{z=h}, \tag{9c}$$

$$\partial_z\Phi|_{z=0} = 0\,, \tag{9d}$$

with $\Delta_2 = \partial_{xx} + \partial_{yy}$ as the 2D Laplacian, and the dimensionless *gravitation number* $G = \dfrac{gh_0\tau^2}{\ell^2}$.

2.4. Laplace equation

The next step is to solve the Laplace equation Eq. (9a), iteratively. Therefore, we expand

$$\Phi(\mathbf{r},t) = \Phi^{(0)}(\mathbf{r},t) + \delta^2\Phi^{(1)}(\mathbf{r},t) + \delta^4\Phi^{(2)}(\mathbf{r},t) + \ldots$$

and find from Eq. (9a) in the zeroth order of δ that

$$\partial_{zz}\Phi^{(0)} = 0\,.$$

Because of the boundary condition, Eq. (9d), this can only be solved if it is independent of z:

$$\Phi^{(0)} = \Phi^{(0)}(x,y,t)\,.$$

In the order δ^2 one then finds

$$\partial_{zz}\Phi^{(1)}(\mathbf{r},t) = -\Delta_2\Phi^{(0)}(x,y,t)\,,$$

which can be integrated twice:

$$\Phi^{(1)}(\mathbf{r},t) = -\frac{z^2}{2}\Delta_2\Phi^{(0)}(x,y,t) + \varphi^{(1)}(x,y,t) \tag{10}$$

with an arbitrary function $\varphi^{(1)}$. Up to the second order one gets

$$\Phi(\mathbf{r},t) = \Phi^{(0)}(x,y,t) + \delta^2\left[-\frac{z^2}{2}\Delta_2\Phi^{(0)}(x,y,t) + \varphi^{(1)}(x,y,t)\right] + O(\delta^4)\,. \tag{11}$$

2.5. The shallow water equations

Inserting Eq. (11) into the two kbc-s, Eqs. (9b)–(9c), and yielding up to the lowest order in δ, the shallow water equations are

$$\partial_t h = -h\Delta_2\Phi^{(0)} - (\partial_x h)(\partial_x\Phi^{(0)}) - (\partial_y h)(\partial_y\Phi^{(0)}), \tag{12a}$$

$$\partial_t\Phi^{(0)} = -G(h-1) - p(h) - \frac{1}{2}\left(\partial_x\Phi^{(0)}\right)^2 - \frac{1}{2}\left(\partial_y\Phi^{(0)}\right)^2. \tag{12b}$$

Now we have reached our goal to derive a 2D system starting from 3D fluid motion. Eqs. (12) constitute a closed system of partial differential equations for the evolution of the two functions $h(x,y,t)$ and $\Phi^{(0)}(x,y,t)$. Using Eq. (11), from the latter one finds the velocity field immediately (up to the order δ^2).

2.6. Numerical solutions

Fig. 2 shows numerical solutions of the shallow water equations, left frame in 1D, right frame in 2D. In 1D, traveling surface waves can be seen clearly, which may run around due to the periodic boundary conditions in x. On the other hand, one can recognize a second wave with a smaller amplitude going to the left hand side. Both waves seem to penetrate each other without further interaction. The reason seems to be the smallness of the amplitude, which results in a more or less linear behavior.

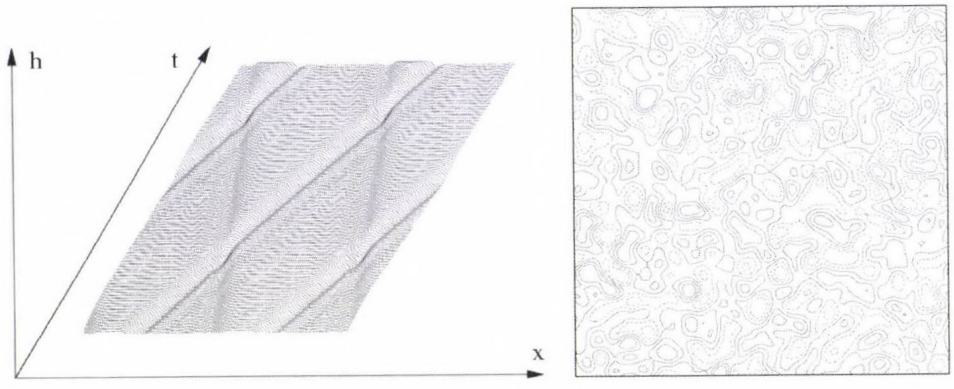

Fig. 2. Numerical solutions of the shallow water equations. (a) Temporal evolution in one dimension. (b) A snapshot in 2D. Dashed contour lines mark troughs, solid ones correspond to peaks of the sea.

In the 2D frame, a snapshot of the temporal evolution of the surface is presented. The initial condition was chosen randomly. For numerical stability reasons, an additional damping of the form

$$\tilde{\nu}\Delta_2\Phi \tag{13}$$

was added to the right hand side of Eq. (12b) in order to filter out the short wave lengths. This could be justified phenomenologically by friction and in the long time limit it leads to a fluid in rest, if only gravity acts.

3. Instabilities

To see if the flat film $h = 1$ is stable against small perturbations, one may perform a linear stability analysis. To this end it is convenient to introduce the (small) variable

$$\eta(x,y,t) = h(x,y,t) - 1 \tag{14}$$

in Eq. (12) and linearize with respect to η and Φ. The two resulting equations can be combined into one wave equation for η or alternatively for Φ:

$$\partial_{tt}\eta - G\Delta_2\eta = 0, \tag{15}$$

where we have assumed constant surface pressure. A solution of Eq. (15) is provided by

$$\eta \sim e^{\lambda t + ikx},$$

from which one finds the dispersion relation

$$\lambda(k) = \pm i|k|\sqrt{G},$$

for waves traveling with the constant phase velocity $\pm\sqrt{G}$.

3.1. Damped wave equation

Since $\mathrm{Re}(\lambda) = 0$, waves do neither growth nor decay in time, they are marginally stable. This changes if damping according to Eq. (13) is included. Then instead of Eq. (15) one finds a kind of telegraph equation having the dispersion relation

$$\lambda(k) = -\frac{\nu k^2}{2} \pm i|k|\sqrt{G - \nu^2 k^2}.$$

Again waves, now with a slightly smaller phase speed, are the solution, but these waves are all decaying in time (if $k \neq 0$), leading finally to a steady state with a flat surface at $h = 1$. So the initial state is now stable.

3.2. Laplace pressure and disjoining pressure

To discuss Eqs. (12) further, we have to elaborate a little on the dependence of the surface pressure on the depth h.

The length scale of the surface structures is proportional to the depth of the fluid layer. If the films are very thin, we expect to have scales in the range or even well below the capillary length

$$a = \sqrt{\frac{\Gamma}{G\rho}}, \tag{16}$$

where Γ denotes the surface tension. Then one has to take into account the additional pressure, which origins from the curvature of the surface, the so-called *Laplace pressure*. It reads for weakly curved surfaces

$$-q\Delta_2 h, \quad q>0. \tag{17}$$

The dimensionless constant q is linked to the surface tension by

$$q = \frac{h_0 \tau^2}{\ell^4 \rho}\Gamma$$

Thus we have to substitute $p(h)$ in Eq. (12b) for the expression

$$p = p_0 - q\Delta_2 h, \tag{18}$$

which changes the dispersion relation to that of (damped) capillary waves

$$\lambda(k) = -\frac{\nu k^2}{2} \pm i|k|\sqrt{G + qk^2 - \nu^2 k^2}\,.$$

Again, no instability with $\mathrm{Re}(\lambda)>0$ can occur.

Now assume, that the pressure p_0 depends also on the absolute value of h in some nonlinear non-monotonic fashion. This can be the case for very thin films, where van der Waals forces between the solid support and the free surface come into play (*Israelachvili*, 1992). But also in thicker films, this should be possible in non-isothermal situations, where the surface temperature and, therefore, the surface tension changes with the vertical coordinate (Marangoni effect).

If we take for instance the polynomial (*Fig. 3a*)

$$p_0 = h(h-1)(h-2) \tag{19}$$

linearization around $h = 1$ leads to the growth rates (*Fig. 3b*)

$$\lambda_{12}(k) = -\frac{\nu k^2}{2} \pm i\left|k^2\right| \sqrt{p'_0 + G + qk^2 - \nu^2 k^2}\,, \tag{20}$$

where

$$p'_0 = \left.\frac{dp_0}{dh}\right|_{h=h_0}$$

and h_0 is the conserved mean thickness of the film. An instability occurs if the expression under the integral can be negative, i.e., for $p'_0 + G < 0$

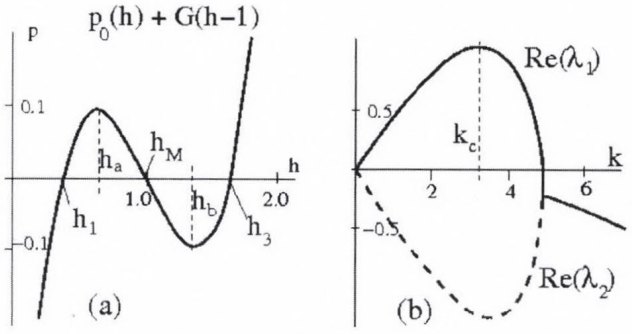

Fig. 3. (a) Non-monotonic generalized pressure with p_0 from Eq. (19). Between the spinodals h_a and h_b, the flat surface is unstable and pattern formation sets in. The binodals h_1 and h_3 follow from a Maxwell construction. (b) Eigenvalues Eq. (20) for the supercritical case.

This corresponds to the region of initial thickness, where the generalized pressure

$$p_0 + G(h-1) \tag{21}$$

has a negative slope (*Fig. 3a*). The two extrema, h_a and h_b are called *spinodals*. For $h_a<h_0<h_b$ the flat film is unstable with respect to infinitesimally small perturbations. The points h_1 and h_2 (the *binodals*) can be found for a general form of the pressure from a Maxwell construction. For the special form of Eq. (19) they coincide with the zeros of Eq. (21). Films having an initial depth in the two regions $h_1 < h_0 < h_a$, $h_b < h_0 < h_3$ are meta-stable. A finite disturbance is necessary to bring the system to an absolutely stable state, that consists of a structured surface. In these regions, pattern formation by nucleation is expected.

Fig. 4 shows a numerically determined time series of a random dot initial condition. The mean thickness h_0 was chosen in the unstable region on the right hand side of the Maxwell point h_M of *Fig. 3a*. The formation shows clearly traveling waves in the linear phase, followed by coarsening to a large scale structure, in this case to one big region of depression, or a hole. This hole gets more and more symmetric, while the velocity decays due to the friction term. Finally, a steady state of a circular big hole remains.

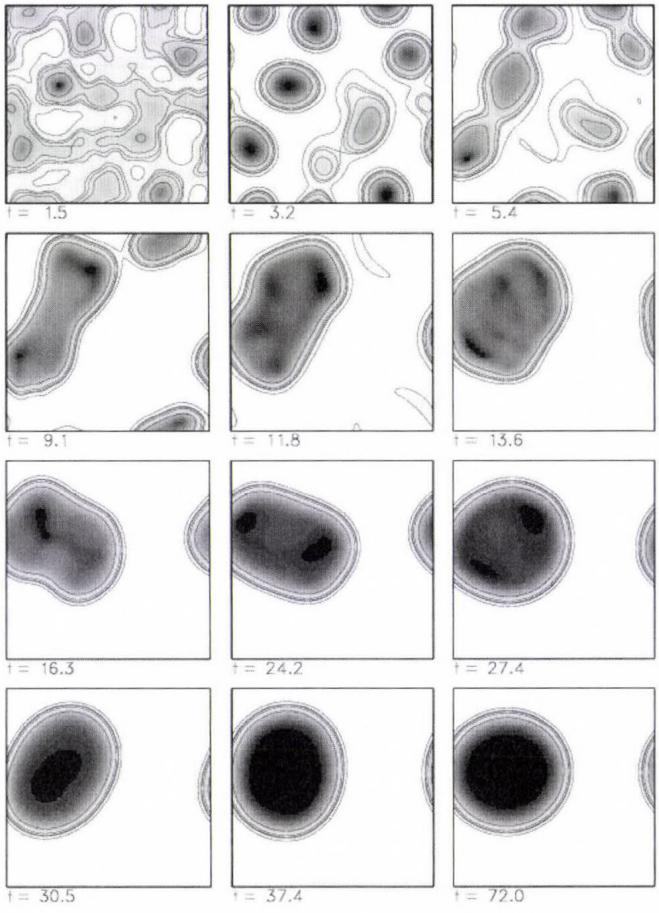

Fig. 4. Time series from a numerical solution of Eq. (12) with damping Eq. (13) and bistable pressure (Eqs. (18), (19), and (21)). Coarsening dominates the non-linear evolution, and eventually, a stationary circular region of surface depression (a hole) remains. Parameters: G=0.5, ν=0.02, q=0.01, h_0=1.3. Periodic boundary conditions in both horizontal directions have been used.

3.3. Parametric excitation of a thin bistable fluid layer

One way to replace the energy lost by a damping according to Eq. (13) is to accelerate the whole layer periodically in vertical direction. This was done first in an experiment by Michael Faraday in 1831. He obtained regular surface patterns mostly in the form of squares (*Faraday*, 1831).

Faraday patterns can be seen as a solution of the shallow water equations, if the gravity constant G is modulated harmonically (*Bestehorn*, 2006):

$$G(t) = G_0 + G_1 \cos(\Omega t). \tag{22}$$

A linear stability analysis leads to the Mathieu equation (now with v=q=p_0=0) (*Abramowitz* and *Stegun*, 1972):

$$\partial_{\tilde{t}\tilde{t}}\,\eta + (b^2 + 2a\cos(2\tilde{t}))\,\eta = 0 \tag{23}$$

with

$$b^2 = \frac{4G_0 k^2}{\Omega^2}, \qquad a^2 = \frac{2G_1 k^2}{\Omega^2}, \tag{24}$$

and the rescaled time $\tilde{t} = t\Omega/2$. The flat film is unstable if frequency and amplitude fall into certain domains, the so-called *Arnold tongues* (*Fig. 5*). There one usually finds squares for not too supercritical values.

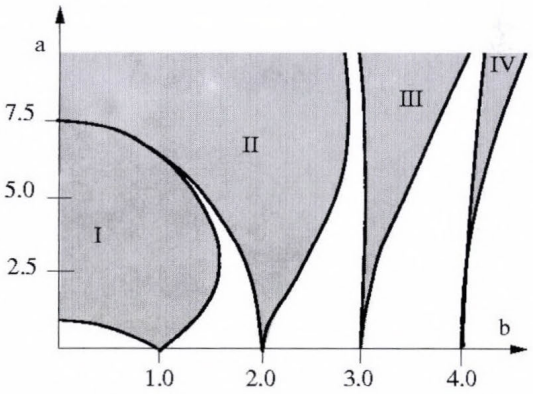

Fig. 5. The stability chart of the Mathieu equation (Eq. (23)) without damping, Arnold tongues. In region I, the pattern oscillates with the half of the driving frequency Ω.

Instead of presenting these results, we finally show a numerical solution of the full equations with v, q, p_0 having the same values as above, but now with

an additional periodic excitation (*Fig. 6*). Coarsening is still present, but now oscillating drops emerge in the form of stars. No time stable structure is found in the long time limit.

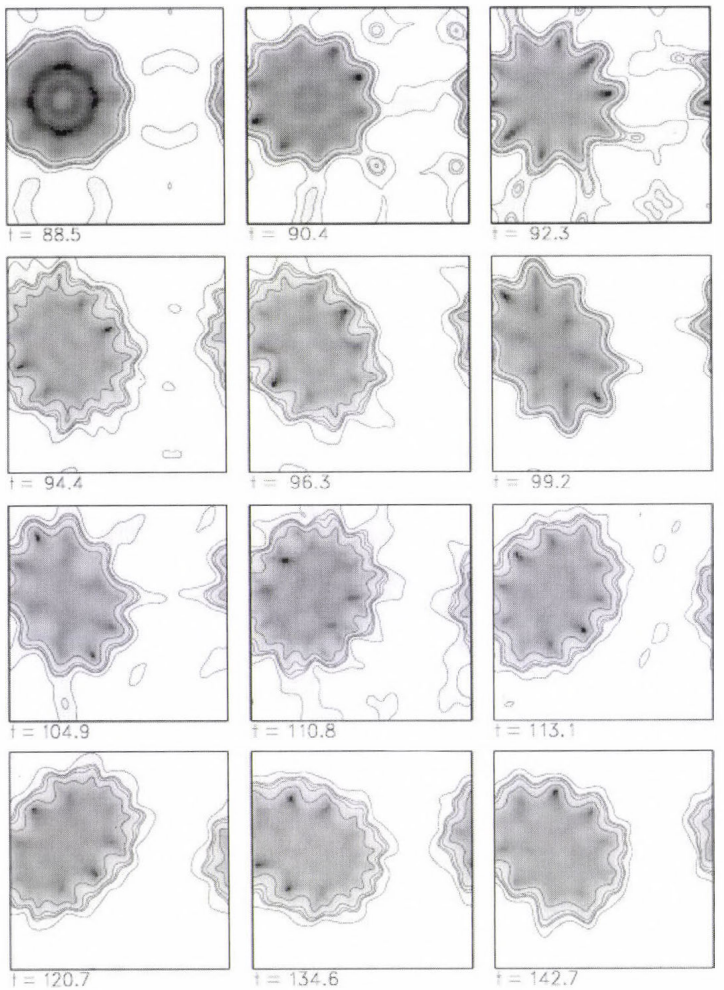

Fig. 6. Continuation of the series of Fig. 4, but with additional parametric excitation according to Eq. (22), switched on at t=72. Instead of stationary patterns, pulsating stars are found.

References

Abramowitz, M. and *Stegun, I.A.*, 1972: *Handbook of Mathematical Functions*. Dover, New York.

Bestehorn, M., 2006: *Hydrodynamik und Strukturbildung*. Springer, Berlin.

Bestehorn, M. and *Neuffer, K.* , 2001: Surface patterns of laterally extended thin liquid films in three dimensions. *Phys. Rev. Lett. 87,* 046101.

Chandrasekhar, S., 1981: *Hydrodynamic and Hydromagnetic Stability*. Dover, New York.

Cross, M.C. and *Hohenberg, P.C.*, 1993: Pattern formation outside equilibrium. *Rev. Mod. Phys. 65,* 851-860.

Drazin, P.G. and *Johnson, R.S.*, 1989: *Solitons: An Introduction*. Cambridge University Press.

Faber, T.E., 1995: *Fluid Dynamics for Physicists*. Cambridge University Press.

Faraday, M., 1831: *Philos. Trans. R. Soc. London 121,* 319 pp.

Haken, H., 2004: *Synergetics. Introduction and Advanced Topics*. Springer, Berlin.

Israelachvili, J.N., 1992: *Intermolecular and Surface Forces*. Academic Press, London.

Kargupta, K. and *Sharma, A.*, 2001: Templating of thin films induced by dewetting on patterned surfaces. *Phys. Rev. Lett. 86,* 4536.

Kundu, M.P.K., 2004: *Fluid Mechanics*. Academic Press.

Reiter, G., 1992: Dewetting of thin polymer films. *Phys. Rev. Lett. 68,* 75-85.

Ward, N. and *Day, S.*, 2001: Cumbre Vieja Volcano – Potential collapse and tsunami at La Palma, Canary Islands. *Geophys. Res. Lett. 28,* 3397.

IDŐJÁRÁS

Quarterly Journal of the Hungarian Meteorological Service
Vol. 111, No. 2–3, April–September 2007, pp. 185–198

Surface patterns on thin liquid films, reduced 2D-descriptions. Part II. Viscous fluids

Michael Bestehorn

Department of Theoretical Physics II, Brandenburg Technical University Cottbus, Erich-Weinert-Str 1, 03046 Cottbus, Germany; E-mail: bes@physik.tu-cottbus.de

(Manuscript received in final form February 13, 2007)

Abstract—We show how a reduced equation describing the spatio-temporal evolution of the surface of a thin viscous liquid film can be systematically derived from the basic hydrodynamic equations. This equation is called thin-film equation. A special form of the interaction between free surface and solid substrate of the film, that has attractive long range and repelling short range properties, is discussed. The formation of holes, drops (spinodal dewetting), as well as nucleation is demonstrated.

Key-words: thin film instabilities, wetting, surface patterns

1. Introduction

In this contribution, we wish to study pattern formation of the surface of thin viscous films. In thin or ultra-thin films, fluid motion described by the velocity field $\mathbf{v}(\mathbf{r},t)$ is usually very slow, and the whole layer can be considered as a boundary layer, where viscous forces are much larger than inertial forces. For that case it is sufficient to consider the Stokes equation

$$\eta\nabla^2\,\mathbf{v}=\nabla P, \tag{1}$$

where η denotes the viscosity of the fluid. Again we assume the fluid to be incompressible:

$$\nabla\cdot\mathbf{v}=0. \tag{2}$$

Further, we restrict us to the case that external terms have a potential, which can be included into the "generalized" pressure: $P = p + U$.

Surface patterns of thin liquid films on a solid support were studied during the last decade in numerous experimental and theoretical contributions (*Rehse et al.*, 2001; *Rockford et al.*, 1999; *Oron et al.*, 1997; *Pototsky et al.*, 2004; *Reiter*, 1992; *Reiter et al.*, 1999; *Jacobs et al.*, 1998; *Colinet et al.*, 2001). Most of the theoretical works is based on an interface equation, often called thin film equation, describing the location $z=h(x,y,t)$ of the free surface of the liquid (*Oron et al.*, 1997; *Vrij*, 1966; *Pismen* and *Pomeau*, 2000; *Bestehorn* and *Neuffer*, 2001). This equation can be derived from Eqs.(1)–(2) using the lubrication approximation, what we shall work out next.

2. *The thin film equation*

2.1. The lubrication approximation

For the sake of simplicity, we shall restrict the derivation of this section to one spatial dimension, say x. The final result will be given also in 2D (for more details see in *Oron et al.* (1997)). As above, the aim is to find an equation for the surface location $h(x,t)$ of the liquid. Such an equation is already provided by the kinematic boundary condition:

$$\partial_t h = v_z|_h - v_x|_h \partial_x h. \tag{3}$$

To compute v_z at the surface $z=h$, one integrates the continuity equation, Eq. (2) with respect to z and finds with the bottom boundary condition $v_z(z=0)=0$, that

$$\int_0^{h(x,t)} \partial_x v_x dz + v_z|_h = 0.$$

Extracting the derivative from the integral yields

$$v_z|_h = -\partial_x \int_0^{h(x,t)} v_x dz + v_x|_h \partial_x h,$$

and inserting into Eq. (3), the desired equation for $h(x,t)$ is

$$\partial_t h = -\partial_x \int_0^{h(x,t)} v_x dz, \tag{4}$$

or in two horizontal dimensions it is

$$\partial_t h = -\nabla_2 \cdot \int_0^{h(x,y,t)} \mathbf{v}_H dz, \tag{5}$$

where $\mathbf{v}_H = (v_x, v_y)$ denotes the horizontal velocity components.

To close the equation, it is necessary to compute v_x (or $\mathbf{v}_H$) as a function of h. This can be done by solving the Stokes equation. It reads, using the same scaling as in Part I,

$$(\delta^2 \partial_{\tilde{x}\tilde{x}} + \partial_{\tilde{z}\tilde{z}})\tilde{v}_x = \partial_{\tilde{x}} \tilde{P}, \tag{6a}$$

$$\delta^2 (\delta^2 \partial_{\tilde{x}\tilde{x}} + \partial_{\tilde{z}\tilde{z}})\tilde{v}_z = \partial_{\tilde{z}} \tilde{P}, \tag{6b}$$

with dimensionless velocity and pressure:

$$v_x = \tilde{v}_x \frac{\ell}{\tau}, \qquad v_z = \tilde{v}_z \frac{d}{\tau}, \qquad P = \tilde{P} \frac{\eta}{\delta^2 \tau},$$

where we use now d instead of h_0 for the uniform depth of the layer at rest. In the limit $d/\ell = \delta \longrightarrow 0$, it follows from (6b), that

$$\partial_{\tilde{z}} \tilde{P} = 0 \qquad \text{or} \qquad \tilde{P} = \tilde{P}(\tilde{x}).$$

Thus, one can integrate Eq. (6a) twice over $\tilde{z}$ and finds with the no-slip condition $\tilde{v}_x(\tilde{x},0) = 0$, that

$$\tilde{v}_x(\tilde{x},\tilde{z}) = f(\tilde{x})\tilde{z} + \frac{1}{2}(\partial_{\tilde{x}} \tilde{P}(\tilde{x}))\tilde{z}^2, \tag{7}$$

with a function $f(\tilde{x})$, which can be determined by the boundary conditions. To this end we consider a constant surface tension. Then the horizontal component of the surface stress has to vanish at the free surface:

$$\eta \partial_z v_x \big|_{z=h} = 0.$$

Inserting Eq. (7) leads to $f(\tilde{x}) = -(\partial_{\tilde{x}} \tilde{P})h$. Substituting everything into Eq. (4) and integrating by $\tilde{z}$ finally yields (all tildes omitted)

$$\partial_t h = -\partial_x \left[-\frac{h^3}{3} \partial_x P \right], \tag{8}$$

or in two dimensions

$$\partial_t h = -\nabla_2 \cdot \left[-\frac{h^3}{3} \right] \nabla_2 P . \tag{9}$$

This is the basic equation for the evolution of the surface of a thin film in the lubrication approximation. It is called the *thin film equation.*

2.2. Laplace pressure and gravity

To discuss Eq. (9) further, one has to express the pressure as a function of the depth:

$$P = P(h),$$

as we shall do now. To include the influence of gravity, one adds the gravity potential ($\rho g\, z$) to the pressure and evaluates it at the surface $z=h$. In the scaling of Eq. (9), the total pressure then reads

$$P = p_0 + G(h-1) \tag{10}$$

with the *gravitation number*

$$G = \frac{d^3 g \tau}{\ell^2 \nu}.$$

If the films are very thin, we expect to have a surface structure with a length scale in the range of or even well below the capillary length

$$a = \sqrt{\frac{\Gamma}{G\rho}}, \tag{11}$$

where Γ denotes the surface tension. Then one has to take into account the additional pressure, which origins from the curvature of the surface. Therefore, we add the *Laplace pressure* to P which reads for weakly curved surfaces

$$-q\Delta_2 h, \quad q>0. \tag{12}$$

The constant q is linked to the so-called capillary number C and follows from scaling as

$$q = \Gamma \frac{\tau d^3}{\ell^4 \eta} = \delta^2 / C .$$

Thus for $P(h)$ we have to substitute the expression

$$P = p_0 + G(h-1) - q\Delta_2 h \tag{13}$$

in Eq. (9), which yields

$$\partial_t h = \nabla_2 \cdot \left[\frac{h^3}{3} \nabla_2 (Gh - q\Delta_2 h) \right]. \tag{14}$$

The stability of a flat surface with thickness h=1 is examined by introducing small deviations:

$$h(x,y,t) = 1 + \eta(x,y,t),$$

and linearizing with respect to η:

$$\partial_t \eta = \frac{1}{3} \left(G\Delta_2 \eta - q\Delta_2{}^2 \eta \right). \tag{15}$$

Assuming plane waves with exponential behavior in time:

$$\eta \sim e^{\lambda t + ikx},$$

one finds the growth rate for the dispersion relation:

$$\lambda = -\frac{1}{3}(Gk^2 + qk^4).$$

Obviously, λ is always real, and for positive G and q and finite k it is always less than zero. Thus the flat film is always stable, both gravity and Laplace pressure act stabilizing.

However, this can be changed if the system is put "upside down", leading to negative G. In the experiments this can be realized by fixing a thin film on the underside of a horizontal plane (*Fig. 1*, left frame). Gravity is now destabilizing for all wave vectors, which have a length less than the cut-off (*Fig. 1*, right frame):

$$k_0 = \sqrt{-\frac{G}{q}},$$

a value that can be expressed by the capillary length a, already defined in Eq. (11), if one goes back to dimensional values:

$$k_0 = \sqrt{\frac{g\rho}{\gamma}} = \frac{1}{a}.$$

The numerical solution of the full Eq. (14) is not very instructive. In the first phase, periodic instabilities with $k \approx k_c$ occur and grow until h takes zero values. Physically this corresponds to a rupture of the film, beyond which the thin film equation cannot be used.

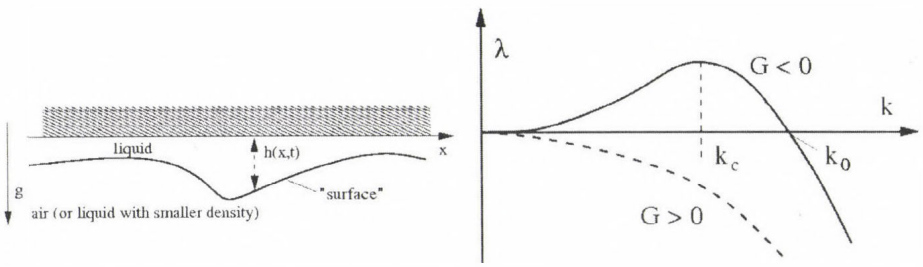

Fig. 1. Left: Sketch of a thin liquid film fixed under a solid plane. The plane surface is unstable due to gravity forces. Fingers are formed and finally the film ruptures.

Right: Growth rates of periodic disturbances of the plane surface with wave number k. The situation shown in the left frame corresponds to the solid line $G<0$ in the right ones. Waves having a wave number $k<k_0$ grow exponentially, the mode with $k=k_c$ has the largest growth rate (most dangerous mode). For $G>0$, the flat film is always stable.

2.3. The disjoining pressure and ultra-thin films

Another instability mechanism is encountered in very thin (ultra-thin) films, where the thickness is some 100 nm or even less. Then, van der Waals forces between free surface and solid substrate can no longer be neglected (*Israelachvili*, 1992).

The van der Waals force depends on the distance between the surface and support, which is the depth h. One can show that it is proportional to h^{-4}. It can be taken into account by adding the interaction potential

$$\Phi(h) = \frac{A_H}{h^3},$$

to the generalized pressure, Eq. (13), where A_H is the *Hamaker constant*. The function Φ is called *disjoining pressure*. If we neglect gravitation for the moment (it plays no role in ultra-thin films), the expression for the total pressure reads

$$P = p_0 + \frac{A_H}{h^3} - q\Delta_2 h. \tag{16}$$

If $A_H>0$, the pressure increases with decreasing depth and an instability may occur. Mathematically this corresponds to the condition (prime means derivative with respect to h):

$$P' = \Phi' < 0,$$

which is the case if $A_H>0$. The flat film is unstable for all initial depths, if the Hamaker constant is positive. As in the case of the Rayleigh-Taylor instability, the dynamics starts with the formation of periodic surface structures followed by a rupture.

On the other hand, there can also exist a repelling force between the surface and substrate, which is modeled taking $A_H<0$ and stabilizes the flat surface. Normally, attractive and repelling forces have different ranges. Usually, the repelling force is short range, the attractive is long range. Then, the initially "thick" film can be unstable due to the attraction, but rupture can be avoided by repulsion. In this way completely dry regions cannot exist, but the substrate remains always covered by an extremely thin film (some nm), called *precursor film*.

The complete expression for such an attractive/repulsive disjoining pressure may read

$$\Phi(h) = \frac{A_n}{h^n} - \frac{A_m}{h^m}, \qquad m>n,$$

with the two positive Hamaker constants A_n and A_m. Different models were discussed in *Oron et al.* (1997) in detail. We shall restrict us here to the "Lennard-Jones potential", which results for n=3 and m=9. Examining the derivative of Φ shows that layers which have a depth bigger than

$$h_a = \left(\frac{3A_9}{A_3}\right)^{1/6}$$

are always unstable. Especially arbitrarily thick films are unstable in this model. This is of course not realistic and has its reason in the neglect of the gravitational force in Eq. (16). If this is also included, one finds, instead of Eq. (16),

$$P = p_0 + \frac{A_3}{h^3} - \frac{A_9}{h^9} + G(h-1) - q\Delta_2 h. \tag{17}$$

The lower and upper stability bounds h_a, h_b for the depth are then solutions of the polynomial

$$Gh^{10} - 3A_3h^6 + 9A_9 = 0,$$

or they can be taken graphically from *Fig. 2*.

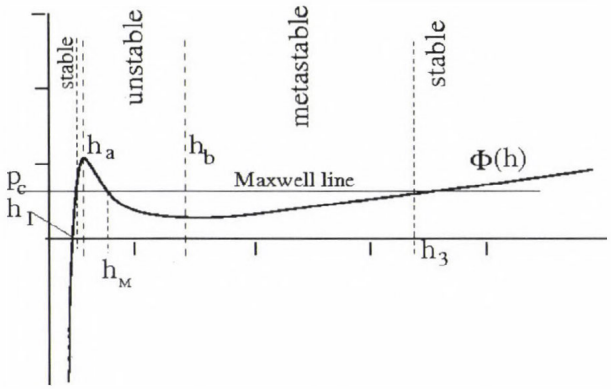

Fig. 2. Disjoining pressure including gravitation, A_3=3, A_9=1, G=0.1. The region of unstable films is bounded by h_a and h_b. The critical pressure (depth), P_c (h_M), where drops turn into holes, is determined by a Maxwell construction (see Section 3.3.1.).

3. Spinodal de-wetting

If a thin liquid film is exposed to a non- or partially wetting substrate, a small perturbation is sufficient to destabilize the flat surface. The fluid then bubbles and many small drops are formed. This phenomenon can be seen for instance if rain falls on a waxed cloth or a well polished car roof. Such a process is called *spinodal de-wetting* and can be described in the frame of Eq. (9) if the disjoining pressure has a negative slope for a certain region of the initial depth h (*Bestehorn* and *Neuffer*, 2001).

3.1. Thin film equation

For the following study we take an attracting/repelling disjoining pressure discussed in the last section (Eq. (17)):

$$\Phi(h) = \frac{A_3}{h^3} - \frac{A_9}{h^9} + Gh\,.$$

This, inserted into Eq. (9), yields the thin film equation:

$$\partial_t h = -\nabla_2 \cdot \left[-\frac{h^3}{3} \nabla_2 (\Phi(h) - \Delta_2 h) \right]. \tag{18}$$

Note that we put q=1. This is possible by a suitable choice of τ and δ. We shall come back to this issue in more detail below.

3.2. Normal form

Instead of further examining Eq. (18), we first wish to convert it to a more convenient form, showing the canonical form of a type II_s instability (*Cross* and *Hohenberg*, 1993). It will have also the advantage to be easier transformable into a numerical scheme.

To this end we introduce a variable that describes deviations from the average reference (initial) depth h_0 (a conserved quantity):

$$\eta(x,y,t) = h(x,y,t) - h_0\,.$$

Inserting this into Eq. (18), on the right hand side one can separate the linear and nonlinear expressions in η:

$$\partial_t \eta = \frac{1}{3} {h_0}^3 D(h_0) \Delta_2 \eta - \frac{1}{3} {h_0}^3 {\Delta_2}^2 \eta - \nabla_2 \cdot \mathbf{j}_{NL}(\eta) \tag{19}$$

with the nonlinear current

$$\mathbf{j}_{NL}(\eta) = -\frac{1}{3}\left(q_2 \nabla_2 \eta - q_1 \Delta_2 \nabla_2 \eta\right)$$

and the abbreviations

$D(h) = d_h \Phi$, $q_1 = 3{h_0}^2 \eta + 3h_0 \eta^2 + \eta^3$, $q_2 = (h_0 + \eta)^3 D(h_0 + \eta) - {h_0}^3 D(h_0)$.

Both functions q_1 and q_2 vanish as $\sim\eta$. From Eq. (19) it is evident, how the linearized problem looks near h_0. One has just to drop the nonlinear expression $\mathbf{j}_{NL}$ and a linear equation of the form Eq. (15) can be obtained. The same approach used there yields the dispersion relation

$$\lambda = \frac{1}{3} h_0{}^3 (-D(h_0)k^2 - k^4). \tag{20}$$

An instability occurs if the "diffusion coefficient" D is less than zero. The dispersion relation then has the form of the solid line in *Fig. 1*, right frame. This of course coincides with the reasoning of Section 2.3. An instability occurs, where the slope of the pressure is negative. Numerically one finds, from

$$D(h_0) = 0,$$

the two limits (for the special choice of A_3=3, A_9=1, G=0.1), the so-called *spinodals*

$$h_0{}^{(1)} = h_a = 1.002, \qquad h_0{}^{(2)} = h_b = 3.08.$$

3.3. Numerical solutions

We present solutions of the fully nonlinear Eq. (19) for the parameters of *Fig. 2* and several initial depths h_0 (*Fig. 3*). As initial condition, a random distribution around the average depth h_0 was chosen.

3.3.1. Spatial and temporal scales

In the early stage of the evolution, structures having a length scale of the critical wave length $\Lambda = 2\pi / k_c$ occur, where k_c is the wave number of the fastest growing mode

$$k_c = \sqrt{-\frac{D}{2}}.$$

This can be called "linear phase", since the amplitudes are still small and nonlinearities play no important role. The structure grows on the typical time scale:

$$\tau = \lambda^{-1}(k_c) = \frac{12}{h_0{}^3 D^2} = \frac{12}{h_0{}^3} (\Phi'(h_0))^{-2},$$

which is inverse to the square of the slope of the disjoining pressure. This is the reason why pattern formation in thicker films takes much longer (right column in *Fig. 3*). As a consequence, the small scale (linear phase) structures are overlayed by holes created by certain seeds (see also in the next paragraph). After the linear phase, the position of h_0 with respect to the Maxwell point (*Fig. 2*) is decisive. If $h_0 > h_M$, holes are formed, for $h_0 < h_M$, one finds drops. If $h_0 \approx h_M$, maze-like patterns are obtained in the form of bended, rather irregular

stripes (*Fig. 3*, middle column). In a last, strongly nonlinear phase, so-called *coarsening* is observed. This is a slow increase of the length size of the structures (holes, drops, or mazes), accompanied by fusion of smaller objects to larger ones. The final structure (long time limit) is often a single entity, one big drop or hole, which is finally time stable. The whole spatio-temporal evolution is transient and can be formulated as a gradient dynamics. The potential plays the role of a generalized free energy reaching its minimum in the steady end state.

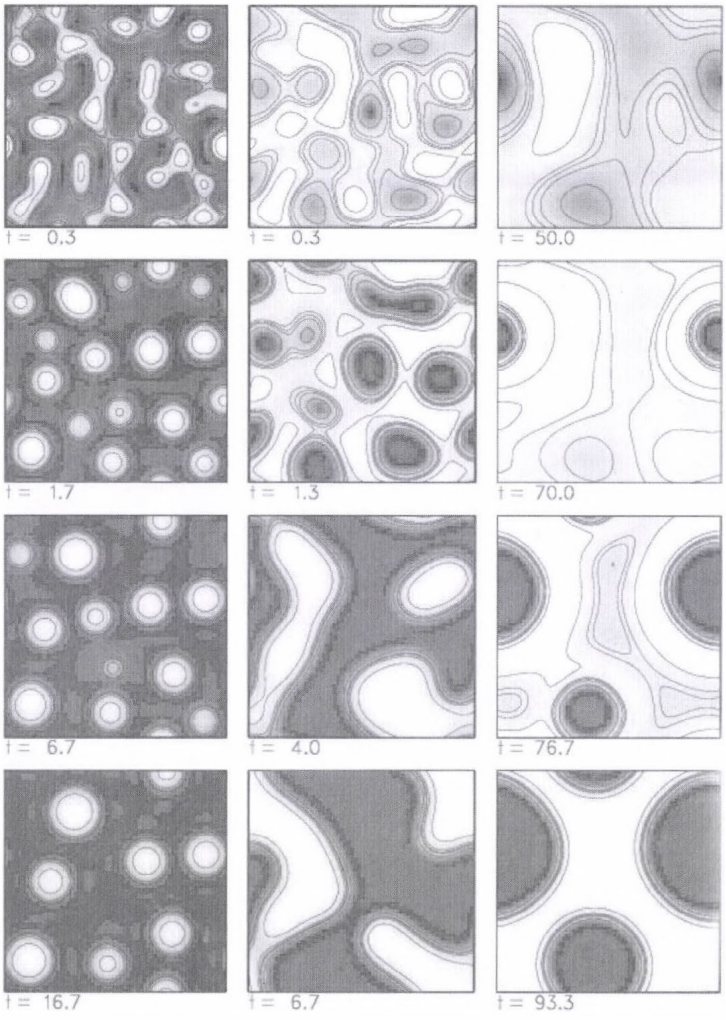

Fig. 3. Time series found by numerical integration of Eq. (19) for h_0=1.2 (left column), 1.862 (middle), and 2.8 (right). Light areas correspond to elevated regions of the surface. Nucleation dominates in the last column.

The critical pressure as well as h_M can be found by a Maxwell construction (*Fig. 2*). One has

$$P_c(h_3 - h_1) = \int_{h_1}^{h_3} \Phi(h)dh,$$

with h_1 (h_3) as left (right) intersection of P with the Maxwell line:

$$\Phi(h_1) = \Phi(h_3) = P_c.$$

From these three conditions one can determine P_c and the three intersection points by numerical iteration:

$$P_c = 0.647, \qquad h_1 = 0.850, \qquad h_M = 1.862, \qquad h_3 = 6.56.$$

3.3.2. Meta-stable region and nucleation

The flat film is unstable with respect to infinitesimal disturbances, if h_0 is in the region between h_a and h_b. On the other hand, two meta-stable domains exist,

$$h_1 < h_0 < h_a, \qquad h_b < h_0 < h_3,$$

where the flat film is stable, although the free energy could be lowered by pattern formation. Then, a finite disturbance is necessary, which can be caused by seeds coming for instance from impurities. Such a process is called *nucleation* and can be seen in the right column of *Fig. 3*. There the seeds were provided by the random dot initial conditions, and two holes are formed. Both processes (nucleation and wetting) concur in this region, and it is a question of time scales, which one emerges first. In experiments, the formation of holes by nucleation is seen quite often. The reason is that the meta-stable hole region is much larger compared to that of drops (*Fig. 2*).

3.3.3. Physical values

To get an idea of the spatial and temporal scales of the experiments, one has to rescale to dimensional variables. For the Hamaker constant A_3 this means

$$\tilde{A}_3 = \frac{\delta^2 \tau}{\eta d^3} A_3 \,, \tag{21}$$

where the variables bearing a tilde are non-dimensional (in our simulations, e.g., $\tilde{A}_3 = 3$). Since we chose q=1, one can determine δ and τ from

$$q = \frac{\pi d^3}{\ell^4 \eta}\gamma = \frac{\delta^4 \tau}{\eta d}\gamma = 1$$

together with Eq. (21):

$$\delta = \frac{1}{d}\left(\frac{A_3}{\gamma \tilde{A}_3}\right)^{1/2}, \qquad \tau = \left(\frac{\tilde{A}_3}{A_3}\right)^2 \eta \gamma d^5 .$$

Knowing δ, the horizontal scale ℓ can be specified:

$$\ell = \frac{d}{\delta} = d^2\left(\frac{\gamma \tilde{A}_3}{A_3}\right)^{1/2}$$

To compute the scaling, we need values for the Hamaker constant A_3 and for the depth d. From the literature we take the values of *Israelachvili* (1992):

$$A_3 = \frac{0.5}{6\pi} \times 10^{-20}\, J .$$

For the depth of the precursor film h_a this gives about 5.5 nm. Then the depths (water as a working substance) of the runs shown in *Fig. 3* correspond to

$d \approx 7$ nm (left), $d \approx 10$ nm (middle), $d \approx 16$ nm (right).

For the time scales we get

$\tau \approx 0.15$ s (left), $\tau \approx 1$ s (middle), $\tau \approx 10$ s (right).

This means that the evolution shown in the left column takes about two seconds, the middle one takes seven seconds, and on the right hand side it is 15 minutes. Finally, we mention the horizontal scales:

$\ell \approx 1.4$ μm (left), $\ell \approx 3.2$ μm (middle), $\ell \approx 7.5$ μm (right),

corresponding to the horizontal dimensions of the shown areas (64×64 mesh points with distance $\Delta x = 0.5$):

$L \approx 45$ μm (left), $L \approx 100$ μm (middle), $L \approx 240$ μm (right).

4. Conclusions

In this and in the preceding paper we showed that it is often sufficient to consider reduced equations instead of the full set of hydrodynamic basic equations (Euler, Navier-Stokes equations). We gave a derivation of such a reduced description for the cases of a perfect fluid as well as of a viscous fluid. The first case leads to the shallow water equations, the latter to the thin film equations. Under both circumstances we studied the influence of a generalized pressure allowing for a bistable depth distribution. In that way the typical coarsening behavior is obtained. For a perfect fluid we add phenomenological damping. The energy lost is balanced by a parametric excitation, leading to very interesting time dependent structures.

References

Bestehorn, M. and *Neuffer, K.*, 2001: Surface patterns of laterally extended thin liquid films in three dimensions. *Phys. Rev. Lett. 87*, 046101.

Colinet, P., Legros, J.C., Velarde, M.G., 2001: *NonlinearDynamics of Surface-Tension-Driven Instabilities*. Wiley-VCH, Berlin.

Cross, M.C. and *Hohenberg, P.C.*, 1993: Pattern formation outside equilibrium. *Rev. Mod. Phys. 65*, 851-860.

Israelachvili, J.N., 1992: *Intermolecular and Surface Forces*. Academic Press, London.

Jacobs, K., Herminghaus, S., and *Mecke, K. R.*, 1998: Thin liquid polymer films repture via defects. *Langmuir 14*, 965.

Oron, A., Davis, S. H., and *Bankhoff, S. G.*, 1997: Long-scale evolution of thin liquid films. *Rev. Mod. Phys. 69*, 931.

Pismen, L.M. and *Pomeau, Y.*, 2000: Disjoining potential and spreading of thin liquid layers in the diffuse-interface model coupled to hydrodynamics. *Phys. Rev. E 62*, 2480.

Pototsky, A., Bestehorn, M., and *Thiele, U.*, 2004: Control of the structuring of thin soft matter films by means of different types of external disturbance. *Physica D199*, 138.

Rehse, N., Wang, C., Hund, M., Geoghegan, M., Magerle, R.., and *Krausch, G.*, 2001: Stability of thin polymer films on a corrugated substrate. *Eur. Phys. J. E4*, 69.

Reiter, G., 1992: Dewetting of thin polymer films. *Phys. Rev. Lett. 68*, 75.

Reiter, G., Sharma, A., Casoli, A., David, M.-O., Khanna, R., and *Auroy, P.*, 1999: Thin film instability induced by long-range forces. *Langmuir 15*, 2551.

Rockford, L., Liu, Y., Mansky, P., Russell, T.P., Yoon, M., and *Mochrie, S.G.*, 1999: Polymers on nanoperiodic, heterogeneous surfaces. *Phys. Rev. Lett. 82*, 2602.

Vrij, A.,1966: Possible mechanism for the spontaneous repture of thin free liquid films. *Discuss. Faraday Soc. 42*, 23.

IDŐJÁRÁS

Quarterly Journal of the Hungarian Meteorological Service
Vol. 111, No. 2–3, April–September 2007, pp. 199–208

Input data representativeness problem in plant disease forecasting models

Lalić Branislava[1*], **Dragutin T. Mihailović**[1], **Slavica Radovanović**[2], **Jelica Balaž**[1] and **Ana Ćirišan**[1]

[1]*Faculty of Agriculture, University of Novi Sad, Dositej Obradović Sq. 8, 21000 Novi Sad, Serbia*

[2]*Hydrometeorological Service of Serbia, Kneza Viseslava 66, Belgrade, Serbia*
E-mails: branka@polj.ns.ac.yu; guto@polj.ns.ac.yu

(Manuscript received in final form February 13, 2007)

Abstract—In this paper, the LAPS surface scheme and the BAHUS biometeorological model are shortly described. LAPS has been applied for within-crown microclimate simulations in an apple orchard at experimental site Rimski Sancevi in the northern part of Serbia. The simulated values of leaf wetness duration, air temperature, and relative humidity within the tree crown are compared with the data measured in the orchard during the 2003 apple growing season. On the basis of biological and meteorological inputs coming from the outputs of either the automatic or the climatological weather station, or LAPS, BAHUS was applied in order to give the messages on occurrence of apple scab and fire blight diseases. BAHUS outputs obtained for the three meteorological input data sets are compared with time and intensity of infections observed in the apple orchard.

Key-words: agrometeorological modeling, SVAT models, data representativeness, diseases forecasting

1. Introduction

The first recorded agrometeorological forecast was made by Réaumur in year 1735 (*Réaumur*, 1735). This pioneer work was related to the forecast of phenological development for several crops based on thermal sum concept. Over almost three centuries, an "army" of scientist coming from different meteorological and agricultural communities has invested a great deal of effort

* Corresponding author

to establish agrometeorology as an applied science. At present level of development, agrometeorology plays the main role in the development of sustainable and economically viable agricultural systems, production and quality improvement, losses and risk reduction, cost decrease, and efficiency increase in the use of water, labor, and energy (*Lalic et al.*, 2005).

Accuracy of agrometeorological modeling depends on: (a) how well the initial observations represent the regional conditions, (b) how homogeneous the regional conditions are, (c) how accurate the observations themselves are, and (d) how sensitive the model is to agrometeorological variables variations (*Lomas*, 1984). In addition, it should be taken into account, how representative certain relations or modeling tools are for particular agroecological conditions, and how uncertainties in the variables will affect the result. More details about the representativeness concept, related to the actual use of measured or calculated parameter value in a numerical model, with an application on documentation system for administration of meteorological parameters at The Norwegain Crop Research Institute, can be found in *Sivertsen* (2005).

The objective of this paper is to emphasise the importance of input data and modeling tools representativeness in providing useful and accurate agrometeorological information. After Section 2, which gives a brief overview of basic agrometeorological techniques, in Section 3, the LAPS surface scheme (*Mihailovic*, 1996; *Mihailovic* and *Kallos*, 1997) and BAHUS biometeorological model (*Mihailovic et al.*, 2001; *Lalic et al.*, 2003) for predicting the occurrence of some frequent plant diseases are described shortly. In Section 4, the observations are presented and compared with the results of the following simulations: (a) orchard microclimate simulation provided using the LAPS scheme and (b) plant diseases occurrence prediction obtained using BAHUS model run with the three different types of meteorological data (gathered at an apple orchard, measured at the meteorological station in the vicinity of the orchard, and simulated by the LAPS scheme). Section 5 summaries the concluding remarks.

2. Agrometeorological modeling techniques and data representativeness

Last decades of the 20th century were denoted by increasing development of modeling tools and techniques in all areas of research and technology. No industry is built before a model is conceived where the controls of all its production processes are known (*Dourado-Neto et al.*, 1998). In agrometeorology, modeling is the art of predicting the vegetation dynamics, crop yield and production, disease and pest appearance, drought development, pasture and animal production, fish catches, and meteorologically induced post-harvest losses (*Gommes et al.*, 1996). Since an agrometeorological model attempts to simulate plant/animal-soil-weather interaction in a quantitative way,

it needs the information and data on the most important factors that relate agricultural production response to its environment, i.e., model inputs. These inputs mainly consist of different biological, meteorological, soil, and management data.

After passing through the "modeling" part of the model, the inputs are converted into a number of outputs. All procedures incorporated into the "modeling" part are based on either empirical relations or parameterized scientific laws. If a variable of interest could be achieved as a result of parameterization (the intensity of canopy evaporation, soil moisture and temperature, horizontal and vertical runoff, the intensity of within canopy deposition, the rate of nitrogen movement, etc.), then the accuracy of modeling strongly depends on the representativeness and the accuracy of forcing data. Particularly, if the chosen variable represents the statement of atmosphere at a certain point and the mathematical formulation of the process of interest is well known, then the output information for this point is as accurate as the input data are. For that purposes, the SVAT model is an irreplaceable part of an agrometeorological model providing a link between the underlying surface and the atmosphere with the strong background focused on the parameterization of environmental fluid dynamics and physiological processes. Depending on the time and space scales of the agrometeorological model, the included SVAT schemes range in complexity from a simple bucket model as used by *Manabe* (1969) to the vertically complex models, such as BATS (*Dickinson et al.*, 1986), SiB (*Sellers et al.*, 1986) and LAPS (*Mihailovic*, 1996; *Mihailovic* and *Kallos*, 1997). The current improvement of the SVAT models is related to the incorporation of sub-grid scale heterogeneity (*Famiglietti* and *Wood*, 1994; *Liang et al.*, 1994; *Mihailovic et al.*, 2005) and to the improvement of plant physiological processes parameterization (*Wang* and *Jarvis*, 1990) increasing the complexity and the number of model parameters (*Dourado-Neto et al.*, 1998). In this way, the SVAT model becomes more sophisticated but, from the point of view of agrometeorological models, its effectiveness decreases.

On the other hand, if the model output is a result of application of empirical relation (appearance of some phenological phases, crop yield, disease and pest appearance), then the accuracy of the agrometeorological modeling depends on the representativeness of forcing data and on the applied formula. Typically, meteorological elements appearing in empirical relations are not defined precisely enough. Moreover, it is not obvious, where the reference level is placed and whether the data are related to within or above the canopy air space. For example, term "air temperature" (without any other comments) in meteorology assumes that it is the temperature of the air at 2meters above the non-vegetated ground. Yet, the outside meteorological community rules are not so strict, and this term could be also related either to the temperature of air surrounding the plant, bacteria, or insects, or to the air temperature above canopy. Additionally, it is a well-known fact, that empirical relations are

representative only of agroecological conditions similar to those for which they are defined in the first place. It assumes that particular relation could not be extrapolated without the adjustment for conditions different from those of its origin.

3. Short descriptions of LAPS scheme and BAHUS model

In order to reconsider the representativeness of different meteorological datasets in agrometeorological forecasting, surface scheme LAPS and biometeorological model BAHUS have been used.

LAPS scheme. This SVAT model describes mass, energy, and momentum transfers between the land surface and the atmosphere. The model is designed as a software package that can be run as part of an environmental model or as a stand-alone one. LAPS includes modeling of the land surface and atmosphere interaction under processes divided into three sections: subsurface thermal and hydraulic processes, bare soil transfer processes, and canopy transfer processes. They are: the interaction of vegetation with radiation, evaporation from bare soil, evapotranspiration including transpiration and evaporation of intercepted water and dew, conduction of soil water through the vegetation layer, vertical water movement in the soil, surface and subsurface runoff, heat conduction in the soil, and momentum transport within and above the vegetation. A single layer "sandwich" approach for canopy is chosen for the physical and biophysical parameterization. The scheme has seven prognostic variables: three temperature variables (foliage, soil surface, and deep soil), one interception storage variable, and three soil moisture storage variables. For the upper boundary conditions the following forcing variables are used: air temperature, water vapor pressure, wind speed, short wave and long wave radiation, and precipitation at a reference level within the atmospheric boundary layer. The surface fluxes are calculated using resistance representation. The soil module is designed as a three-layer model, which is used to describe the vertical transfer of water in the soil. LAPS uses the morphological and physiological characteristics of the vegetation community for deriving the coefficients and resistances that govern all the fluxes between the surface and atmosphere. More details and descriptions can be found in *Mihailovic* (1996) *Mihailovic* and *Kallos* (1997), while the review of the new approaches was reported at the „Workshop on Environmental Fluid Mechanics as Elements in Agrometerological Modeling" (*Mihailovic* and *Lalic*, 2006).

BAHUS model. It is a biometeorological model conceptualized for providing the messages of occurrence of plant diseases and the proper time for pesticide application (*Mihailovic et al.*, 2001; *Mihailovic et al.*, 2002). Components of this model are: (1) input module – providing meteorological and biological data that are representative of a selected area, (2) modeling module – consisting of empirical relations and conditions related to the disease appearance

and intensity of infection, and (3) output module – giving the following messages: the risk of infection, the duration of incubation period, the time of the first symptoms, etc. Depending on the method selected in the modeling module, following meteorological data should be provided by the input module: maximum air temperature, minimum air temperature, mean daily temperature, actual values of temperature, relative humidity, precipitation, and the duration of leaf wetness. Since in the literature (indicated bellow) used for developing each diseases routine, there is no precise information about the reference level related to the meteorological variables, it was supposed, in all calculations, that these variables describe conditions within the crown air space. In the modeling module, the BAHUS uses method defined by *Mills* (1944), later modified by *Jones et al.* (1980), based on air temperature, relative humidity, and the duration of leaf wetness in order to describe the intensity of apple scab infection. Requirements for fire blight blossom infection defined by *Steiner* (1990) are incorporated in Degree-day (*Mills*, 1955) and MARYBLIGHT methods (*Steiner* and *Lightner*, 1992). These methods are based on accumulation of degree-days (DD) and degree-hours (DH), which are defined as a number of degrees over the base temperature during one day and one hour, respectively (*Zoller* and *Sisevich*, 1979; *Mills*, 1955). For a particular forecasting day model outputs are: (i) the intensity of apple scab infection ranged as none, weak, medium, and strong infection, and (ii) for a fire blight blossom infection event with a description of risk as none, low, moderate, and high infection. Let us note that this module also produces other outputs, but for the purpose of this paper we have selected the aforementioned ones.

4. Numerical experiment

In the numerical experiment, appearance of fire blight and apple scab diseases, during the 2003 apple growing season in Serbia, was forecasted by the BAHUS model, that is its the first run with real data (*Lalic et al.*, 2003). In that purpose, three sources of meteorolopgical data were used: (i) a data set measured by an ADAS mini weather station placed in the apple orchard, (ii) a data set measured on the weather station Rimski Sancevi in the vicinity of apple orchard ($\approx$ 1 km), and (iii) a data set obtained as a result of the simulation of apple orchard microclimate using the LAPS scheme. In the further text these data sets are denoted by DS1, DS2, and DS3, respectively. The main idea of using these three different data sets is to explore its representativeness for apple orchard disease forecasting. As a first step in this numerical experiment, the LAPS scheme was run on hourly basis to provide simulated values of leaf wetness duration, air temperature, and relative humidity within the tree crown. Obtained results compared with *in situ* measured data illustrate that LAPS can provide an accurate simulation of daily variation of within-crown air temperature and

relative humidity (*Figs. 1* and *2*). Some deviations between the simulations and measurements are seen only for extreme values of variables. Regarding leaf wetness duration, results presented in *Fig. 3* show that, for the particular period, LAPS simulates two wet periods, while the ADAS station registered only one. After short inspection of the data related to precipitation, it becomes absolutely clear that there are two wet periods, but the first one (April 24 and 25) was caused with such a small amount of precipitation (0.4 mm and 0.1 mm) that leaf wetness sensor placed within the tree crown did not become wet. On the other hand, LAPS recognized these rain episodes like sources of leaf wetness.

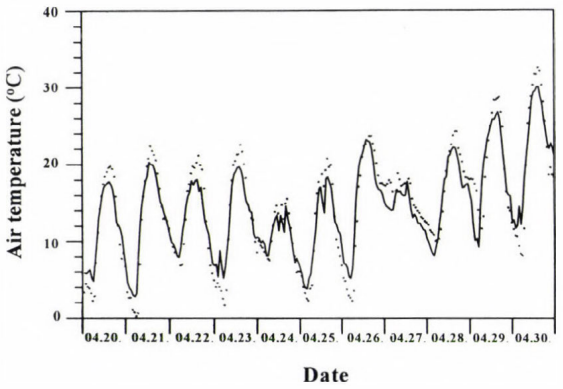

Fig. 1. Within-crown air temperature, measured by the ADAS weather station (dots) and simulated using the LAPS model (line), during the last decade of April 2003.

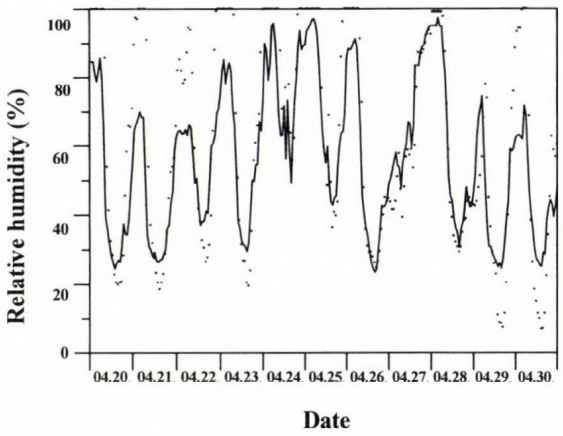

Fig. 2. Within-crown relative humidity, measured by the ADAS weather station (dots) and simulated using the LAPS model (line), during last decade of April 2003.

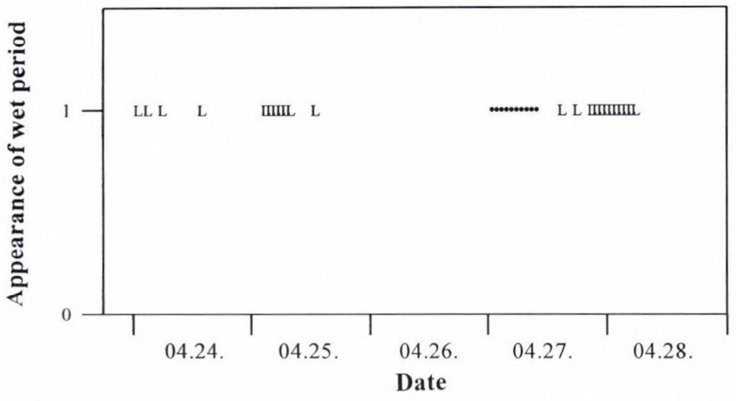

Fig. 3. Appearance of wet period, measured by the ADAS weather station (dots) and simulated using the LAPS model (L), during the last decade of April 2003.

From April 21st, when flowering and the accumulation of degree days (DD) and degree hour (DH) units started, the indicators for *Erwinia amylovora* development, as well as the leaf wetness necessary for releasing the *Venturia inaequalis* ascosporic, were pursued. Accumulated DH units and related epiphytic infection potential (EIP) representing possibility of fire blight blossom infection are calculated using the above mentioned data sets. The results presented in *Table 1* indicate that, in all cases, the infection practically starts on April 29 since there are small differences in EIP among methods in the range of error of measurements. However, the appearance and intensity of apple scab infection are too complex and cannot be described with only two parameters. For that reason, in *Table 2* only critical days and expected intensity of infection are presented. Obviously, in all cases, April 27 is the critical day for apple scab infection appearance with small differences in expected infection intensity. Following the information that comes from phytopathologists, the results presented in *Table 1* and *Table 2* correspond to the observed fire blight blossom appearance and the intensity of apple scab infection in the apple orchard at Rimski Sancevi.

Table 1. Accumulated DH and epiphytic infection potential (EIP) calculated using DS1, DS2, and DS3 data sets (days without DH accumulation are omitted)

Date	DS1		DS2		DS3	
	DH (°C)	EIP	DH (°C)	EIP	DH (°C)	EIP
04. 27	0.5	0.5	31.8	35.3	35.4	31.9
04. 28.	38.2	34.4	27.5	24.8	27.6	24.9
04. 29.	117.1	105.5	109.5	98.6	109.7	98.9
04. 30.	246.5	222.1	248.6	224.0	249.0	224.3

Table 2. Intensity of apple scab infection calculated using DS1, DS2, and DS3 data sets (days, when leaves were dry, are omitted)

Date	DS1	DS2	DS3
04. 24	no infection	no infection	no infection
04. 25	no infection	no infection	no infection
04. 26	no infection	no infection	no infection
04. 27	weak infection	weak infection	moderate infection

5. Concluding remarks

In this paper, the LAPS scheme has been applied for apple orchard microclimate simulations. The BAHUS biometeorological model was used in order to forecast appereance of blossom fire blight and apple scab infection in an apple orchard during the 2003 growing season at the experimental site Rimski Sancevi. Three meteorological input data sets coming from automatic weather station, climatological weather station, as well as the LAPS scheme were used in order to compare the BAHUS outputs with the observations and to explore the representativeness of these meteorological inputs for the purpose of disease forecasting.

The obtained results indicate that, sometimes significantly, the differences between DS1, DS2, and DS3 data sets are not considerable in disease forecasting. This situation is strongly affected by the non-sophisticated nature of the prognostic methods incorporated into a BAHUS model and could be taken as an advantage till differences between forecasted and observed time of infection is one or two days. Yet, for larger differences it is obvious, that the applied method is too simplified, avoiding factors and processess strongly affecting the disease development. Consequently, in the absence of *in situ* measurements, the data measured at a weather station in the vicinity of orchard or simulated using the LAPS scheme could be used as meteorological inputs for the BAHUS model, at the present level of sophistication.

However, it is hard to balance the appetite for commonly available input data with internal complexity of the method. Even *in situ* measurements could not guarantee accurate agrometeorological forecast, if they are not harmonized with the applied modeling techniques. Therefore, it is of the utmost importance, that the agrometeorological model is followed by a list of incorporated processes and a precise documentation of parameters and variables used, see *Sivertsen* (2005). From that particular point one can try to provide data sets and parameters as realistic as possible. In the near future, a realistic challenge of the operational use of agrometeorological models will be the extended availability of data from different sources like weather stations, weather radars, satellite, and tools for integrating the data ought to be developed. In order to integrate data from different sources, it is important to document the data thoroughly.

References

Dickinson, R.E., Henderson-Sellers, A., Kennedy, P.J., and *Wilson, M.F.,* 1986: Biosphere-Atmosphere Transfer Scheme (BATS) for the NCAR Community Climate Model. *NCAR Tech. Note TN-275_STR*, Boulder, Co., 72 pp.

Dourado-Neto, D., Teruel, D.A., Reichardt, K., Nielsen, D.R., Frizzone, J.A., and *Bacchi, O.O.S.,* 1998: Principles of crop modeling and simulation II. The implications of the objective in model development. *Sci. Agric., Piracicaba, 55 (Número Especial),* 51-57.

Famiglietti, J.S. and *Wood, E.F.,* 1994: Application of Multi-Scale Water and Energy Balance models on a Tallgrass Prairie. *Water Resour. Res. 30,* 3079-3093.

Gommes, R., Bernardi, M., and *Petrassi, F.,* 1996: Agrometeorological Crop Forecasting. *Environment and Natural Resources Service (SDRN), FAO Research, Extension and Training Division*, 23 pp.

Jones, A.L., Lillevik, S.L., Fisher, P.D., and *Stebbins, T.C.,* 1980: A microcomputer-based instrument to predict primary apple scab infection periods. *Plant Dis. 64,* 69-72.

Lalic, B., Mihailovic, D.T., Balaz, J., and *Koci, I.,* 2003: Prediction of occurrence of plant diseases using the coupled atmosphere-land surface models. *Sixt European Conference on Applications of Meteorology*, September 15-19, Rome (Italy), Abstracts, 13 p.

Lalic, B., Koci, I., and *Mihailovic, D.T.,* 2005: Agrometeorological modeling – powerful tool of modern agriculture. *Proc. of the International Conference on Sustainable Agriculture and European Integration Processes*. 19-24 September 2004. *Savremena poljoprivreda 54,* 312-317.

Liang, T., Lai, H., and *Chen, N.,* 1994: When Client/Server isn't enough: Co-ordinating Multiple Distributed Tasks. *IEEE Computer, Vol. 27,* No. 5. 73-79.

Lomas, J., 1984: CAgM Report No. 22. Chairman of a Working Group of CAgM. Agrometeorological Services in Developing Countries. 35 pp.

Manabe, S., 1969: Climate and the ocean circulation 1. the atmospheric circulation and the hydrology of the earth's surface. *Mon. Weather Rev. 97,* 739-774.

Mihailovic, D.T., 1996: Description of a land-air parameterization scheme (LAPS). *Global Planet. Change 13,* 207-215.

Mihailovic, D.T. and *Kallos, G.,* 1997: A sensitivity study of a coupled-vegetation boundary-layer scheme for use in atmopsheric modeling. *Bound.-Lay. Meteorol. 82,* 283-315.

Mihailovic, D.T., Koci, I., Lalic, B., Arsenic, I., Radlovic, D., and *Balaz, J.,* 2001: The main features of BAHUS – biometeorological system for messages on the occurrence of diseases in fruits and vines. *Environ. Modell. Softw. 16,* 691-696.

Mihailovic, D.T., Eitzinger, J., Koci, I., Lalic, B., Arsenic, J.I., and *Balaz, J.,* 2002: Biometeorological system BAHUS for predicting the occurrence of plant diseases and ensuring their efficient control. *Int. Workshop on Environmental Risk Assessment of Pesticides and Integrated Pesticide Management in Developing Countries,* Kathmandu, Nepal, 6-9 November. *Landschaftsökologie und Umweltforschung 38*, 120-129.

Mihailovic, D.T., Rao, S.T., Alapaty, K., Ku, J.Y., Arsenic, I., and *Lalic, B.,* 2005: A study on the effects of subgrid-scale representation of land use on the boundary layer evolution using a 1-D model. *Environ. Modell. Softw. 20*, 705-714.

Mihailović, D.T. and *Lalic, B.,* 2006: Land-Air Parameterisation Scheme (LAPS) as a Component in Agrometeorological Modelling. Abstracts of *Workshop on Environmental Fluid Mechanics as Elements in Agrometeorological Modelling.* June 6-9, Ås (Norway).

Mills, W.D., 1944: Efficient use of sulfur dusts and sprays during rain to control apple scab. *N.Y. Agric. Exp. Stn. Ithaca Bull. 630*, 4 pp.

Mills, W.D., 1955: Fire blight development on apple in western New York. *Plant Dis. Rep. 39,* 206-207.

Réaumur, R.A.F., 1735: Observation du thermometre, faites to Paris pendant l'année 1735, comparées avec celles qui ont été faites sous la ligne, to the l'Isle of France, to Alger et en quelques-unites of in the l'Amérique isles. *Mém. Acad. give Sci., in the 545,* Paris.

Sellers, P.J., Mintz, Y., Sud, Y.C., and *Dalcher, A.,* 1986: A simple biosphere model (SIB) for use within general circulation models. *J. Atmos. Sci. 43*, 505–531.

Sivertsen, T.H., 2005: Discussing the scientific method and a documentation system of meteorological and biological parameters. *Phys. Chem. Earth 30*, 35-43.

Steiner, P.W., 1990: Predicting apple blossom infection by *Erwinia amylovora* using the Maryblyt model. *Acta Horticulturae 273*, 139-148.

Steiner, P.W. and *Lightner, G.W.*, 1992: MARYBLYT: A Predictive Program for Forecasting Fire Blight Disease in Apples and Pears. *University of Maryland, Version 4.0.*

Wang, Y.P. and *Jarvis, P.G.*, 1990: Description and validation of an array model. MAESTRO. *Agr. Forest Meteorol. 51*, 257-280.

Zoller, B.G. and *Sisevich, J.*, 1979: Blossom populations of Erwinia amilovora in pear orchards vs. accumulated degree hours over 18.3 Celsius, 1972-1976. *Phytopatology 69*, 1050 p.

IDŐJÁRÁS

Quarterly Journal of the Hungarian Meteorological Service
Vol. 111, No. 2–3, April–September 2007, pp. 209–220

An essay on modeling problems of complex systems in environmental fluid mechanics

Dragutin T. Mihailović[1*] and **Igor Balaž**[2]

[1]*Faculty of Agriculture, University of Novi Sad,*
Dositej Obradović Sq. 8, 21000 Novi Sad, Serbia; E-mail: guto@uns.ns.ac.yu

[2]*Scientific Computing Laboratory, Institute of Physics,*
P.O. Box 57, 11001 Belgrade, Serbia

(Manuscript received in final form January 29, 2007)

Abstract—In this essay we point out the current problems in the modeling of complex biophysical systems, particularly in environmental fluid mechanics, which requires quite new methodological and mathematical approaches. We give a short overview of some epistemological attitudes arisen from the 20th century onwards, which have converged on establishing of endophysics. Then, we generally discuss the establishment of the relations between the two different kinds of reasoning (causal and inferential) by pointing out a possibility of using two-state (teleological) model in modeling of complex systems. Using an example from environmental fluid mechanics, i.e., solving the energy balance equation for the Earth-atmosphere interface, we show that uncertainties can occur in predictions because of non-linear relations in the system under consideration.

Key-words: environmental fluid mechanics, endophysics, complex systems, modeling, epistemology, non-linear processes, deterministic chaos, teleological dynamics

1. Introduction

Regardless of the word "balance" being used either globally or locally in any given context, it is undoubtedly the keyword in the increasing number of environmental problems. The underlined sketch is a proper introduction to the question: Why are the environmental problems in the focus now? One particular answer can be found in the hierarchy of the main scientific problems of the 21st century, as seen by the community mostly consisting of physicists. According to them, in the 21st century the world of the scientific community will be occupied by the problems linked to superconductivity, quantum teleology, and

* Corresponding author

environmental problems that are primarily expressed through the problem of climate changes. A unique characteristic of these problems is their close connection with the questions of different aspects of the existence of individual human being, i.e., the questions of technological capability, origin of the consciousness and survival on the Earth. This is the first time in the history of science, when the environmental problems take the place at the front of the sciences. The question, why it is happening now and why it will go on happening in the future, could be answered by the well known fact, that in the scientific as well as in other worlds the main "drama of event" takes place at the interface between either two media or two states (*Mihailovic,* 2006).

The field of environmental sciences is abundant with various interfaces, and it is the right place for application of new fundamental approaches leading towards better understanding of environmental phenomena. We defined the environmental interface as an interface between the two either abiotic or biotic environments, which are in a relative motion exchanging energy through biophysical and chemical processes and fluctuating temporally and spatially regardless of its space and time scale. To our mind, this definition broadly covers the unavoidable multidisciplinary approach in environmental sciences and also includes the traditional approaches in sciences, that are dealing with the environmental space less complex than any one met in reality. The wealth and complexity of processes at this interface determine that the scientists, policy-makers, and the public, as it often seems, are more interested in a possibility of non-linear dislocations and surprises in the behavior of the environment than in a smooth extrapolation of current trends and a use of the approaches close to the linear physics. To overcome the current situation we have to do the following: (a) to establish a way in approaching non-linear physics and the non-linearity in describing the phenomena in environmental sciences, and (b) to solve or, at least, understand the problem of predictability. These two problems are *par excellence* problems of the methodology. Their successful solving will help us to avoid the current problems in mathematical, biophysical, and chemical interpretation of the nature, as well as in design of corresponding software. The environmental discipline that will be under consideration in this essay is the environmental fluid mechanics dealing with a broad range of environmental problems, which are, for example, picturesquely described and defined in *Cushman-Roisin et al.* (2006). Because of the thought behind this essay, this definition will be given in detail.

All forms of life on earth are immersed in a fluid, either the air of the atmosphere or the water of a river, lake, or ocean; even soils are permeated with moisture. So, it is no exaggeration to say that life, including our own, is bathed in fluids. A slightly closer look at the situation reveals further, that it is the mobility of fluids that actually makes them so useful for the maintenance of life, both inside and outside living organisms. For example, it is the flow of air through our lungs that supplies oxygen to our blood stream. The forced air flow

created by our respiration, however, is not sufficient. Namely, without atmospheric motion around us, we would sooner or later choke to death with the carbon dioxide exhaled by ourselves. Likewise, most aquatic forms of life rely on the natural transport of water for their nutrients. Our industrial systems, which release pollution on a continuing basis, would not be permissible in the absence of transport and dilution of nearly all emissions by ambient motions of air and water. In sum, natural fluid motions in the environment are vital, and we have a strong incentive to study the naturally occurring fluid flows, particularly those of air in the atmosphere and of water in all its streams, from underground aquifers to surface flows in rivers, lakes, estuaries, and oceans.

The study of these flows has received considerable attention over the years, and several distinct disciplines have emerged: meteorology, climatology, hydrology, hydraulics, limnology, and oceanography. Whereas the particular objectives of each of these disciplines, such as weather forecasting in meteorology and design of water-resource projects in hydraulics, encourage disciplinary segregation, environmental concerns compel experts in those disciplines to consider problems that are essentially similar: the effect of turbulence on the dispersion of a dilute substance, the transfer of matter or momentum across an interface, the flow in complex geometries, the rise of a buoyant plume, and the impact of flow over a biotic system. The common points encourage interdisciplinarity to a degree, that it is increasing in proportion to the acuteness of our environmental problems. This overlap between various disciplines concerned with the environmental aspects of natural fluid flows has given rise to a body of knowledge, that has become known as environmental fluid mechanics.

This short essay aims just to point out the current problems in modeling of complex biophysical systems, particularly in environmental fluid mechanics, that require quite new methodological and mathematical approaches.

2. A short overview of some epistemological points from the 20th century onwards

Until recently, discussions about scientific truth were filled with numerous metaphysical assumptions. They usually converged at one question (more or less explicitly stated): "How can we reach objective truth about natural processes?" However, during the 20th century, this question first became less important and then gradually disappeared from the epistemological scene as a relict from the age of naive realism. Now, in contemporary epistemology of science, it is well established that there is a fundamental difference between phenomenon and noumenon. Therefore, the object of scientific analysis cannot be the nature by itself, but only highly constructivistic products, i.e., conceptually embedded sets of observer's experiences. Accordingly, scientific theories are now understood

as logical instruments of organization of human thought, through which we can interpret and organize experimental laws (*Nagel,* 1961). Also, since they have constructivistic character, their relation to the nature should not be considered through the vocabulary of logic; they are not truth statements and they are not logical derivatives of observed facts, but only sets of rules and guiding principles for analysis of empirical facts (*Nagel,* 1961). Therefore, in the development of a scientific theory, it is not a problem to make approximations that can never reach reality. It is inevitable. But believing that relations of abstractions are exactly the same as relations in nature can be very problematic. Firstly, it can usually become a source of unfruitful debates about the "true" nature of the nature. Secondly, from such a perspective it is impossible to see and analyze the consequences of the interface perspective, where the observer is within the universe he observes.

A clear example of both mentioned problems can be found in the development of the contemporary physics. At the very beginning of the 20th century, Pierre Duhem asserted that physical theories are not simple (straightforward) reflexions of natural processes, but rigorous logical systems, which operate with abstract symbols and which are connected with nature through system of measurements and scales (*Duhem,* 1906). Such approaches put forward the process of encoding of natural processes into the domain of formal systems, as the first and crucial step in the development of a physical theory. However, in his opinion, a pattern of encoding depends almost entirely on the previously accepted theories. Therefore, empirical observations cannot be separated from the current state of affairs in a given scientific discipline, since theoretical assumptions determine what will be observed, how it will be observed, and how results will be interpreted. Although Duhem's approach can be characterized as conventionalism, his contribution to the general trend of development of thought in theoretical physics remains immense.

Few decades later, the explosive growth of quantum mechanics raised some fundamental questions about the status of observation in physics, and how our measurement procedures can affect the observed physical properties ("measurement problem"). In short, Einstein, opposing the Copenhagen interpretation of physical properties of quantum systems, claimed that under ideal conditions, observations reflect the objective physical reality (*Einstein et al.,* 1935). On the other hand, Bohr asserts that in quantum mechanics the measured quantum system and the measuring macroscopic apparatus cannot be considered as separate within a scope of scientific consideration. In other words, the physical properties of quantum systems are essentially dependent on the applied experimental apparatus. One of the most famous moments of the debate is now well-known as Einstein-Podolsky-Rosen paradox (*Einstein et al.,* 1935). In the short paper they showed, that if the quantum mechanic description of reality is complete, then the non commutable operators corresponding to two physical quantities can have simultaneous reality. In other words, quantum

mechanics is inconsistent with the reduction of the wave-packet postulate. Later, Bell (*Bell,* 1964) revealed, that the EPR paradox stands only under the set of supplementary assumptions, among which there is the assumption of locality. Moreover, within quantum mechanics there is no need to accept them all. Although it can look like a closing chapter in the debate on "measurement problem", this question evolved from the limited scope of quantum mechanics and took a more general form: "how the observations are affected by the fact that the observer is within the universe he observes?". This is certainly not a new question in the history of human though, but (until recent partial attempts) in the natural sciences it never gets a formal explanation. In philosophy, after Kant, it is one of the elementary topics, in developmental psychology Piaget clearly demonstrated, that elementary categories of human thought are construed during one's development, and how externality of cognitive entities is re-structured in accordance with its functional purposes through the process of assimilation of external changes with the operative schematism of that entity (*Piaget,* 1973a; *Piaget,* 1973b), and finally, in the world of logic and formal systems, Gödel shook the scientific community with his proof of incompleteness of formal systems (for extensive discussion see *Nagel* and *Newman,* 1958; *Rosen,* 1991). Now, in the natural sciences this problem is finally recognized and dispersed attempts of its formal treatment fall under the umbrella of discipline called endophysics. This term was originally suggested by David Finkelstein in personal communication with Otto Rössler. Later, it was comprehensively elaborated in details by *Rössler* (1998), although his *magnum opus* is loaded with inconsistencies.

We see the outside world, i.e., the world of phenomena (*ambience*) from the observer's perspective (its inner world). In the ambience there are *systems* of different level of complexity and their *environments*. A system in the ambience is a collection of precepts while whatever lies outside, like the component of a set, constitutes the environment. The fate of science lies in the fact that it is focused on the system (*Rosen*, 1991). Furthermore, to anticipate something, the system gets described by *states* (determined by observations), while the environment is characterized through its effects on the system. The trend in contemporary science and mathematics is to try to dispense with extralinguistic referents entirely and replace them with purely syntactic structures, that only recognize and manipulate the symbols out of which the propositions are built. This process is called *formalization* (*Kleene,* 1952). The crucial thing to bear in mind is that both theory and any formalisation of it are the systems of *entailment*. It is the *relation* between them, or more specifically, the extent to which these schemes of entailment can be brought into congruence. That is of primary interest. The establishment of such congruences is the essence of the *modeling relation* (*Rosen,* 1991). In the precise sense, the incompleteness theorem of Gödel asserts that formalization, in which each entailment is a syntactic entailment, is too poor in entailment to be congruent with the number

theory, no matter how we try to establish such a congruence. This kind of situation is termed complexity (*Rosen,* 1977). In this light, Gödel's theorem says that the number theory is more complex than any of its formalizations. Following the message and the fundamental consequences of this theorem, we call the complex system such a system that is more complex than its any formalization.

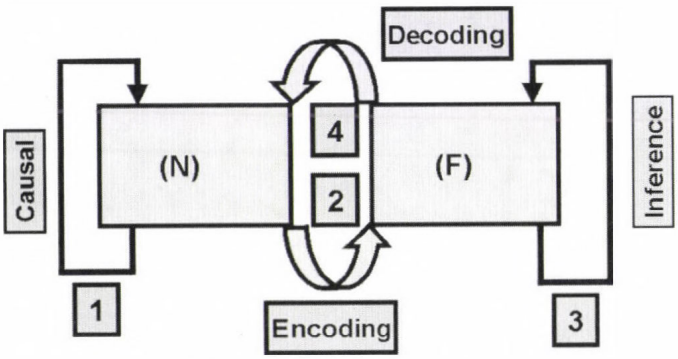

Fig. 1. Schematic diagram representing both (i) comparison of two formalisms F_1 and F_2, and (ii) modeling relation when we have given a natural system N, and a formal system F.

Fig. 1 schematically depicts a comparison of two formalisms F_1 and F_2. To compare two formalisms we need to make two dictionaries. The first of them, which translates from F_1 to F_2, is an *encoding* dictionary while the other, translating from F_2 back to F_1, is a *decoding* dictionary. Let us note, that we do not require any relation at all between them. If we find the encoding and decoding for which the diagram of *Fig. 1 always commutes*, in such a case, we have in fact brought at least a part of the inferential machinery of F_1 into congruence with a corresponding part of the inferential machinery of F_1. We will then say that F_2 is a *model* of F_1, or equivalently, that F_1 is a *realization* of F_2. Also we can say that a *modeling relation* exists between the two inferential structures. We can use the inferential structure of the model to study its realization, to *predict,* in effect, from the encoded hypothesis (via the pathway $2 + 3 + 4$ in the diagram in *Fig. 1*), theorems of F_1 from theorems in F_2. In mathematics, there are a lot of procedures of formal modeling of one kind of inferential structure into another. It seems that the category theory comprises, in

fact, the general theory of formal modeling, the comparison of different modes of inferential or entailment structures.

Fig. 1 also schematically depicts a modeling relation, when a natural system N and a formal system F are given. As before, the two arrows represent the respective entailment structures; inference in formalism F, causality in N. Now, the two established dictionaries provide an encoding of the phenomena of N into the propositions of F and a decoding of the propositions of F back to the phenomena in N. As we said before, there are two paths in the diagram: (1) and (2) + (3) + (4). According to *Rosen* (1991), the first of them (the path (1)) represents a causal entailment within N (what an observer, simply sitting and watching what happens in, will see). The arrow (2) encodes the phenomena in N into the propositions in F. In this route we must use these propositions as hypothesis, on which the inferential machinery of the formal system F may operate (denoted by the arrow (3)). It generates theorems in F, entailed precisely by the encoded hypotheses. Finally, we have to decode these theorems back into the phenomena of N, via the arrow (4). At this point, the theorems become *predictions* about N. Then the formal system F is called a *model* of the natural system N, if we always get the same answer, regradless of the fact, whether we follow path (1) or path (2) + (3) + (4).

Finally, in this section we cannot avoid the question of time in the modeling relation. A usual approach in physics is that the present state is strictly a result of its evolution from the past. However, recently it has been shown that some phenomena in the real world can be explained, if we accept that the *present state* of a system is defined by its *past*, in the sense that the past determines the possible states that are to be considered, and by its *future*, in the sense that the selection of a possible future state determines the effective present state (*Nedeljkovic* and *Nedeljkovic,* 2003a; *Nedeljkovic* and *Nedeljkovic,* 2003b among others); regarding that a concise and illustrative differentiation between causal and teleological dynamics is given by *Van Loocke* (2002). According to them, in a large part of the present-day physics, the fundamental physical laws are compatible with the teleological as well as with the causal dynamics (the term 'causal' is used in the restricted sense of 'governed by influences from the past'). Considering a system that is characterized by a set of variables $x_i(t)$ $(I = 1,\ldots, n)$, where t is the time variable, he makes a differentiation between the causal and the teleological dynamics by the following definitions:

(1) A system behaves causally and deterministically if there is a law that determines the values of $x_i(t)$ given the values of $x_i(t–1)$ at the previous time step.

(2) A system behaves causally and non-deterministically, if there is a law that produces the probability distributions for possible values of $x_i(t)$ giving the probability distributions for possible values of of $x_i(t–1)$ at the previous time step.

(3) A system is teleological and deterministic if there is a law that determines the values of $x_i(t)$ giving the values of $x_i(t+1)$ at the next time step.

(4) A system is teleological and non-deterministic, if there is a law that produces the probability distribution for possible values of $x_i(t)$ giving the probability distributions for possible values of $x_i(t+1)$ at the next time step. We will not further speculate with the question about time. This is just a short reminder for the environmental fluid mechanics community that, in the modeling of complex biophysical processes, we should bear in mind a possibility of using two-state (teleological, *Nedeljkovic* and *Nedeljkovic,* 2003a) models.

3. An example of modeling at the Earth-atmosphere interface

There is still no information available in the environmental fluid mechanics literature about the application of the methods and approaches of the endophysics as mentioned in Section 2. Recently *Sivertsen* (2005) discussed the hypothetico-deductive principle, bearing in mind an observer who looks at the ambience representing the biological world. More precisely, he was dealing with a biological system reacting to the atmospheric environment through meteorological parameters. The outcome of the discussion in this paper, which is an extension of the work in *Sivertsen* (2004), is a proposal of a documentation system for the quantitative meteorological and biological parameters, either measured or the parameters derived by model calculation. Undoubtedly, a growing demand for modeling of more complex systems in environmental fluid mechanics will shift the attention towards the endophysics and the methods of modeling of the complex systems. In this section, we will give an example of the modeling at the Earth-atmosphere interface. In particular, we will point out some uncertainties, which can occur in prediction, because of the non-linear relations in system under consideration.

Environmental fluid mechanics modelers base their calculations on mathematical models for simulation and prediction of different processes, which are exclusively non-linear, describing relevant quantities in the field of consideration. Many investigators, for example *Boccaletti et al.* (2000), have proved that complex dynamical evolutions lead to chaotic regime. Finite precision computer realizations of non-linear models give unrealistic solutions, because of the deterministic chaos, a direct consequence of round-off error growth in iterative numerical computations, which doubles on average for each iteration of iterative computations. Round-off error propagates to the mainstream computation and gives unrealistic solutions for different geophysical models, which incorporate thousands of iterative computations in longer-term numerical integration schemes (*Selvam* and *Fadnavis,* 1998). Also, in solving of

the model partial differential equations, depending on numerical procedure, the problem of sensitivity to initial conditions may occur. Namely, a small "tuning" of initial conditions may lead the numerical model to instability, if the system is a chaotic one. The aforementioned instabilities can be generated in temporal fluctuations on all space-time scales ranging from turbulence to climate. These kinds of uncertainties take place preferably at the interface between two mediums in geophysical space (*Mihailovic et al.,* 2001). The land-atmosphere interface is a suitable area for the occurrence of irregularities in the temporal variation of some geophysical quantities. Here we will analyze the occurrence of deterministic chaos in the surface temperature obtained by solving the energy balance equation, which describes the exchange of energy at the land-atmosphere interface.

Solar radiation provides almost all of the energy received on the surface of the Earth. Some of the radiant energy is reflected back to space. The Earth also radiates, in the thermal waveband, some of the energy received from the sun. The quantity of the radiant energy remaining on the earth surface is the net radiation R_n (the net radiation energy available on the surface, when all inward and outward streams of radiation have been considered). The net radiation drives certain physical processes important to us. The energy balance may be expressed as

$$C_g \partial T_g / \partial t = R_n - H - \lambda E - S - PS - M, \tag{1}$$

where C_g is the surface heat capacity, T_g is the surface temperature, S is the flux heat out of the soil, H is the flux of sensible heat between the surface and air, λE is the flux of sensible heat between the surface through vaporization (evaporation) of water condensation, PS is the energy fixed in plants photosynthesis, and M is the energy involved in a number of miscellaneous processes as respiration and heat storage in the crop canopy. Eq. (1) is applicable on the scale of a single plant or cropped field, explaining how energy is provided to warm up the soil crop and to evaporate water. The equation is not less valid on the global scale, explaining how energy is provided to the continents and oceans, where vast quantities of heat and vapor are delivered to or extracted from the atmosphere (*Rosenberg et al.,* 1983). Neglecting terms M and PS, which have much smaller values comparing to other terms, leads us to the equation (*Mihailovic* and *Lalic,* 2006)

$$C_g \partial T_g / \partial t = R_n - H - \lambda E - S, \tag{2}$$

that is more appropriate for further analysis. In the resistance representation, the last equation gets the form

$$C_g \partial T_g / \partial t = C_R (T_g - T_r) - C_L [E(T_g) - e_r] - C_H (T_g - T_r) - C_D (T_g - T_r), \quad (3)$$

where the symbols introduced have the following meaning: C_R is a constant in the net radiation term (*Bhumralkar,* 1975; *Holtslag* and *van Ulden,* 1983), T_r is the air temperature at the reference level, C_L is the water vapor transfer coefficient, $E(T_g)$ is the saturated water vapor pressure at the surface temperature, e_r is the water vapor pressure at the reference level, C_H is the heat transfer coefficient, and C_D is the coefficient of conduction. To solve Eq. (1) numerically, for simplicity we use the foreword difference scheme, as it is usual in environmental fluid mechanic modeling, which has the form

$$T_g{}^{n+1} = T_g{}^n + \Delta t F^n / C_g, \quad (4)$$

where F^n is the right hand side term of Eq. (1) at the nth time step, while Δt is the time step. Because Eq. (1) is a non-linear partial differential equation, it could be expected that its solution exhibits not only periodic but even chaotic behavior under some conditions. One set of those conditions leading to chaotic behavior of the surface temperature is considered in *Mihailovic* (2006). Under those conditions, Eq. (3) can be written as

$$\partial \xi / \partial t = [a_c - C_L b E(T_r) / C_g] \xi - [C_L b^2 E(T_r) / 2C_g] \xi^2, \quad (5)$$

where $a_c = C_R - C_H - C_D$ and $\xi = T_g - T_r$, while $b = 0.06337$ J °C^{-1} is a constant for temperatures around 20 °C (*Hrigan,* 1978), which occurs in expanding the expression for $E(T_g)$ in Taylor's series. If we write Eq. (5) in the finite difference form, we reach the equation having the form

$$\xi_{n+1} = A_1(C_g)\xi_n - A_2(C_g)\xi_n^2, \quad (6)$$

where the symbols introduced have the following meaning $A_1(C_g) = (C_R - C_L b E(T_r)\Delta t / C_g) + 1$ and $A_2(C_g) = C_L{}^2 b E(T_r)\Delta t / (2C_g)$. Eq. (6) is one form of the so-called logistic equation. As a non-linear equation, it can produce a chaotic solution for some values of A_1 and A_2. It is very interesting to analyze Eq. (6), in the $(\lambda_L, \Delta t)$ phase space, for different values of A_1 and A_2. Here we define the Lyapunov exponent λ_L for this equation, which has a single degree of freedom ξ depending on discrete "time" n. It has the form

$$\lambda_L = \lim_{n \to \infty} (1/n) \sum_{j=1}^{n} \ln \left| F'(\xi_n) \right|, \quad (7)$$

where $F(\xi) = A_1(C_g)\xi - A_2(C_g)\xi^2$.

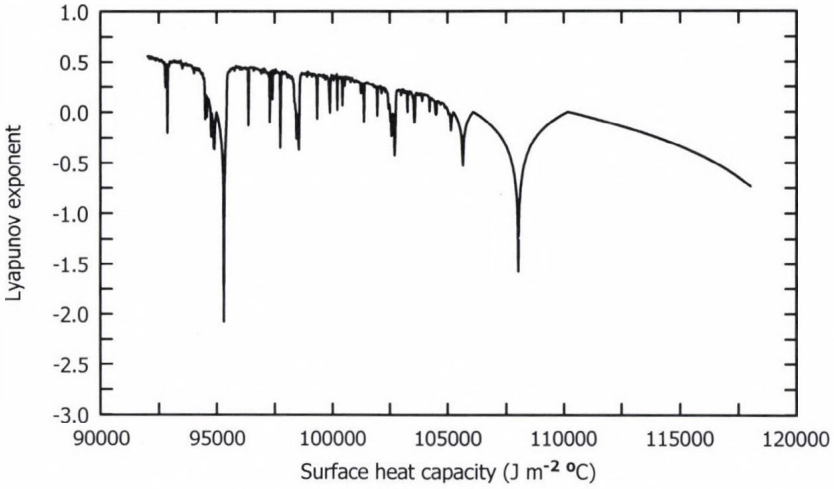

Fig. 2. Dependence of Lyapunov exponent λ_L on soil surface heat capacity C_g (*Mihailovic*, 2006).

Fig. 2 depicts the changes of exponent depending on the variation of the surface heat capacity. It is seen from this figure, that the considered dynamical system, i.e., the soil-atmosphere interface, mostly exhibits chaotic behavior manifested through the positive value of λ_L, while the soil surface heat capacity takes the values from the 92,500–107,500 J m^{-2} °C^{-1} interval. Outside of this interval the considered system is stable, since the Lyapunov exponent takes the negative values. This example points out, that the way to the phenomenon of N via the arrow (4) in *Fig. 1* is not a simple one, even in the case of a relatively simple model. In other word, that attempt is methodologically difficult in the non-linear world.

Acknowledgements—The research work described in this paper has been funded by the Serbian Ministry of Science and Environmental Protection under the project "Modeling and numerical simulations of complex physical systems", No. ON141035 for 2006-2010. The authors would like to thank *Mr. Nebojsa Vukov* for proofreading of the paper.

References

Bell, J.S., 1964: On the Einstein Podolsky Rosen paradox. *Physics 1*, 195-200.

Bhumralkar, C.M., 1975: Numerical experiments on the computation of ground surface temperature in an atmospheric general circulation model. *J. Appl. Meteorol. 14*, 1246-1258.

Boccaletti, C.M., Grebogi, C., Lai, Y-C., Mancini, H., and *Mazaret, D.*, 2000. The control of chaos: Theory and applications. *Phys. Rep. 329*, 108-109.

Cushman-Roisin, B., Gualtieri, C., and *Mihailovic, D.T.*, 2006: *Introduction*. In *Fluid Mechanics Processes at the Environmental Interfaces* (eds.: *C. Gualt*ieri and *D.T. Mihailovic*). Taylor and Francis, London (in press).

Duhem, P. 1906: *The Aim and Structure of Physical Theory* (in Serbian). Izdavacka knjizarnica Zorana Stojanovica, Novi Sad, 2003, 271 pp.

Einstein, E., Podolski, B., and *Rosen, N.,* 1935: Can quantum-mechanical description of physical reality be considered complete? *Phys. Rev. 47,* 777-780.

Holtslag, A.A and *van Ulden, A.P.,* 1983: A simple scheme for daytime estimates of the surface fluxes from routine weather data. *J. Appl. Meteorol. 22,* 517-529.

Hrigan, A.H., 1978: *Fizika atmosfery* (in Russian), *Tom 2.* Gidrometeoizdat, Leningrad, 319 pp.

Kleene, S.C., 1952: *Introduction to Metamathematics.* van Nostrand, New York.

Mihailovic, D.T., 2006: Chaotic time fluctuations of surface temperature occurring in the ecological modeling from local to global scale. Plenary Talk on *Ecological problems of our days – from global to local scale: Vulnerability and adaptation,* 30 November – 1 December, Keszthely (Hungary). CD ROM. Internet: http://www.georgikon.pate.hu/tanszekek/Meteor/programfuzet.htm.

Mihailovic, D.T., Kapor, D.V., Lalic, B., and *Arsenic, I.,* 2001: The chaotic time fluctuations of ground surface temperature resulting from energy balance equation for the soil-surface system. *Abstracts of the 26th General Assembly of European Geophysical Society,* 20-25 March, Nice (France).

Mihailović, D.T. and *Lalic, B.,* 2006: Land-Air Parameterisation Scheme (LAPS) as a component in agrometeorological modeling. Invited lecture on *Workshop on Environmental Fluid Mechanics as Elements in Agrometeorological Modelling,* 6-9 June, Ås (Norway).

Nagel, E., 1961: *The Structure of Science: Problems in the Logic of Scientific Explanation.* Harcourt, Brace World, inc. New York, 618 pp.

Nagel, E. and *Newman, J.R.,* 1958: *Gödel's Proof.* New York University Press, New York, 128 pp.

Nedeljković, Lj.D. and *Nedeljkovic, N.N.,* 2003a: Rydberg-state reionization of multiply charged ions escaping from solid surfaces *Phys. Rev. A 67,* 032709.

Nedeljković, Lj.D. and *Nedeljkovic, N.N.,* 2003b: Reconstruction of the past in quantum teleology of the ion - surface interaction. *Fifth General Conference of Balkan Physical Union.* Vrnjačka Banja, Serbia and Montenegro, August 25-29.

Piaget, J., 1973a: *Introduction to Genetic Epistemology. 1) Mathematical thought* (in Serbian). Izdavacka knjizarnica Zorana Stojanovica, Novi Sad, 1994, 322 pp.

Piaget, J., 1973b: *Introduction to Genetic Epistemology. 2) Physical thought* (in Serbian). Izdavacka knjizarnica Zorana Stojanovica, Novi Sad, 1996, 318 pp.

Rosen, R., 1977: Complexity as a systems property. *Int. J. Gen. Systems 3,* 227-232.

Rosen, R., 1991: *Life Itself: A Comprehensive Inquiry into the Nature, Origin, and Fabrication of Life.* Columbia University Press, New York, 285 pp.

Rosenberg, N.J., Blad, B.L., and *Verma, S.B.,* 1983: *Microclimate: The Biological Environment.* John Wiley & Sons, New York, 528 pp.

Rössler, O.E., 1998: *Endophysics: The World as an Interface.* World Scientific Publishing Co. Pte. Ltd., Singapore, 204 pp.

Selvam, A.M. and *Fadnavis, S.,* 1998: Signatures of a universal spectrum for atmospheric interannual variability in some disparate climatic regimes. *Meteorol. Atmos. Phys. 66,* 87-112.

Sivertsen, T.H., 2004. Invitation to conceptual discussions concerning the scope of the scientific method and classification systems of meteorological phenomena and meteorological parameters. *Selected papers of the International Conference "Fluxes and Structures in Fluids".* St. Petersburg, Russia, 23–26 June 2003. Moscow. IPM RAS, 6 p.

Sivertsen, T.H., 2005: Discussing the scientific method and a documentation system of meteorological and biological parameters. *Phys. Chem. Earth 30,* 35-43.

Van Loocke, Ph., 2002: Deep teleology in artificial systems. *Mind. Mach. 12,* 87–104.

GUIDE FOR AUTHORS OF *IDŐJÁRÁS*

The purpose of the journal is to publish papers in any field of meteorology and atmosphere related scientific areas. These may be

- research papers on new results of scientific investigations,
- critical review articles summarizing the current state of art of a certain topic,
- short contributions dealing with a particular question.

Some issues contain "News" and "Book review", therefore, such contributions are also welcome. The papers must be in American English and should be checked by a native speaker if necessary.

Authors are requested to send their manuscripts to

Editor-in Chief of IDŐJÁRÁS

P.O. Box 39, H-1675 Budapest, Hungary

in three identical printed copies including all illustrations. Papers will then be reviewed normally by two independent referees, who remain unidentified for the author(s). The Editor-in-Chief will inform the author(s) whether or not the paper is acceptable for publication, and what modifications, if any, are necessary.

Please, follow the order given below when typing manuscripts.

Title part: should consist of the title, the name(s) of the author(s), their affiliation(s) including full postal and e-mail address(es). In case of more than one author, the corresponding author must be identified.

Abstract: should contain the purpose, the applied data and methods as well as the basic conclusion(s) of the paper.

Key-words: must be included (from 5 to 10) to help to classify the topic.

Text: has to be typed in single spacing with wide margins on one side of an A4 size white paper. Use of S.I. units are expected, and the use of negative exponent is preferred to fractional sign. Mathematical formulae are expected to be as simple as possible and numbered in parentheses at the right margin.

All publications cited in the text should be presented in a *list of references*, arranged in alphabetical order. For an article: name(s) of author(s) in Italics, year, title of article, name of journal, volume, number (the latter two in Italics) and pages. E.g., *Nathan, K.K.,* 1986: A note on the relationship between photo-synthetically active radiation and cloud amount. *Időjárás 90,* 10-13. For a book: name(s) of author(s), year, title of the book (all in Italics except the year), publisher and place of publication. E.g., *Junge, C.E.,* 1963: *Air Chemistry and Radioactivity*. Academic Press, New York and London. Reference in the text should contain the name(s) of the author(s) in Italics and year of publication. E.g., in the case of one author: *Miller* (1989); in the case of two authors: *Gamov* and *Cleveland* (1973); and if there are more than two authors: *Smith et al.* (1990). If the name of the author cannot be fitted into the text: *(Miller,* 1989); etc. When referring papers published in the same year by the same author, letters a, b, c, etc. should follow the year of publication.

Tables should be marked by Arabic numbers and printed in separate sheets with their numbers and legends given below them. Avoid too lengthy or complicated tables, or tables duplicating results given in other form in the manuscript (e.g., graphs)

Figures should also be marked with Arabic numbers and printed in black and white in camera-ready form in separate sheets with their numbers and captions given below them. JPG, GIF, or XLS formats should be used for electronic artwork submission.

The text should be submitted both in manuscript and in electronic form, the latter on disks or in e-mail. Use standard 3.5" MS-DOS formatted diskette or CD for this purpose. MS Word format is preferred.

Reprints: authors receive 30 reprints free of charge. Additional reprints may be ordered at the authors' expense when sending back the proofs to the Editorial Office.

Information on the last issues: http://www.met.hu/Journal-Idojaras.php

Published by the Hungarian Meteorological Service

Budapest, Hungary

INDEX: 26 361

HU ISSN 0324-6329